Joana de Freitas Fresco Rodrigues Costa

Sca*l*e for mapping the brain:

the role of stargazin in regulating dendritic spine morphology

Dissertação apresentada à Universidade de Coimbra para cumprimento dos requisitos necessários à obtenção do grau de Mestre em Biologia Celular e Molecular, realizada sob orientação científica da Doutora Luísa Cortes (Centro de Neurociências e Biologia Celular, Universidade de Coimbra) e pela Professora Doutora Ana Luísa Carvalho (Departamento de Ciência da Vida, Universidade de Coimbra) e apresentada ao Departamento de Ciências Da Vida da Universidade de Coimbra.

Julho de 2016

· U C ·

UNIVERSIDADE DE COIMBRA

Cover Legend: Hippocampal neuron expressing mCherry.

The present work was performed in the Synapse Biology group of the Center for Neurocience and Cell Biology (Universidade de Coimbra, Portugal), headed by Professor Ana Luísa Carvalho.

This work was supported by a NARSAD Independent Investigator Grant from the Brain and Behavior Research Foundation, by national funds through the Portuguese Science and Technology Foundation (FCT; PTDC/SAU-NMC/4888/2014 and UID/NEU/04539/2013), by the European Union – European Fund for Economic and Regional Develoment funding through the Operational Competitiveness Program (COMPETE), and by Programa Mais Centro (CENTRO-07-ST24-FED ER-002002, 002006, 002008).

Dedicatória

À minha mãe

Agradecimentos

À minha orientadora, Professora Doutora Ana Luísa Carvalho, pela sua orientação, disponibilidade, apoio e encorajamento que foram para mim fundamentais na concretização deste projeto.

À minha orientadora, Doutora Luísa Cortes, pela sua disponibilidade e colaboração na procura de respostas para o trabalho.

À Doutoranda Gladys Caldeira, pelo seu apoio e paciência, por me ter ensinado tanto.

Ao meu grupo no Laboratório, pela ajuda e colaboração, pela cumplicidade, pelos momentos alegres e travessos que partilhámos.

Aos grupos Growth Factor Signaling and Brain Ischemia e Neuronal Circuits and Behaviour e, em particular, ao Doutorando Mohamed Hussien, pela sua infinita paciência no ensino e apoio ao trabalho com o NeuronStudio.

Ao Gang do Tremoço Bravo, por me ensinarem o valor da amizade e por me fazerem rir com coisas que não lembram a ninguém.

Ao meu irmão por ser um idiota querido.

À minha mãe, pela sua importância nesta jornada.

Table of contents

Abbreviations

ADF	Actin depolymerizing factor
AMPA	α-amino-3-hydroxy-5-methyl-4-isoxazole propionic acid
AMPAR	AMPA receptor
ASD	Austim spectrum disorder
ARC	Activity-Regulated Cytoskeleton-associated protein
BDNF	Brain-derived neurotrophic factor
CaMKII	Calcium/calmodulin-dependent protein kinase II
CDC42	Cell division control protein 42 homolog
CNS	Central nervous system
CP-AMPAR	Calcium permeable AMPAR
CTD	Carboxy-terminal domain
DIV	Days in vitro
DISC	Disrupted in schizophrenia 1
DLPFC	Dorsolateral prefrontal cortex
DNA	Deoxyribonucleic acid
DNM	*De novo* mutation
ER	Endoplasmic reticulum
GABA	Gamma-Aminobutyric acid
GDP	Guanosine diphosphate
GFP	Green fluorescent protein
GTP	Guanosine-5'-triphosphate
HEPES	N-(2-hydroxyethyl)piperazine-N'-(2-ethanesulfonic acid)
HBSS	Hank's balanced salt solution
ICC	Immunocytochemistry
ID	Intellectual disability
iGluR	Ionotropic glutamate receptors
IP3	Inositol 1,4,5-triphosphate
IRSp53	Insulin receptor substrate p53
KAR	Kainate receptor
kDa	Kilodalton
LBD	Ligand binding domain
LC	Light chain
LPM	Liters per minute
LTD	Long-term depression
LTP	Long-term potentiation
MAP2	Microtubule associated protein 2

MAGI-2	Membrane-associated guanylate kinase inverted 2
mGluR	Metabotropic glutamate receptor
NMDA	N-methyl-D-aspartate
NMDAR	NMDA receptor
NTD	Amino-terminal domain
P	Postnatal day
PACT	Passive clarity technique
PARS	Perfusion-assisted agent release
PBS	Phosphate buffered saline
PCR	Polymerase chain reaction
PDZ	Postsynaptic density 95-discs large-zona occludens 1
PEG	Polyethylene glycol
PICK1	Protein interacting with C kinase
PKA	Protein kinase A
PKC	Protein kinase C
PSD	Postsynaptic density
PSD-95	Postsynaptic density protein 95
RIMS	Refractive index matching solution
S-SCAM	Synaptic scaffolding molecule
SEM	Standard error of the mean
shRNA	Short-hairpin Ribonucleic Acid
SCZ	Schizophrenia
SNP	Single Nucleotide Polymorphism
SR	Serine racemase
S-SCAM	Synaptic scaffolding molecule
Stg	Stargazin
TARP	Transmembrane AMPAR-regulatory protein
TBS	Tris-buffered saline
TDE	2,2’-thiodiethanol
TTX	Tetrodotoxin
VGAT	Vesicular GABA Transporter
VASP	Vasodilator-stimulated phosphoprotein
VGLUT	Vesicular glutamate transporter
WASF1	Wiskott-Aldrich syndrome protein family member 1
WAVE	WASP-family verprolin homologous protein

Resumo

Esquizofrenia e Deficiência intelectual são duas doenças que hoje em dia afetam entre 1 e 3% da população mundial, respetivamente. Estudos recentes demonstram a relevância de mutações em genes que codificam proteínas sinápticas na patogénese de doenças neuropsiquiátricas (Volk et al., 2015). Um desses genes é o *CACNG2* que codifica a stargazina, uma proteína de 37 kDa, transmembranar, auxiliar dos recetores AMPA e que se localiza na pós-sinapse. A stargazina influencia o tráfico sináptico e propriedades biofísicas dos AMPAR (Chen et al., 2000; Letts et al., 1998; Roberts et al., 2011). Para além disto, a stargazina também afeta a complexidade da arborização dendrítica (resultados não publicados) e medeia a plasticidade homeostática (Louros et al., 2014). Dado o papel sináptico da stargazina e também a sua interação com proteínas do citoesqueleto, colocámos a hipótese de a stargazina poder ter um papel na modulação da morfologia das espículas dendríticas. Para testar esta possibilidade, silenciámos a expressão da stargazina em neurónios de fatias organotípicas de hipocampo usando RNA de interferência tendo como alvo a stargazina. Analisámos a morfologia das espículas em neurónios de hipocampo transfetados e observámos que o silenciamento da stargazina afeta o balanço entre espículas imaturas e maduras, levando a um aumento de cerca de 65% na ocorrência de estruturas do tipo filopodia, ou seja, precursores de espículas. De acordo com o nosso conhecimento, este trabalho fornece a primeira evidência da influência da stargazina na morfologia das espículas em neurónios de hipocampo. Também gerámos e caraterizámos um vetor lentiviral capaz de expressar mCherry e stargazina *wild-type* ou variantes de stargazina associadas a doença. Este vetor lentiviral ajudar-nos-á, no futuro, no estudo da influência de mutantes de stargazina associados a doença na morfologia das espículas e na arborização dendrítica.

Finalmente, otimizámos e implementámos os métodos Sca*l*eA2 e Sca*l*eS, protocolos de *clearing* de tecido que nos ajudarão a adquirir imagens de microscopia em profundidade em tecidos biológicos. Com este tipo de protocolos poderemos usar secções espessas de cérebro para análise da morfologia neuronal. Com estes protocolos conseguimos obter sinal fluorescente endógeno em camadas mais profundas em cérebros de ratinho. Para isto usámos microscopia confocal para obter images de *z-stack*

que variaram entre 200-500 µm para o Sca*l*eA2 e cerca de 250 µm para Sca*l*eS. Por outro lado, usando o microscópio multifotão conseguimos obter 1 mm de espessura de imagens de *z-stack*. Acreditamos que este tipo de metodologia será extremamente importante em futuras investigações no estudo do papel da stargazina e variantes de stargazina associadas a doença.

Palavras-chave: stargazina, *CACNG2*, Sca*l*eA2, Sca*l*eS, morfologia de espículas.

Abstract

Schizophrenia and Intellectual Disability are two disorders that affect 1 and 3% of the worldwide population, respectively. Recent genetic studies point the relevance of mutations in genes coding for synaptic proteins in the pathogenesis of neuropsychiatric disorders (Volk et al., 2015). One of those genes is *CACNG2*, which encodes for stargazin, a 37 kD AMPA receptor (AMPAR), transmembrane, auxiliary protein that localizes postsynaptically and binds physically to AMPAR. Stargazin influences AMPAR synaptic traffic and biophysical properties (Chen et al., 2000; Letts et al., 1998; Roberts et al., 2011). Additionally, stargazin affects neuronal dendritic arborization complexity (unpublished data) and mediates homeostatic plasticity (Louros et al., 2014). Given the synaptic roles of stargazin, and also its interaction with cytoskeletal proteins, we hypothesized that stargazin may have a role in modulating the morphology of dendritic spines, the sites that house the postsynaptic element of excitatory synapses. In this project, we tested this hypothesis. In order to do so, we silenced stargazin expression in neurons in organotypic hippocampal slices using interference RNA to target stargazin. We analyzed spine morphology in transfected hippocampal neurons and found that the deletion of stargazin affects the balance between immature and mature spines, leading to a ~65% increase in the occurrence of filopodia-type structures, which are spine precursors, at the expense of thin and mature spines. To our knowledge, this work provides the first evidence for stargazin influence on spine morphology in hippocampal neurons. We also generated and characterized a lentiviral vector expressing mCherry and wild-type or disease-associated variants of stargazin. This lentiviral vector will help us study, in the future, the influence of stargazin-disease related mutants in spine morphology and dendritic arborization.

Finally, we have optimized and implemented Sca*l*eA2 and Sca*l*eS methods, tissue clearing protocols that allow in depth imaging of biological tissue. With this type of protocol, we can use thick brain sections to image neuronal morphology. With these protocols we could obtain endogenous fluorescence signal in deep layers of the mouse brain. In order to do so, we used confocal microscopy to obtain 200-500 µm for Sca*l*eA2 and ~250 µm for Sca*l*eS thick image stacks. Multiphoton microscopy allowed us to obtain

1 mm thick image stacks. We believe that this type of methodology will be extremely important for the study of the role of stargazin and its disease-associated variants in the brain.

Key words: stargazin, *CACNG2*, Sca*l*eA2, Sca*l*eS, spine morphology.

Chapter I

Introduction

1. Glutamatergic synapses

Within the central nervous system (CNS) it is possible to find two different types of specialized communications: chemical and electrical synapses. These synapses allow the communication between different neurons, neurons and muscles or even neurons and gland cells.

Chemical synapses can be classified in two groups: excitatory or inhibitory synapses, depending on the effect of neurotransmitter release. If GABA (g-aminobutyric acid) is the chemical compound released from the pre-synaptic neuron, then the postsynaptic neuron will undergo hyperpolarization of the membrane. If glutamate is release instead, the postsynaptic neuron will suffer a depolarization and if this depolarization reaches the threshold, an action potential will occur. These type of synapses are called excitatory synapses (Siddoway et al., 2011).

In the vertebrate CNS, the major excitatory neurotransmitter is the glutamate whereas GABA is the major inhibitory neurotransmitter (Siddoway et al., 2011). In the CNS, glutamate signal is vital for several processes such as cognition and sensory processing. Disruption of this type of signaling has been associated with several disorders such as autism spectrum disorder (ASD), intellectual disability (ID) and schizophrenia, reason why it is vital a better understanding of how the glutamatergic system might be affected in a disease context (Volk et al., 2015).

1.1. Glutamate receptors

Glutamate receptors can be distinguished in two different functional groups: the metabotropic receptors also known as glutamate-activated G protein–coupled receptors, which are subdivided in three families. These families are: mGluR I which includes mGluR1 and 5, postsynaptically localized, mGluR II composed by mGluR2 and mGluR3 and finally, mGluR III which are mostly presynaptic and composed by mGluR4 and mGluR6-8. The second group is composed by ionotropic ligand-gated ion channels, constituted by α-amino-3-hydroxy-5-methyl-4-isoxazolepropionic acid (AMPA) receptors (AMPAR), Kainate

(KA) receptors and N-methyl-D-aspartate (NMDA) receptors (NMDAR), whose designations are related to their affinity for the glutamate analogues AMPA, KA and NMDA, respectively. These receptors are vital for chemical synapses and synaptic plasticity processes. It is due to these type of receptors that, during development, the CNS may refine their synapses and circuits, a process fundamental for adaptive cognitive processes such as learning and memory (Palmer et al., 2005; Volk et al., 2015).

1.2. NMDAR

NMDAR are heterotetrameric synaptic channels permeable to monovalent cationic ions and calcium ions (Volk et al., 2015). NMDAR at resting membrane potential are blocked by magnesium, which is released after depolarization of the neuron when these same receptors are bound to glutamate and glycine (or D-serine), allowing the opening of this channel (Zito and Scheuss, 2009).

More recently, a study regarding serine racemase enzyme (SR), an enzyme responsible for the conversion of L-serine to D-serine, points out that there is a possible cross-talk between NMDAR and AMPAR, a cross-talk where AMPAR activation enhances NMDAR transmission. In this work it was found that SR could bind both PSD-95 and stargazin forming, possibly, a quinary complex with AMPAR and NMDAR. In resting conditions, SR is bound to stargazin, PSD-95 and AMPAR rendering this enzyme inactive. After the activation of AMPAR, the previous mentioned complex is dissociated, releasing SR. The free SR is then able to generate D-serine which, together with glutamate will activate NMDAR (Ma et al., 2014).

1.3. AMPAR

AMPAR are synaptic monovalent cationic glutamate receptors composed by a complex of tetrameric proteins GluA1-4 whose properties depend on their subunits composition (Palmer et al., 2005; Soto et al., 2008). For example, GluA2 subunit is modified at its Q/R site within the pore region by posttranscriptional RNA editing and AMPAR lacking this edited subunit are permeable to calcium ions and have an elevated single-channel conductance. Besides, these AMPAR that are lacking this edited subunit

can be blocked endogenously by intracellular polyamines which alters the channel properties (as reviewed in Soto et al. 2008).

In terms of structure, all subunits have an intracellular C-terminus, responsible for the interaction with several proteins, an extracellular N-terminus and four hydrophobic transmembrane domains, TM1 – 4. Besides these structures, there is still the ligand-binding core which is responsible for AMPAR pharmacological specificity (Palmer et al., 2005).

In terms of kinetics, after glutamate binding, AMPAR open very quickly and also desensitize in a rapid manner. After the unbinding of glutamate from the receptor, the AMPAR channel closes - a process called deactivation (Tomita et al., 2006).

1.4. Stargazin and other TARPs

TARPs are a family of transmembrane AMPAR regulatory proteins (Ziff, 2007). This family can be divided in two classes, according to their influence on AMPAR modulation: class I, which includes γ2 (stargazin) (expressed in cortex, midbrain, hippocampus, cerebellum, pons and thalamus), γ3 (expressed in the cerebral cortex), γ4 (olfactory bulb), and γ8 (hippocampus) and class II which includes γ5 and γ7 (hippocampus) (Kim et al., 2010; Tomita, 2010). Another difference between the elements of both classes are the PDZ domain-binding motif, while class I is characterized by a –TTPV PDZ binding motif at its C-terminal, class II contains a −S/TTPC PDZ binding motif, at its C-terminal (Tomita, 2010).

Structurally, TARPs have two intracellular termini and four transmembrane domains. Four of the eight known TARPs (namely stargazin, γ3, γ4 and γ8) are vital for AMPAR function, modulating AMPAR receptor activity (Kim et al., 2010; Ziff, 2007). TARPS have a variable stoichiometry, ranging from one unit to four, depending on TARP concentration levels, region of the brain and neuronal cell types (Kim et al., 2010; Shi et al., 2009). Moreover, each TARP is able to bind AMPAR independently and without cooperative binding properties (Kim et al., 2010).

The first AMPAR auxiliary subunit to be identified was stargazin, which is able to interact physically with AMPAR not only in plasmatic membrane but also in intracellular organelles (Chen et al., 2000; Cuadra et al., 2004; Tomita et al., 2004, 2005a).

Stargazin is a 37-kDa protein encoded by the *CACNG2* gene and is enriched at the excitatory postsynaptic plasma membrane, with high expression in the cortex (Chen et al., 2000; Inamura et al., 2006; Letts et al., 1998; Roberts et al., 2011).

Stargazin is a membrane-spanning protein with four transmembrane domains that may exist in monomeric or dimeric form (Letts et al., 1998; Roberts et al., 2011). Stargazin is also characterized for having two intracellular tails (N and C tail) and an extracellular loop, with an ectodomain (represented as the prominence in Fig. 1). This extracellular loop is flanked by the two first transmembrane domains (represented as green rectangles in Fig. 1) (Letts et al., 1998; Roberts et al., 2011).

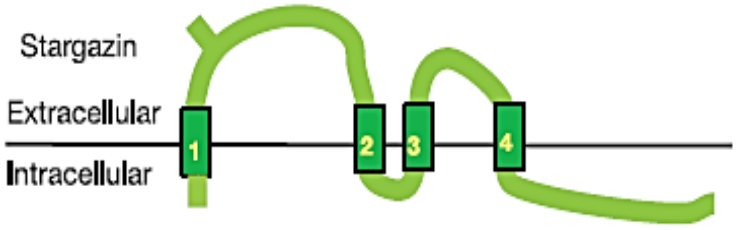

Fig. 1 – Schematic representation of stargazin secondary structure. Stargazin is composed by four transmembrane domains, two cytoplasmatic tails and an extracellular loop with an ectodomain between the first and second transmembrane domain. Adapted from (Tomita et al., 2005a).

Stargazin C-terminal contains nine serine residues that can be phosphorylated and a PDZ binding site which is responsible for its interaction with several proteins in the PSD, such as PSD-95 (Choi et al., 2002; Tomita et al., 2005b). The interaction between stargazin and PSD-95 through the PDZ domains revealed to be vital in AMPAR subunits clustering (Chen et al., 2000; Schnell et al., 2002; Tomita et al., 2001, 2005b).

Stargazin postsynaptic localization appears to be dependent not only on its PDZ domain but also on its aminoacids within C-tail (Cuadra et al., 2004). The phosphorylation of the serine residues leads to conformational changes, which extend stargazin C-tail length into the cytoplasm facilitating and enhancing its interaction with PSD-95 (Fig. 2). The interaction between stargazin and PSD-95 leads to a decrease in AMPAR lateral

diffusion between extrasynaptic and synaptic sites potentiating, consequently, synaptic function (Hafner et al., 2015; Sumioka et al., 2010). Stargazin phosphorylation may be mediated by PKA, PKC and CaMKII, with different results in terms of stargazin and PSD-95 binding and, consequently AMPAR clustering on the membrane (Chetkovich et al., 2002; Choi et al., 2002; Inamura et al., 2006; Opazo et al., 2010; Sumioka et al., 2010; Tomita et al., 2005a, 2005b). Moreover, calpains have also been associated with stargazin regulation since they truncate stargazin C-tail, decreasing its expression on the membrane with obvious consequences to AMPAR synaptic localization (Yu et al., 2011).

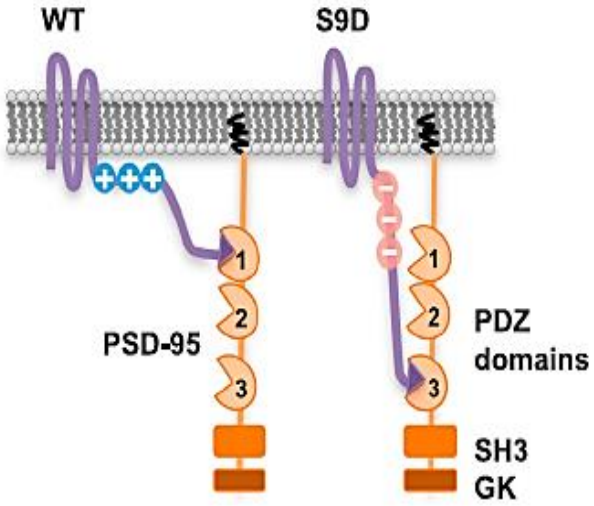

Fig. 2 - Schematic model of stargazin C-tail extended length upon stargazin phosphorylation. Upon phosphorylation, stargazin C-tail extends through the cytoplasm where it binds with higher affinity to the second and third PDZ domains of PSD-95. PDZ perpendicular position regarding the plasma membrane facilitates this binding. WT- wildtype stargazin; S9D – phosphomimetic mutant for stargazin. From (Hafner et al., 2015).

Many other stargazin partners besides AMPAR have been reported. Some of these partners are MAGI-2, claudin-1 and Arc (Deng et al. 2006; Price et al. 2005; Zhang et al. 2015). Stargazin by interacting with these proteins might not only be important for their function but also in processes in which these proteins take action.

Stargazin, in particular, is vital for AMPAR biosynthesis and maturation, trafficking, clustering and AMPAR channel properties (Bats et al., 2012; Shanks et al., 2010; Tomita et al., 2006; Vandenberghe et al., 2005). This enormous influence is due to different interactions between this TARP and AMPAR: trafficking is mediated by AMPAR interaction

with stargazin cytoplasmatic C-tail, whereas channel properties are dependent on extracellular loop (Tomita et al., 2004, 2005a). One example of such effect on channel properties is the influence of stargazin on calcium permeable (CP)-AMPAR (channels that lack GluA2 subunit but are composed by GluA1, GluA3 or GluA4 subunits).

AMPAR delivery to the membrane involves the participation of stargazin, occurring in an independent manner of stargazin PDZ binding domain, nPIST (which helps AMPAR-stargazin complexes insertion within extrasynaptic regions), and PSD-95 (Chen et al., 2000; Cuadra et al., 2004; Schnell et al., 2002). AMPAR clustering in turn, occurs in a dependent manner from stargazin PDZ binding domain (Bats et al., 2007; Borgdorff and Choquet, 2002; Chen et al., 2000; Schnell et al., 2002; Tardin et al., 2003).

After reaching its destination, AMPAR are able to diffuse along the membrane between synaptic and extrasynaptic sites if they translocate in a complex where stargazin is present. AMPAR movement along the membrane is then, most likely due to a disruption of stargazin-PSD-95 interaction, as a consequence of stargazin phosphorylation by PKA, since other forms of phosphorylated stargazin are able to associate with PSD95 (Chetkovich et al., 2002; Choi et al., 2002).

1.5. Synaptic plasticity

Plasticity is a process by which the brain adapts constantly to a changing world such as the challenges from the surrounding environment. Besides, these adaptations are extremely important for processes such as learning and memory. One of such adaptations is the pruning of the synapses, through which the brain deletes the connections that are no longer needed and strengths the ones that are necessary. In other cases, the brain reorganizes the synaptic networks by strengthening or weakening synapses or even balancing excitatory/inhibitory transmission in order to make them not only more efficient, but also to make sure that the brain maintains its balance (Kourosh Arami and Jameie, 2015). These modifications are often accomplished by two phenomena: Hebbian and Homeostatic plasticity.

1.5.1. Hebbian plasticity

Hebbian plasticity is an activity-dependent form of plasticity that occurs during development and during the maturation and refinement of neuronal circuits (Martens et al., 2015; Toyoizumi et al., 2014; Turrigiano, 2007). This type of plasticity includes both long-term potentiation (LTP) and long-term depression (LTD) and has been considered important for some types of memory (Amtul and Atta-ur-Rahman, 2015; Toyoizumi et al., 2014).

LTP is a mechanism responsible for an increase in synaptic strength due to the activation of the signaling pathways that ultimately lead to functional and morphological alterations. In experimental terms, LTP can be induced by a high frequency tetanic stimulation which allows the entrance of calcium ions through NMDAR and consequent activation of phosphorylation cascades. This alteration on calcium concentration leads to activation of the CaMKII which translocates to the synapse, phosphorylating the S831 residue in GluA1. This enhances single channel conductance and opening probability of AMPAR. Besides S831, during LTP, S845 may also be phosphorylated by PKA and S818 by PKC. Nevertheless, the level of phosphorylation is dependent on the activity history of the synapse as well as on the age of the animal used in the experiments. After phosphorylation one of the first modifications observed is the increase of AMPAR number at the synapse since this phosphorylation is responsible for AMPAR trapping within the synapse, decreasing their surface diffusion (Chater and Goda, 2014).

Besides LTP, LTD may also occur. LTD is responsible for a decrease in synaptic response and may or may not involve protein synthesis, depending on the type of glutamate channel activated during the process: mGluRs or NMDAR (Ramiro-Cortés and Israely, 2013). Protein synthesis induced in mGluR-LTD is postulated to be necessary for AMPAR trafficking (Rosch and Bonhoeffer, 2003). mGluR-dependent LTD is distinct from NMDAR-dependent since it does not require the activation of phosphatases (Rosch and Bonhoeffer, 2003).

The induction of these opposite responses (LTD/LTP) is most probably due to variations in the intracellular calcium ion concentrations which activates different downstream pathways responsible for distinct functional and morphological responses

(Sala and Segal, 2014). LTP is induced by high increase in calcium concentration with consequent activation of kinases (like CaMKII) which phosphorylates several substrates such as PKC and AMPAR, namely GluA1 subunit, leading to synaptic potentiation (Chater and Goda, 2014; Rosch and Bonhoeffer, 2003). On the other hand, LTD induces only moderate rises of intracellular calcium that activate phosphatases (like PP1 and PP2A) which in turn dephosphorylate CaMKII and GluA1 subunit, leading to synaptic depression through the removal of AMPAR from the synapse (Chater and Goda, 2014; Rosch and Bonhoeffer, 2003). These modifications lead to AMPAR channel properties changes and alteration of AMPAR number within the synapse (Rosch and Bonhoeffer, 2003). In this type of plasticity, it seems that the dephosphorylation of S845 of GluA1 is required (Chater and Goda, 2014). Interactions between AP2, a multimeric protein involved in the clathrin-mediated endocytosis, and GluA2 also seem to contribute to LTD. This interaction between AP2 and GluA2 allows endocytosis of the AMPAR and, consequently AMPAR removal from the synapse leading to synaptic depression (Lee et al., 2002). The endocytosis occurs after GluA2 phosphorylation at S880 (Chater and Goda, 2014). Even though this interaction leads to internalization of AMPAR, Lee and colleagues stated that AP2 might interact with this receptor and induce its internalization through other ways, which is in accordance with the recent suggestion that AP2 might interact with stargazin (Lee et al., 2002).

Besides Hebbian plasticity, homeostatic plasticity also plays an important role in the regulation of neuronal transmission.

1.5.2. Homeostatic plasticity

In order to avoid a disturbance in neuronal function and maintain the neuronal circuits stable, the neurons display a mechanism called homeostatic plasticity. Homeostatic plasticity prevents an already saturated synapse to undergo even further (de)potentiation, maintaining the entire network stable, without extreme and uncontrolled over/under excitation (Pozo and Goda, 2010).

Homeostatic plasticity can be subdivided in global and local homeostatic plasticity. Global plasticity occurs in all of the synapses, as a result of postsynaptic firing, whereas the local plasticity only acts on individual or a small group of synapses, as a result of modifications in postsynaptic receptor activation or a presynaptic release, in a particular synapse (Turrigiano, 2012).

So, which are the mechanisms that lead to homeostatic plasticity? First of all, an alteration in network activity, strong enough to be detected by neurons or even glial cells is necessary. These cells will activate several mechanisms responsible for numerous types of modifications according to the initial stimulus. These modifications might involve the modifications of presynaptic release and/or alteration of the number of postsynaptic receptors, such as AMPAR.

Synaptic scaling is a type of homeostatic plasticity and accounts for the variation in the number of glutamate receptors at the synaptic sites allowing the control of the synaptic strength (Louros et al., 2014). This phenomenon might involve activation of gene expression with consequent local protein synthesis of AMPAR and Arc/Arg3.1. Synaptic scaling might still alter the status of activation of the eEF2 – a translational effector that in its activated form promotes dendritic protein synthesis (Fig. 3) (Pozo and Goda, 2010).

Besides this, this type of plasticity might still release BDNF (which can control, in a negative manner, the upregulation of dendritic excitability during homeostatic plasticity and modulate dendritic protein synthesis), TNF-α and retinoic acid, as summarized in Fig. 3 (Pozo and Goda, 2010).

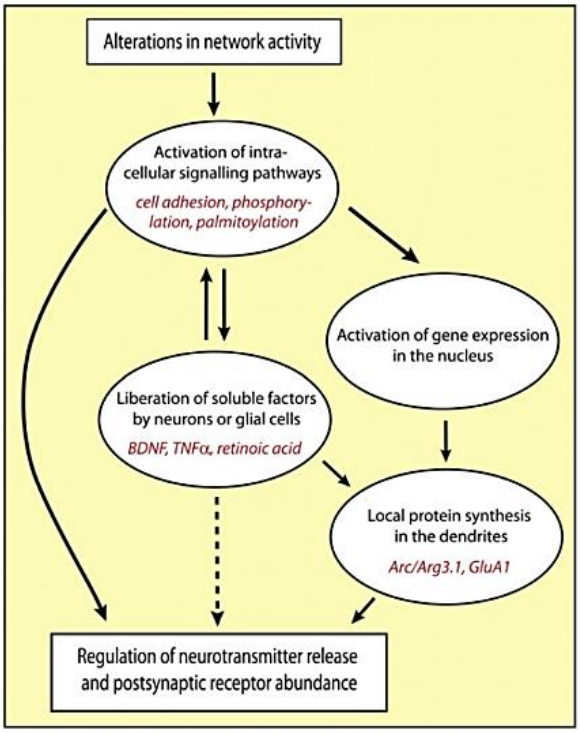

Fig. 3 - Summary of the molecular mechanisms underlying homeostatic plasticity. From (Pozo and Goda, 2010).

In homeostatic plasticity there are modifications in both presynaptic and postsynaptic sites (Vitureira et al., 2012). Using firstly the neuromuscular junction in *Drosophila* and then cultured neurons, it has been shown that presynaptic function can indeed be modified through the adjustment of synaptic efficacy in order to compensate modifications in network activity. Such modifications involve an increase in release probability due to an increased number of readily releasable vesicles, enhanced vesicle recycling and increased frequency of mEPSC. The opposite occurs when there is a persistent increase of neuronal activity. Moreover, changes in expression of VGLUT1 (glutamate transporter) may also occur (Pozo and Goda, 2010).

Some works suggest that this presynaptic homeostatic adaptations are dependent on the postsynaptic site through the use of retrograde signals that modulate the presynaptic site (Pozo and Goda, 2010). Postsynaptic strength modifications during homeostatic plasticity occur as a result of modifications of AMPAR number in the membrane, a process dependent on interaction between stargazin, PSD-95 and AMPAR, and its composition. In situations of chronic activity deprivation newly synthesized

AMPAR usually accumulate on the membrane since they are translated in the dendrites instead of being synthesized on the soma. Until now there is no consensus about which type of AMPAR receptors are inserted in the membrane in response to inactivity but some studies suggest that it is the insertion of GluA1-containing AMPAR that functions as a signal for a following insertion of GluA2-containing AMPAR for synaptic scaling (Pozo and Goda, 2010). Interestingly, stargazin was shown recently to be required for the scaling-up of GluA1-containing AMPAR. Furthermore, the phosphorylation of stargazin was shown to act as a switch controlling AMPAR synaptic accumulation and trapping (Louros et al., 2014).

1.5.3. Stargazin and its role in plasticity

Stargazin (de)phosphorylation has been characterized as a pivotal phenomenon regarding hippocampal synaptic plasticity induction. Hippocampal LTP is induced upon stargazin phosphorylation by CaMKII/PKC, decreasing its lateral diffusion which allows a higher trapping of stargazin-AMPAR complex within the membrane. Moreover, this phosphorylation promotes conformational changes within stargazin C-tail which leads to a higher synaptic targeting of this TARP and AMPAR, increasing synaptic response. LTD, however, can be induced upon activation of PP1 and PP2B which will dephosphorylate stargazin, preventing its access to the synaptic site. The prevention of stargazin and AMPAR complex targeting to the synapse will lead consequently to an induction of LTD, as shown in Fig. 4 (Tomita et al., 2005b).

Dephosphorylation of stargazin by calcineurin, which has been reported to induce LTD in hippocampus and Purkinje cells in cerebellum, also releases stargazin-AMPAR complex from the postsynaptic site (Fig. 4) (Nomura et al., 2012). Releasing stargazin-AMPAR complex from the postsynaptic site allows lateral diffusion of this complex and its arrestment in an endocytic region where it binds to AP2 (as shown in Fig. 4, D and E). Binding to AP2 allows complex interaction with PIP2, leading to the endocytosis of this complex (Fig. 4, E). After endocytosis, the complex can follow two pathways: a) recycling to the membrane (Fig. 4, F), or b) lysosome pathway through the releasing of AP2 and consequent binding to AP3 (Fig. 4, G) (Matsuda et al., 2013).

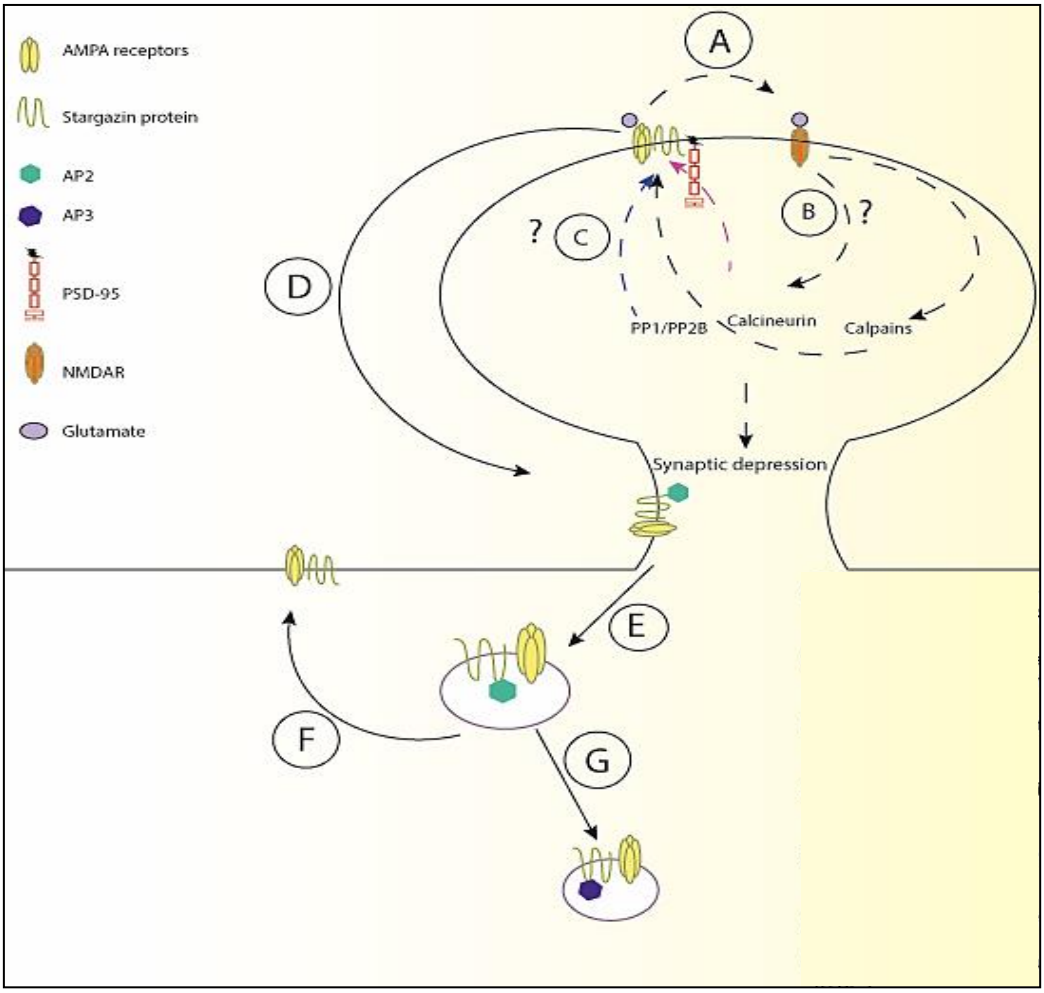

Fig. 4 - Stargazin biological role in neuronal cells: AMPAR trafficking from the membrane with consequent synaptic depression. **A)** Binding of glutamate to AMPAR leads to NMDAR magnesium blockade release; glutamate binds to NMDAR. **B)** NMDAR induces activation of different pathways: PP1/PP2B or calcineurin; it also activates calpains that truncate stargazin C-tail; **C)** Stargazin is dephosphoryated by kinases which leads to conformational changes decreasing its affinity to PSD-95 PDZ domains; **D)** Dephosphorylation increases lateral diffusion of stargazin-AMPAR complexes; **E)** Stargazin within the endocytic zones binds with AP2, promoting endocytosis; **F)** AMPAR-stargazin may recycle to the membrane after dissociation of AP2; **G)** Stargazin-AMPAR may undertake the lysosomal pathway if stargazin binds to AP3. Adapted from (Bats et al., 2007; Chen et al., 2000; Chetkovich et al., 2002; Choi et al., 2002; Cuadra et al., 2004; Elias et al., 2006; Hafner et al., 2015; Matsuda et al., 2013; Opazo et al., 2010; Roberts et al., 2011; Schnell et al., 2002; Sumioka et al., 2010; Tomita et al., 2005b).

Besides its role in Hebbian plasticity, stargazin was recently shown to play a role in homeostatic plasticity and in particular in synaptic scaling. In this study, the knockdown of stargazin followed by protein levels rescue was performed through the transfection of cortical neurons with the pLL-shRNA#4 which promotes knockdown of stargazin, as shown in Fig. 5 bellow. The rescue of protein levels was performed by the co-transfection of the neurons with the pLL-shRNA#4 and a WT stargazin, resistant to this shRNA. A few days after the transfection, the cells were stimulated with TTX, a compound that blocks

sodium channels and consequently action potentials, leading to the increase of GluA1 surface levels in comparison to the control, mechanism known as synaptic scaling. In synaptic scaling, in order to maintain a balanced neuronal transmission, the cell counteracts the stimulus (TTX) through the insertion of GluA1 in the membrane. With the knockdown of stargazin, a reduction of GluA1 levels was observed and no significant modifications were observed in the presence of TTX, which indicates that stargazin is required for synaptic scaling. Accordingly, the rescue of stargazin levels led to a significant increase of GluA1 levels on the membrane in the presence of TTX. Besides stargazin requirement for the scaling-up of GluA1-containing AMPAR it was also shown that stargazin phosphorylation acts as switch, controlling AMPAR synaptic accumulation and trapping (Louros et al., 2014). Furthermore, stargazin was shown to play an indispensable role for experience-dependent plasticity and in the development of the retinogeniculate synapse (Louros et al., 2014).

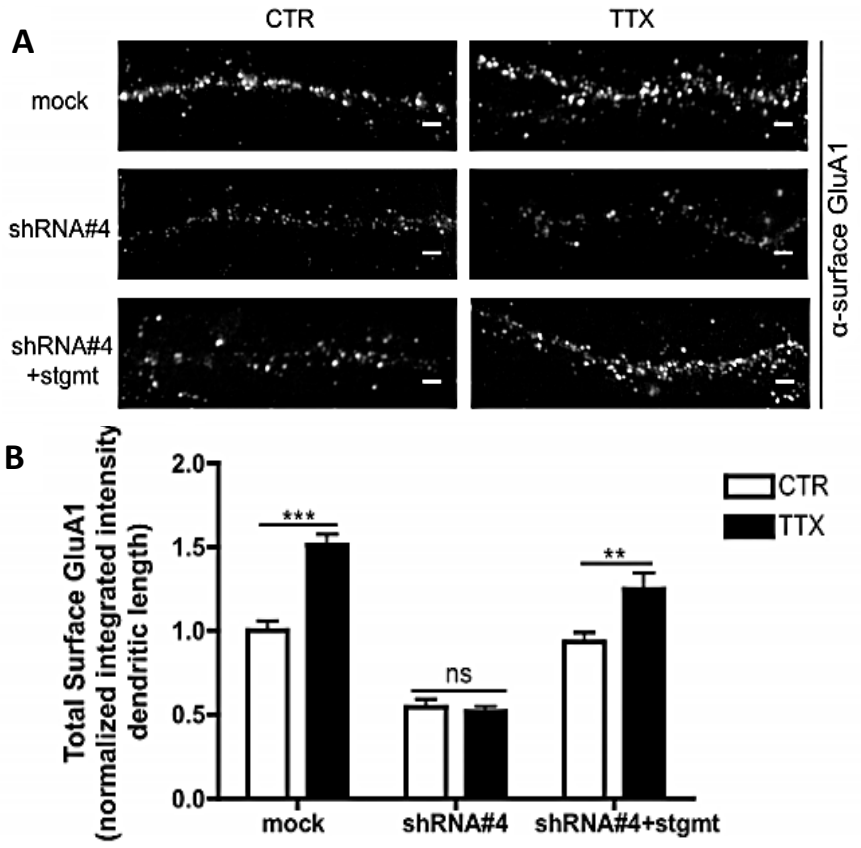

Fig. 5 - Quantification of surface GluA1 immunocytochemistry in cortical neurons. Immunocytochemistry was applied to 11 DIV cortical neuronal cells transfected with pLL-mock or pLL-shRNA#4 at DIV 4 and stimulated with TTX at DIV 9 **(A).** Total surface intensity/dendritic length of GluA1 clusters was quantified **(B)** from more than 26 cells each condition, from 3 independent experiment; **p<0,01; ***p<0,001. Adapted from (Louros et al., 2014).

1.5.6. Stargazin and its role in neuropsychiatric and neurodevelopment disorders

Stargazin has been associated with several disorders such as schizophrenia (unpublished data) and ID (Hamdan et al., 2011).

ID is a neurodevelopment disorder that affects one to three percent of the entire human population and might have several phenotypes and several degrees of severity, ranging from mild to profound in terms of symptomatology (Topper et al., 2011; Volk et al., 2015). ID is characterized by limitations not only in terms of intellectual function but also in behavior that occur before the age of eighteen (Hamdan et al., 2011; Volk et al., 2015). These individuals experience problems to adapt to new and unfamiliar situations (as reviewed in Hamdan et al., 2011). ID can be divided in syndromic and nonsyndromic forms. Syndromic forms are associated with other illnesses, such as autism, dysmorphic features and epilepsy and in the nonsyndromic form, the patients diagnosed with this illness came from families without history of this disease or without any associated illnesses (Sala and Segal, 2014; Topper et al., 2011; Volk et al., 2015). This disorder might be related with genetic abnormalities for the most severe causes (ranging from point mutations, epigenetic alterations to cytogenetic abnormalities) and external facts such as environmental insults and premature births (Volk et al., 2015). Even though most of the times it is difficult to understand which modifications might underlie this type of disorders, for one case of mild ID it has been described a *de novo* mutation (DNM) in the third transmembrane domain of stargazin, p.Val143Leu. This DNM was shown to decrease stargazin binding to GluA1 and GluA2 subunits. Besides this consequence, a decrease in mEPSC amplitude and frequency was reported, which suggests a decrease in glutamatergic transmission (Hamdan et al., 2011).

Schizophrenia on the other hand has later onset, in comparison to ID, starting in adolescence or even in early stages of adulthood (Howard et al., 2000). Schizophrenia affects about one percent of the worldwide population and is characterized by three types of symptoms such as positive symptoms that include delusions, hallucinations and paranoia, negative symptoms such as apathy, social withdrawal and anhedonia and finally cognitive symptoms such as deficits in attention and confusion thoughts (as reviewed in

Volk et al., 2015). Schizophrenia is a multifactorial disease with a strong genetic component and many susceptibility genes have been pointed as possible players in the development of the disorder. Furthermore, it is thought that these patients are more susceptible to social and environmental stressors (Day et al., 1987).

Interestingly, chromosome 22 has been pointed out as a suggestive link between schizophrenia and psychotic bipolar disorder (DeLisi et al., 2002; Kelsoe et al., 2001; Potash et al., 2003). Within this chromosome, three single nucleotide polymorphism (SNP) variants were found in a set of genes (*RASD2*, *MYH9* and *CACNG2*) suggesting that this same set might be susceptibility genes for the disease (Liu et al., 2008). More recently, another SNP in the *CACNG2* gene was also reported and associated with lithium treatment (Nissen et al., 2012).

In another study, involving schizophrenic and bipolar patients, aberrations at four loci that contain genes such as *AKAP5*, *GLUR7* and finally *CACNG2* were found, suggesting a role for glutamate signaling in these disorders (Wilson et al., 2006). More recently, copy number variations were found in the *CACNG2* gene, in a set of patients that suffer from Velo-Cardio-Facial Syndrome (VCFS), which is characterized by a hemizygous microdeletion at 22q11 chromosome. The patients that suffer from this disorder have high rates of incidence of psychiatric disorders, namely schizophrenia and bipolar disorder (Kumar et al., 2012).

Taking together, it seems that some of the susceptibility genes for these disorders encode proteins involved in glutamatergic transmission. A recent study from our laboratory, in collaboration with Dr. Carlos Pato, led to the identification of a mutation in *CACNG2* gene associated with schizophrenia. Whole-genome sequencing data from schizophrenia and control patients from the Portuguese Island cohort resulted in the identification of a missense mutation in *CACNG2* in a 25-year-old individual with undifferentiated schizophrenia, with one affected sibling. Both mutations in the *CACNG2* gene, identified in an ID patient and in a schizophrenia patient are located in the 3rd transmembrane domain and, using the Poly-Phen-2 prediction tool, were predicted to be damaging to the function of the protein (Fig. 6).

Mutation from schizophrenia patient
(Stg^{SCZ})

Using Polyphen2, this mutation is predicted to be
probably damaging, with a score of 0.982
(sensitivity: 0.75; specificity: 0.96)

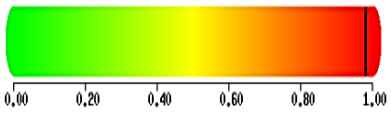

Mutation from intellectual disability patient
(knock-in) (Stg^{ID})

Using Polyphen2, this mutation is predicted to be
probably damaging, with a score of 0.967
(sensitivity: 0.77; specificity: 0.95)

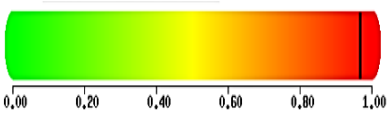

Fig. 6 - Prediction analysis of the impact on protein structure and function of the Stg^{ID} and Stg^{SCZ} variants of stargazin. Results kindly provided by Gladys Caldeira.

Previous *in vitro* data from our lab, showed that both mutations affect AMPAR trafficking, Stg^{ID} variant affects homeostatic plasticity (Fig. 7), whereas Stg^{SCZ} affects the number of inhibitory synapses and dendritic arborization of cortical neurons (Fig. 8).

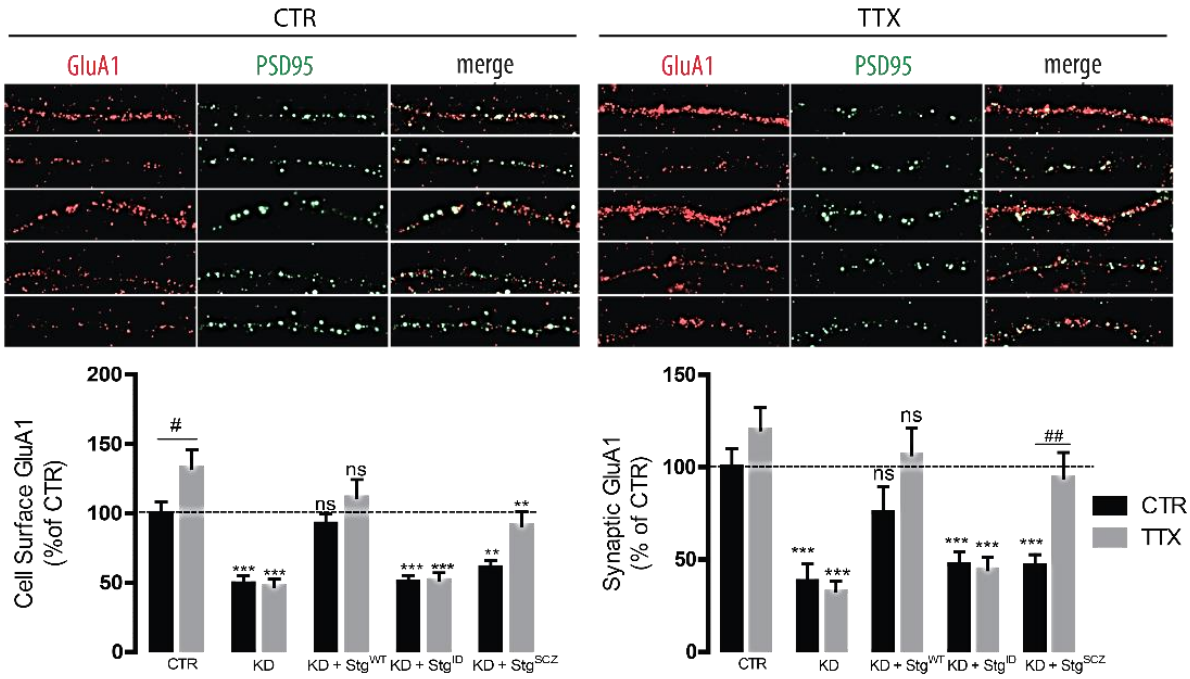

Fig. 7 - Quantification of surface GluA1 immunocytochemistry. Stg^{ID} and Stg^{SCZ} do not rescue the total levels of surface GluA1 or the levels of GluA1 puncta colocalizing with PSD95, after the knockdown of endogenous stargazin, even following TTX treatment. ***p <0,001; *p<0,05, significantly different from CTR; #p<0,05 significantly different from CTR equivalent condition, two-way ANOVA, Bonferroni test. Data presented as mean ± SEM. Kindly provided by Gladys Caldeira.

Interestingly, patients with both schizophrenia and ID seem to be more susceptible to both social and environmental stressors which, in some schizophrenia cases, might trigger disease onset (Beards et al., 2013; Corcoran et al., 2002, 2003). Studies show that in some psychiatric disorders, patients present synaptic disturbances, in fact, it has been previously suggested that the underlying cause for schizophrenia was an abnormal synaptic pruning, a theory that has not yet been discarded (Faludi and Mirnics, 2011).

Several reports suggested that alterations such abnormal dendritic spine density in the cortex and enlargement of ventricles could arise from abnormal synaptic pruning (Faludi and Mirnics, 2011). Furthermore, it was suggested that the decrease in the number of synapses or in the levels of presynaptic genes and proteins such as SNAP-25, synaptophysin, syntaxin-1 and SNARE complex formation could explain some neuroanatomical changes (Faludi and Mirnics, 2011). Besides the presynaptic site, the

postsynaptic region is also affected namely in the glutamate, monoamine and GABA systems. However these alterations seem to be related with functional and not anatomical deficits (Faludi and Mirnics, 2011).

Besides schizophrenia, ID also seems to be associated with mutations in synaptic proteins such as SynGAP, a Ras-GAP important for dendritic spine structure that also been shown to be mutated in ID cases. Besides SynGAP, OPHN1, a Rho-GAP that regulates AMPAR trafficking has also been implicated in ID. OPHN1 loss is known to impair both synapse and spine maturation (as reviewed in Volk et al., 2015).

As seen so far, these types of disorders are associated with disturbances within the synapse and problems regarding neuronal transmission, namely glutamate transmission. A better understanding of the reason behind such modifications and how they affect the entire system might help to comprehend some physiological, molecular and even behavioral aspects that affect these patients, whose treatment is presently insufficient. Concluding, a more profound study would help in the future to create new tools to treat the symptoms of these patients.

As mentioned before, Stg^{SCZ} variant affects dendritic arborization in cortical neurons. Accordingly, the knockdown of stargazin led to a modification in the dendritic arborization of cortical neurons that could be rescued by reintroducing wild-type stargazin or the ID-associated variant but not by the SCZ-associated variant (Fig. 8).

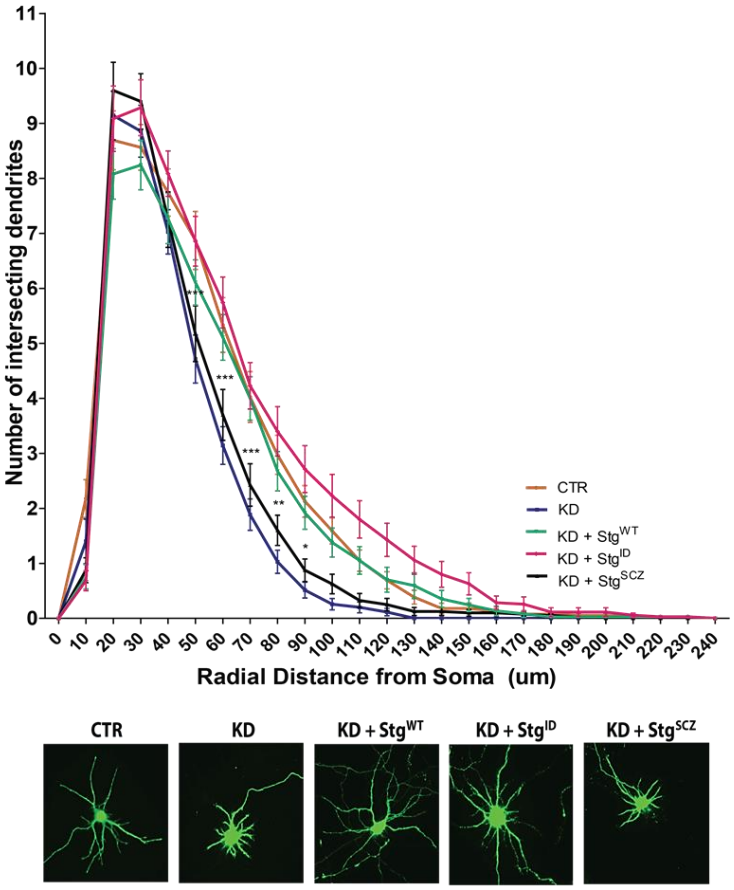

Fig. 8 – Sholl analysis of cortical neurons transfected with pLL-shRNA#4 and/or stargazin variants. Both the knockdown of stargazin and the Stg^{SCZ} point mutation cause shortening of the dendrites. Representative examples of GFP labelling in cortical neurons. ***p<0,001, *p<0,05, significantly different from CTR, one-way ANOVA, Bonferroni test. Data presented as mean ± SEM. Kindly provided by Gladys Caldeira.

It is not yet known how stargazin single point mutations impact dendritic arborization. More information about stargazin interactors and how these interactions could be affected by protein mutations could shed some light on the mechanisms taking place. Even though a better knowledge regarding stargazin interactors would be very important in order to understand how this is caused, it would be also necessary to study if such modifications are maintained in *in vivo* systems. Such assessment is fundamental to a more realistic approximation to what might happen in patients with these disorders.

Besides its role in dendritic arborization, it is possible that stargazin affects dendritic spines. Throughout this thesis we will explore this possibility. Thus, the next chapter will focus on proteins that are important regulators of dendritic spine structure and function as well as some cytoskeleton components that might be interacting with stargazin.

2. Cytoskeleton and dendritic spine structure

2.1. Dendritic spines and filopodia structure and function

Dendritic spines are highly dynamic specialized structures whose form varies across development. During development, there is a high dynamism in dendritic structures with constant appearance and elimination of spines and filopodia (Zuo et al., 2005). Indeed, some spines disappear within a short period of time after their appearance, whereas others remain within the branch for longer periods of time, remaining throughout life (Holtmaat et al., 2005; Zuo et al., 2005). During development, there is a trend to a decrease in spine elimination and, consequently, maintenance of spine number and distribution. Even though a high stability is observed in adulthood, this does not imply that spines cannot suffer alterations in synaptic strength, quite the opposite. This spine pruning might be experience-dependent as stated by Zuo and coworkers (2005), and this dynamism is possible due to several pathways and molecular components within the spine (Zuo et al., 2005).

Dendritic spines may be classified as thin, stubby, mushroom and cup-shaped (Harris et al., 1992; Hering and Sheng, 2001; Peters and Kaiserman-Abramof, 1970). Besides density and size, spines may also be variable in terms of PSD structure whose size is correlated to the number of AMPAR. AMPAR distribution is also highly correlated with spine morphology (Harris et al., 1992; Holtmaat et al., 2005; Matsuzaki et al., 2001; Peters and Kaiserman-Abramof, 1970).

Each spine is isolated from their homologous and from other cell components by a neck whose size and function has been implicated in plasticity in different periods throughout the development (Harris et al., 1992; Hering and Sheng, 2001). Because of this, the dendritic spines offer a specialized microenvironment able to receive inputs. These inputs are received by the receptors located at the membrane such as AMPAR and NMDAR, which activate several downstream pathways, leading to morphological and dendritic density modifications (as reviewed in Hering & Sheng 2001).

Besides spines, it is also possible to find protrusions called filopodia. Unlikely spines, filopodia are long and thin structures without a bulbous head, composed by

parallel actin fibers with the barbed end oriented to the membrane (Blanchoin et al., 2014; Zuo et al., 2005). Filopodia have been referred as precursors of dendritic spines and, in comparison to spines, have a smaller AMPAR content (as reviewed in Matsuzaki et al. 2001; Zuo et al. 2005). Moreover, filopodia are pointed out as environmental detectors, which might be important for cell migration, cell contacts, signal transmission and cell dynamics, all activities highly dependent on actin cytoskeleton (Blanchoin et al., 2014).

The conversion of filopodia into spines is dependent on myosin-II which acts as a depolymerizing agent in the branch, actin and N-cadherin. It is the balance of the forces from transynaptic N-cadherin between axons-dendrites (on the spines actin network) and the forces from myosin II that dictates the shape of the spine (Chazeau et al., 2015).

This transynaptic interaction of N-cadherins with actin filaments is vital to spine morphology and maturation since the disruption of such interaction leads to the appearance of a filopodia structure (Chazeau et al., 2015).

2.2. Molecular components involved in spine dynamics

Besides neurotrophins such as BDNF (Brain Derived Neurotrophic Factor), spine dynamics alterations rely on the interaction between actin networks and their correspondent regulators with components of the PSD, which act as an organizer center for actin nucleation, as shown in Fig. 9 (Alonso et al., 2004; Chazeau et al., 2014).

Within the PSD, it is possible to find Arp2/3 and WAVE complexes, whose regulatory complex besides controlling actin dynamics is also able to bind several partners. These partners have been associated to neuropsychiatric disorders such as schizophrenia. After reaching the PSD region by cytosolic diffusion, Arp2/3 is immobilized and activated by WAVE complexes promoting thereby, nucleation of F-actin and, consequently, formation of a new branch (Chazeau et al., 2014).

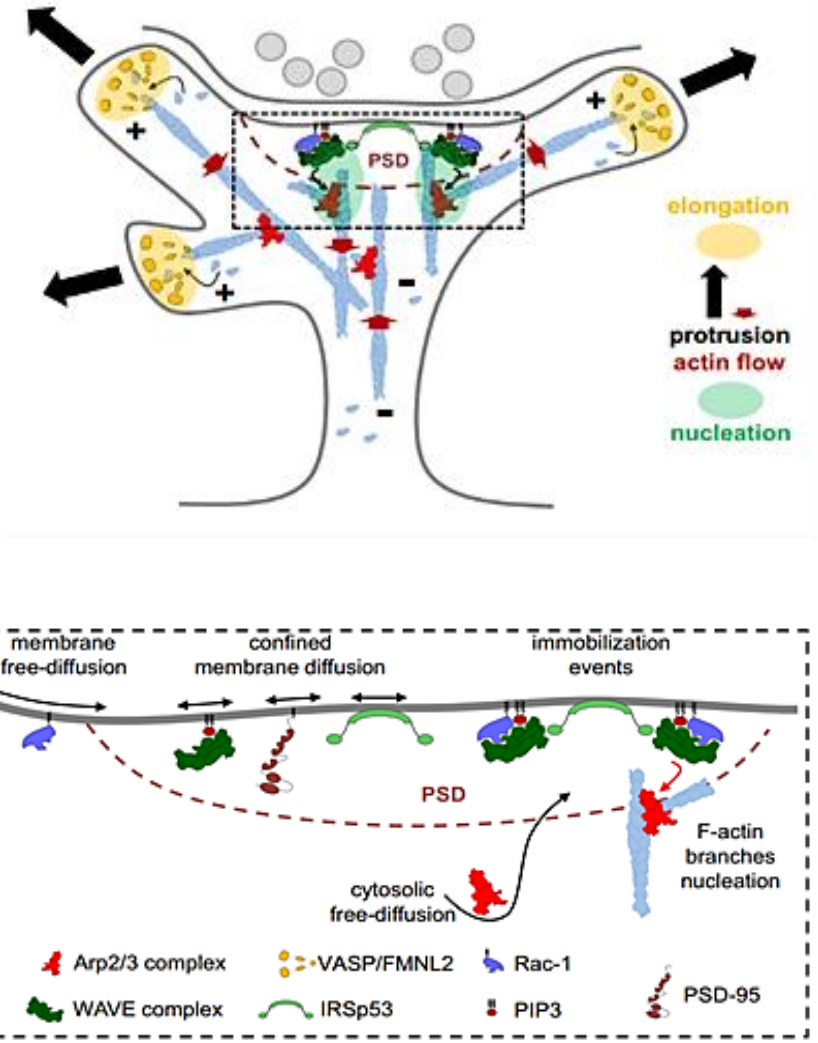

Fig. 9 - Dendritic structure and organization with magnification of the PSD region where several components such as Arp2/3, WAVE complex, Rac1, PSD-95 and IRSp53 co-localize and together dictate dendritic structure. Adapted from: (Chazeau et al., 2014).

In the organizer center, Shank3, a scaffolding protein, is also able to interact with Arp2/3 complex, forming complexes *in vivo,* regulating spine morphology and density (Durand et al., 2012; Han et al., 2013). Shank3 action as a scaffolding protein brings together several compounds, allowing formation of actin networks (Han et al., 2013).

Actin elongation on the other hand occurs in a distinct space from the nucleation step. Elongation occurs at protrusion tips and is induced by VASP and formins (Chazeau et al., 2014). Elongation, with the help of formins and profilin II, occurs at the barbed ends of F-actin (Ackermann and Matus, 2003; Kovar et al., 2006). mDia1, a formin, besides being involved in elongation can also be involved in actin retraction since they may engage in the formation of mechanical forces that lead to actin retraction (Jégou et al., 2013).

Besides these components, many others are involved in spine dynamics such as capping proteins and severing proteins such as ADF/cofilin (Saarikangas et al., 2010).

Besides these proteins that allow the constant growth and retraction of the cytoskeleton, others such as CaMKII are able to modulate and regulate the dendritic structure. CaMKII seems to interact with a scaffolding protein that co-localizes with PSD-95 at the PSD, called axin. Axin is involved in spine shaping, stability (since its downregulation decreases the number and dendrite length), maintenance and finally, complexity of the dendritic arborization. Axin, through a Rho-GTPase called Cdc42, is able to modulate cytoskeleton reorganization. In order to do so, axin acts as a scaffolding protein with CaMKII, given its ability to bind both α and β CaMKII subunits (Chen et al., 2015). Besides interacting with CaMKII, axin is also able to bind MAGI-2 also known as S-SCAM, an already known stargazin binding partner (Deng et al., 2006; Hirabayashi et al., 2004). However, much is still unknown about Axin-Cdc42 pathway regarding dendritic reorganization.

CaMKII β, a CaMKII subunit, has been reported to bind in a reversible manner to the postsynaptic membrane and F-actin, which allows CaMKII to localize in PSD, in a process dependent on calcium (Fink et al., 2003; Lin and Redmond, 2008; Okamoto et al., 2009, 2007; Shen and Meyer, 1999; Shen et al., 1998). CaMKII β binding to F-actin besides being reversible, is stronger when F-actin is more stable, which is vital not only for the dendritic structure maintenance in resting synapses, but also for microspikes formation (Lin and Redmond, 2008; Park et al., 2012; Shen et al., 1998). On the other hand, CaMKII α has also been associated with hippocampal dendritic spine morphology and particularly, on spine maturation (Park et al., 2012). After dissociation from F-actin, CaMKII translocates to PSD and binds components within this structure, in order to phosphorylate them (Shen and Meyer, 1999). When the neuron is stimulated, CaMKII in its autophosphorylated form acquires another function as a signal component, activating several pathways involving GTPases that are able to modulate actin due to glutamate receptor activation, returning afterwards to its structural role when the neuron activity returns to its basal levels (Okamoto et al., 2009, 2007).

Lastly, a protein whose action is dependent on cell activity and is able to bind polymerized actin is Arc (activity-regulated cytoskeleton-associated protein). The interaction between actin and Arc is believed to modify dendritic structures according to cell activity, influencing Hebbian and non-Hebbian synaptic plasticity (as reviewed in Guzowski et al. 2000; Zhang et al. 2015; Peebles et al. 2010). Arc is a postsynaptic protein that is associated with AMPAR traffic (namely its endocytosis) linking, consequently two types of plasticity, functional and structural. Arc is able to change dendritic structure, promoting increase of the proportion of thin spines (Peebles et al., 2010). Moreover, Arc is also able to bind CaMKII, which in turn is able to phosphorylate stargazin (as reviewed in Zhang et al. 2015; Opazo et al. 2010; Tomita, Stein, et al. 2005).

Modifications within spine structure (besides number and density) is closely related with activity within the cell since changes in cell activity will alter dendritic spine morphology and, in some cases, dendritic tree, as it is possible to understand in the next section.

2.3. Activity dependent regulation

Spines have been shown to alter their morphology, their number (through formation or elimination) according to the plasticity protocol applied, LTP or LTD (Sala and Segal, 2014).

LTP is able to induce spine formation with consequent synapse formation. However, it is still controversial the period of time that such formation lasts (Knott et al., 2006; Nägerl et al., 2007; Sala and Segal, 2014). Besides formation, this type of protocol is also able to change spine volume, increasing it in all types of spines, not just in small ones (Yang et al., 2008). These spine modifications are dependent on NMDAR for its initial expansion, GluA1 insertion for spine enlargement stabilization and kinases, for long lasting enlargement. Some pathways involved in the regulation of spine dynamics during LTP are shown in Fig. 10.

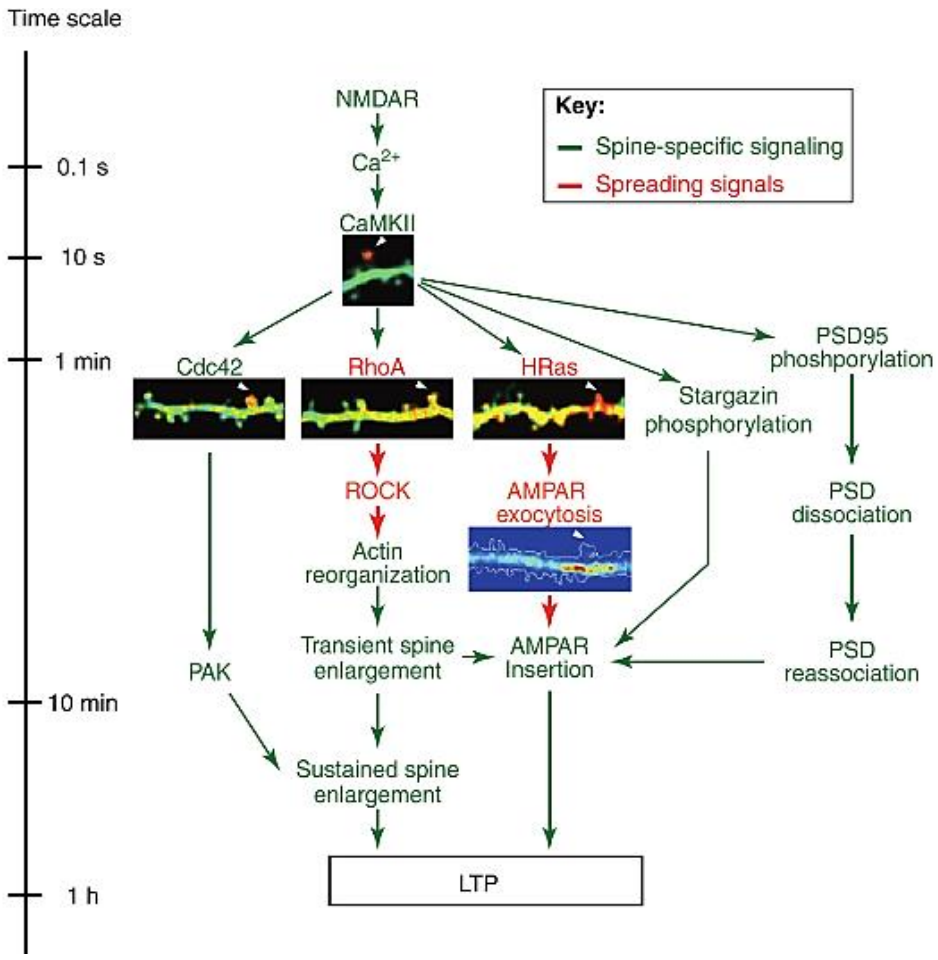

Fig. 10 - Molecular pathways involved in dendritic spine dynamics during LTP. Adapted from: (Murakoshi and Yasuda, 2012).

LTD on the other hand, is much less explored in comparison to LTP, sharing, however, the same types of controversies: some experiments points to a spine retraction whereas others state there is spine loss (Sala and Segal, 2014). As in LTP case, LTD was also reported to be dependent on NMDAR and has been reported to be mediated by type I metabotropic glutamate receptors (Nägerl et al., 2004). Indeed, activation of mGluA1/5 is responsible for long lasting shrinkage and spine loss induction in an independent manner of spine size, a phenomenon that requires protein synthesis, which is in contradiction on what was shown by Schubert and coworkers, where an activation of these receptors leads to an increase in spine length (Ramiro-Cortés and Israely, 2013; Schubert et al., 2006).

2.4. Dysregulation of Dendritic spine dynamics and morphology in neuropsychiatric/neurodevelopment disease

Several disorders, such as autism and schizophrenia seem to have several dendritic morphological modifications. Both autism, schizophrenia and ID disorder have been associated with point mutations in *SHANK3* gene located in the 22q13 chromosome region (Durand et al., 2012; Han et al., 2013). Shank3 was suggested to act as a scaffolding protein that brings together profilinI and II, Mena (that also interacts with profilinII), Arp2/3 complex, Cortactin and WASF1. So, it is proposed that alterations within Shank3 protein modifies spine dynamics leading, consequently, to a change in E/I balance which is in accordance with an increase of VGLUT1 marker and decrease of VGAT marker (Han et al., 2013).

Besides Shank3, another scaffolding protein has been related to deregulation of spine dynamics in schizophrenia: DISC1, which interacts with components involved in spine morphogenesis and spine morphology (Sala and Segal, 2014). In addition to Shank3 and DISC1, CDC42 signaling pathway has also been associated to schizophrenic patients within dorsolateral prefrontal cortex (DLPFC). It is proposed that alterations in these signaling pathways alter actin dynamics through cofilin which, in schizophrenic patients, will be inhibited, perturbing depolymerization of actin and, consequently, actin dynamics leading to a spine reduction (Datta et al., 2015).

Finally, MAP2, a microtubule interacting protein, has been recently associated with schizophrenia since it is significantly reduced in the auditory cortex of patient tissue samples. Furthermore, it was shown that MAP2 reduction was correlated with a decrease in spine number and density in a particular subset of schizophrenia patients (Shelton et al., 2015).

In ID disorder on the other hand, non-syndromic X-linked ID is associated with mutations in tetraspanin7, which is thought to be involved in formation of filopodia and dendritic spines (Abidi et al., 2002; Bassani et al., 2012).

As shown so far, many disorders show alterations in dendritic trees and synapses since many genes that confer susceptibility to the development of these disorders encode

for proteins involved in glutamatergic signaling, scaffolding proteins and proteins involved in the cytoskeleton regulation and modulation.

3. Stargazin and cytoskeleton protein interactions: a possible dendritic arborization regulation mechanism?

In the past years, the understanding regarding stargazin protein namely its structure, biological function and partners has been evolving. However, reports relating stargazin and cytoskeleton components are still very scarce.

The first report of an interaction between stargazin and a cytoskeleton member was in a study performed by Ives and colleagues (2014) where they described a direct interaction between stargazin and the microtubule-associated protein 1 light chain 2. Furthermore, in this work it is hypothesized that stargazin and LC2 might form a complex with GluA2 AMPAR subunit in two processes: trafficking to the plasma membrane and/or during its diffusion to the synapse site (Ives et al., 2004). LC1/2 are not the only components that are able to bind stargazin since Arc was also shown to associate with this TARP (Zhang et al., 2015).

Arc protein has been shown to be important for GluA1 downregulation during homeostatic plasticity. However, this downregulation is only possible due to the binding between Arc protein and stargazin since Arc does not bind directly to AMPAR (GluA1). Moreover, this interaction seems to be regulated by stargazin phosphorylation (Zhang et al., 2015).

Another interesting stargazin partners is MAGI-2 which has been shown to interact with axin, a compound involved in the cytoskeleton dynamics (Deng et al., 2006).

To summarize, several hypotheses have been related to the development of these disorder and many have been the methodologies applied in order to study them. However, several of these studies lack *in vivo* confirmations. Besides this, technical problems also prevent the manipulation and study of the fragile neuronal structures with high resolution, low scattering, low quenching without damaging the cells. Although until recently these setbacks have been circumvented by several methods, now it is possible to analyze the entire brain without the need of sectioning it, which allows the gathering of

more realistic information since the neurons are 3D structures that may spread across many layers of the brain and sectioning it might lead to loss of information. Now it is possible to do such type of analysis through the use of a new set of methodologies such as clearing methods.

4. New methods to image the brain

Until now, several have been the studies using thin tissue sections since it is easier to observe and to gather information about cellular components in two-dimensional sections in comparison to thicker tissues. However, now it is becoming relevant to understand cellular structures in 3D, which requires the use and handling of thicker samples. One of the science fields that take advantage on the study of 3D structure is Neuroscience since neurons extend in many directions, crossing many brain layers and thinner sections may lead to loss of information. For some time, it was possible to obtain 3D information by reconstructing it through the use of a serial of thin sections which, unfortunately, leads to distortion of individual sections leading to an unsatisfactory reconstruction. Another way to obtain 3D information was to image the surface of a block of tissue and sequentially shaving its surface but this is an irreversible method. Moreover, thicker samples such as the whole brain present a milky and opaque appearance which prevents the imaging of inner regions. This occurs due to light scattering, a phenomenon that occurs when light is deviated, which is a big impediment to a proper and high quality imaging acquisition in thicker volumes (Richardson and Lichtman, 2015). Nevertheless, light scattering problems can be overcome through the use of clearing methods which renders the tissue a transparent appearance, decreasing light scattering and, consequently, allowing the imaging acquisition at higher depths. Even though there is still much to do, there are now several available protocols to study, in a more detailed way, several organs, including the brain. Some of the most known approaches are solvent based, aqueous and finally hydrogel embedding methods. All the advantages and disadvantages regarding all different techniques mentioned can be found in table 1 and table 2, respectively.

4.1. Solvent based clearing

In a general way, this type of methodology renders the brain a transparent appearance through the matching of the refractory indexes between different tissue layers of a thicker sample (Ertürk et al., 2012). This process dissolves lipids and dehydrates the samples, followed by elimination of these compounds and refractive index matching (Marx, 2016). Within this set of clearing methods it is possible to find protocols that use organic solvents such as 3DISCO or iDISCO, a 3DISCO upgrade (Renier et al., 2014; Richardson and Lichtman, 2015). These organic solvents are not as popular as the aqueous-based ones since the previous ones cause degradation of protein fluorescence, due to water removal from the sample during the procedure, tissue shrinkage and, unfortunately, are not applicable for the entire brain (Kim et al., 2013; Richardson and Lichtman, 2015). Taking into account these limitations other methods were developed (Hama et al., 2011).

4.2. Aqueous clearing methods

As aforementioned, aqueous clearing methods arose from the need to overcome the disadvantages presented by organic solvent based methods such as fluorescence quenching and morphological changes. This type of clearing methods may use different approaches to minimize light scattering due to refractive index reduction by sample lipid removal (such as Sca*l*e and CUBIC) or by simple immersion on clearing solution (such as FocusClear, SeeDB, TDE, Clear^{T}) whose refractive index reveals to be similar to the tissue (Richardson and Lichtman, 2015).

Simple immersion methods involve the use of sucrose, fructose and TDE. Biological samples are placed in these aqueous solutions which promotes its gradual clearing due to the presence of molecules with an elevated refractive index (Hama et al., 2011; Richardson and Lichtman, 2015).

Sca*l*e technique is a clearing method based on lipid removal followed by hyperhydratation, mediated by urea in the presence of glycerol. This maintains the internal water so it won't affect protein fluorescence. However, Sca*l*e method was shown to cause protein fluorescence degradation and protein denaturation because of the

presence of urea (Kuwajima et al., 2013; Yang et al., 2014). Moreover, samples treated with Sca*l*eA2 become soft, fragile and even showed tissue expansion even though its proportions and shape remain the same (Hama et al., 2011). However, the problems regarding tissue expansion and sample fragility are possible be circumvented through modification in urea and glycerol content, which led to the development of a longer procedure called Sca*l*eU2. According to the same group that developed Sca*l*eA2, the long incubation periods that characterize Sca*l*eU2 can, in turn, be overcome by the use of another reagent: Sca*l*eB4. Sca*l*eB4 reagent has a higher urea concentration, 8M, in comparison to Sca*l*eU2 with 4M (Hama et al., 2011). Another improvement made on Sca*l*e method involves the addition of sorbitol, a hydrophilic sugar alcohol, to the Sca*l*e reagent making the sample to return to its original size since this compound causes dehydratation. This new method is called Sca*l*eS. This method involves the application of a sequential set of reagents called S0, S1, S2, S3, desca*l*ing solution and finally S4, with an overall lower incubation period comparing to Sca*l*eA2 protocol (Hama et al., 2015).

Nevertheless, in comparison to some of the clearing processes, Sca*l*eA2 unveiled a very desirable quality: it is reversible and compatible not only with immunohistochemistry but also with tomography after tissue return to its original state. Another advantage of Sca*l*eA2 and Sca*l*eS is the fact that the economic burden is small and the reagent content can be modified and optimized according to the users intents (Hama et al., 2011).

Clear^{T} is another aqueous clearing method that uses the same principle as Sca*l*eA2. Clear^{T} uses formamide instead of urea. Formamide is responsible for clearing biological samples, through a hyperhydratation of the sample. Clear^{T} however is not compatible with immunohistochemistry labeling even though it was shown to be compatible with lipophilic dyes such as DiI staining. Taking into account the Clear^{T} incompatibility with immunohistochemistry labeling lead, consequently, to the development of Clear^{T2} protocol. (Kuwajima et al., 2013). Clear^{T2} is a method based on the previous clearing procedure and uses polyethylene glycol (PEG) which is able to stabilize protein conformation (Kuwajima et al., 2013).

SeeDB contains fructose and α-thioglycerol, to avoid browning and autofluorescence accumulation, as a result of high temperatures and high incubation periods with fructose, accordingly to the Maillard reaction (Ke et al., 2013).

Besides Clear^{T}, Clear^{T2} and SeeDB, CUBIC is another simple clearing method that involves the employment of several immersion steps followed by its corresponding washing step using, for that end, different set of reagents that use chemical mixtures containing aminoalcohols (Susaki et al., 2014).

4.3. Hydrogel embedding methods

The previous methods unfortunately reveal themselves to be quite limiting in several aspects, reason why methods such as CLARITY, PARS and PACT were developed. These methods use in a very general way, a hydrogel embedding step followed by lipid removal with consequent tissue immersion on immersion solutions.

CLARITY is based on the substitution of the lipidic portion of the brain by a porous (yet firm) supportive infrastructure hydrogel-based. This substitution is achieved by a cold infusion of small organic hydrogel monomers, crosslinkers (such as formaldehyde) and compounds that initiate polymerization when the temperature increases. After this infusion, the system is heated up to 37°C in order to induce polymerization of the hydrogel monomers within the brain. As a result, a hydrogel mesh is formed, linking existing cellular compounds, such as nucleic acids, proteins and neurotransmitters, with the exception being the phospholipids from the membrane, which lack the reactive group. After this step, lipids may be removed in two different manners: eletrophoretically, with the help of ionic detergents, or passively (Chung and Deisseroth, 2013; Chung et al., 2013; Tomer et al., 2014). The lipid removal is the crucial concept in this methodology since these compounds prevent antibodies access and provokes light scattering (Chung et al., 2013; Kim et al., 2013).

Having CLARITY as basis, PACT (*pa*ssive *c*larity *t*echnique) and PARS (*p*erfusion-assisted *a*gent *r*elease) methods were developed. In PACT, the clearing reagents are delivery intracraniously whereas in PARS it is made through the vasculature, *in situ*. PARS, however is only applicable to fixed brains and requires that clearing step to be done *in*

situ. Both methods, involve a crosslinkage and hybridization step at hydrogel monomers in order to stabilize macromolecules, followed by lipid removal from the tissue-hydrogel matrix formed previously. Lastly, the tissue is embedded in RIMS (*r*efractive *i*ndex *m*atching *s*olution) for long-term storage or to image (Yang et al., 2014).

Table 1 - Advantages of several clearing methods: SeeDB, PARS, PACT and CLARITY. Chung *et al.,* 2013 a) and b); Ertürk *et al.,* 2012; Hama *et al.,* 2011; Ke *et al.,* 2013; Kim *et al.,* 2013; Kuwajima *et al.,* 2013; Reiner *et al.,* 2014; Tomer *et al.,*2014; Yang *et al.,* 2014; Zheng & Rinaman, 2015; Susaki e*t al.,* 2014; Tainaka *et al.,* 2014.

Approach	Advantages															
	High range of tissue applicability	No alterations/deformations	Reversibility of the procedure	Tissue preservation	Compatible with lipophilic dyes	Low light scattering	No induction fragility in samples	No volume alterations	Returns to normal volume	Suitable to endogenous fluorescent reporters	Imunohistochemistry and labeling	Fast/ Easy	Economic	No quenching	Possibility of applying passive method	Multiple rounds of molecular interrogation
SeeDB		•	•	•	•		•	•			•	• (both)				
Sca*l*e	•		•	Not specified		•			(only after reversiblity of procedure)	•	•	•	•		•	
Clear^{T}	•	•		•	•	•	Not specified	•				• (faster than Sca*l*eA2)				
Clear^{T2}	•	•		Not specified	•	(more scattering than the previous)	Not specified	•		•	•	•	•	•		
DISCO3	•					•		•			•	•				
iDISCO	•			•					•	•	•	•	•	•		•
CUBIC	•	•		Not specified		•	Not specified	Not specified	Not specified	•	•	• (than Sca*l*e)	•	•		Not specified
PARS		•										•		•		
PACT	•	•				•			•	•	•	•	•	•	•	
CLARITY 2014	•	Not specified		•	Not specified	•			•	•	•	• (fast - eletrophoretic)		•	•	•
CLARITY 2015	•	Not specified		•		•	•		•	Not specified	•	• (easier; slightly faster	• (more than 2014)	•	•	•

Table 2 Disadvantages of several clearing methods: SeeDB, PARS, PACT and CLARITY. Chung *et al.,* 2013 a) and b); Ertürk *et al.,* 2012; Hama *et al.,* 2011; Ke *et al.,* 2013; Kim *et al.,* 2013; Kuwajima *et al.,* 2013; Reiner *et al.,* 2014; Tomer *et al.,*2014; Yang *et al.,* 2014; Zheng & Rinaman, 2015; Susaki e*t al.,* 2014; Tainaka *et al.,* 2014.

Approach	Disadvantages							
	Requires fixation step	Expansion/contraction	Not appropriated for big volumes or adult brain mice	Low image resolution and brightness	Quenching of fluorescence proteins	Requiers specific devices	Slow Expensive Complicated	Destruction in some steps
SeeDB	•		•	•	•	• (objectives)		
Scale	•	•			•		• (slow for Sca*l*eU)	• (protein loss & denaturation)
Clear^{T}	•	•			•			
Clear^{T2}		•						
DISCO3	•				•			• (clearing agents dehydrate tissues and dissolve lipids)
iDISCO	•	•					• (if reduced antibody bioavailaty)	
CUBIC	•	Not specified					• (slower than CLARITY)	
PARS		•						
PACT		•						
CLARITY 2014		•				• (ETC, objectives)	•	• (ETC)
CLARITY 2015		•				• (objectives)		

5. Objectives

Stargazin is a 37-kDa protein that belongs to a class of proteins called TARPs. This protein can be found at the glutamatergic synapses and is involved in the AMPAR biosynthetic pathway, clustering and trafficking. Besides this, stargazin has also been implicated in mechanisms of synaptic plasticity such as LTP and LTD, which have been associated with memory. Moreover, stargazin has been shown to be relevant for homeostatic plasticity, which might be affected in psychiatric disorders. In psychiatric and neurodevelopment disorders such as schizophrenia and ID, as already mentioned before, it was shown that stargazin might influence the organization of the dendritic arborization and the number of synapses (unpublished data from our Lab) (Hamdan et al., 2011). Taking this into consideration, the main objective of this work is to understand if stargazin influences spine morphology in the hippocampus, which has never been addressed. In order to achieve this goal, the project was divided in several tasks:

Task 1. To test whether stargazin affects spine morphology, stargazin expression was silenced in neurons in hippocampal organotypic slice cultures. Effects on spine morphology were determined by analyzing the density of the different spine categories in control neurons and in neurons lacking stargazin.

Task 2. In order to evaluate the role of stargazin in determining spine morphology and dynamics *in vivo*, we aim to silence stargazin expression in different brain regions, through stereotaxic injection of lentivirus expressing interference RNA to silence stargazin expression. These viruses are already available in our laboratory. Nevertheless, to test for the ability of disease-associated variants of stargazin to perform stargazin's role in modulating spine morphology, we aim to introduce either wild-type stargazin or disease-associated mutant forms of stargazin in neurons where endogenous stargazin is deleted. Therefore, we generated and characterized lentiviral vectors expressing mCherry and wild-type stargazin or disease-associated variants of stargazin (Fig. 11). The main objective of this task was to produce the lentiviral vectors that will be used in the future to produce lentivirus and address the function of disease related mutants of stargazin in modulating spines.

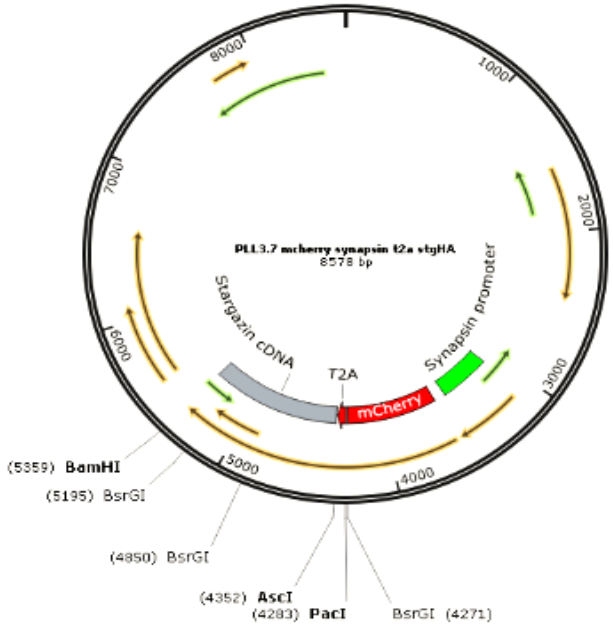

Fig. 11 - pLentilox mCherry-T2A-stargazinHA final vector.

Task 3. Optimization and implementation of Sca*l*e method, a tissue clearing protocol (Hama et al., 2011, 2015). Optical clearing of biological tissues has revealed an immense and extraordinary importance, particularly in neuroscience. The implementation of these type of methodologies, such as Sca*l*eA2 and Sca*l*eS allows a better and more realistic understanding of how the brain might be affected in health or disease context, since it allows a deeper neuronal structure imaging without the need of brain sectioning. In this task, we performed a qualitative evaluation of different versions of these techniques in order to optimize the method for future applications. In the future, one of our goals is to apply these set of techniques to brain samples of animals infected with the mutants described in task 2 and analyze spine morphology and dendritic arborization not only in the hippocampus but also in other brain regions, namely the cortex.

Chapter II

Materials and Experimental Procedures

1. DNA constructs

Sh4 and sh6 DNA constructs used in this work were previously generated in our Lab (Louros et al., 2014). For the generation of the stargazin short-interfering RNA construct, sh4, the DNA oligonucleotides presented below were annealed and subcloned into the XhoI and HpaI sites of the pll3.7 vector:

5'-TGAAGAACGAGGAAGTTATGTTCAAGAGACATAACTTCCTCGTTCTTCTTTTTT-3' and

5'-ACCTTCAATACTGGGTAAGGAAGTTCTCTCCTTACCCAGTATTGAAGGAAAAAA-3'

On the other hand, stargazin wildtype plasmid with an HA tag, was a kind gift from Dr. Daniel Choquet (Institute for Interdisciplinary Neuroscience, Bordeaux, France). This plasmid was used to produce a WT stargazin Sh resistant plasmid. The modified nucleotides were the following:

5'-GCGAGCAAAAAGAATGAGGAAGTCATGACCCATTC-3' primer

After producing WT resistant plasmid, this plasmid served as a base to introduce site directed point mutations in cDNA with the objective of producing the ID and SCZ constructs. The V143L (ID) and S148N (SCZ) single point mutations introduced, by site directed-mutagenesis were, respectively:

5'-GCCGGCATCTTCTTCCTGTCTGCAGGTCTGAG-3' and

5'-CGTGTCTGCAGGTCTGAATAACATCATTGGCATCA-3'

All the sequencing analysis done in this work were performed by Stabvida through Sanger sequencing.

2. Task 1: Hippocampal organotypic cultures

Organotypic hippocampal slices were obtained from 6 day old Wistar rat pup (P6) as previously described (Stoppini et al., 1991). Briefly, the brain was removed and placed in ice cold gassed (5% CO_2) dissection solution (10 mM glucose, 4 mM KCl, 24 mM $NaHCO_3$, 234 mM sucrose, 0.5 mM $MgCl_2$, 0.7 mM $CaCl_2 \cdot 2H_2O$, 0.03 mM phenol red, at pH 7.4) under the flow chamber. The hippocampus from each hemisphere was isolated from the rest of the brain and 300 µm thick hippocampal slices were cut using an automatic shopper (McIalwain tissue shopper). Hippocampus slices were then transferred to a new dissection medium plate and selected under a stereomicroscope (Carl Zeiss Stemi™ DV4), according to their structural quality, placed on a culture membrane, Millicell culture plate inserts (Merck Millipore), and incubated at 35°C, 5% CO_2. The culture medium used is composed by: Minimum Essential Media (MEM; GIBCO, Invitrogen) supplemented with 20% (v/v) horse serum (GIBCO, Invitrogen), 1 mM glutamine Sigma-Aldrich, 1 mM $CaCl_2$, 2mM $MgSO_4$, 1 mg/l insulin, 0.0012% (w/v) ascorbic acid, 30 mM HEPES, 13 mM glucose, 5.2 mM $NaHCO_3$ (Sigma-Aldrich), at pH 7.25, and final osmolarity of 320 mOsm/l.

This medium was supplemented with 0,01% (v/v) of the antibiotics penicillin and streptomycin (GIBCO), in order to avoid contaminations, during the first 2 days following dissection. The culture medium was changed every 2-3 days.

For the biolistic transfection the bullets were prepared as previously described (Woods and Zito, 2008) and a total of 45-48 µg of DNA was used. In order to produce the bullets, 100 µl of 50mM of spermidine were added to 8-10 mg of gold particles with 1 µm diameter. The gold particles and spermidine were vortexed and sonicated. To this solution, cDNA of interest was added and the sample was vortexed and briefly sonicated. Afterwards, 100 µl of 1 M $CaCl_2$ was added dropwise while vortexing and the solution was sonicated briefly and it was allowed to precipitate for 10 min at RT. After the 10 min, the solution was centrifuged at 13000 rpm for 2 min and the supernatant carefully discarded. The sample was washed with 1 mL of absolute ethanol and briefly sonicated. This process was repeated 3 times. Following these washes, 1 mL of absolute ethanol (followed by a briefly sonication) and 8 µl of PVP (20 mg/mL) were added. The mix was vortexed and transferred to a 15 mL falcon tube containing 2 mL of absolute ethanol and was vortexed

vigorously before transferring it to the Tefzel tubing (BioRad), that was previously exposed to N_2 gas with 0.4 liters per minute (LPM). After transferring the solution to the Tefzel, with a 10 mL syringe, the gold particles were allowed to settle for 20 min. After this period of time, the solution was slowly pulled by a 10 mL syringe and the Tefzel tube was placed in the tubing station with N_2 gas, with LPM of 0.4, for 30 min. Finally, the Tefzel tube was removed from the station and cutted in small pieces. These bullets were maintained at 4°C until use. Biolistic transfection was performed using a gene gun apparatus (Biorad) as previously described (Woods and Zito, 2008). For each condition, we used different sterilized nets/holders. We performed a second shooting two hours after the first shooting in order to increase the transfection rate.

2.1. Dendritic spine morphology acquisition and analysis through the use of NeuronStudio software

2.1.1. Laser-scanning confocal microscopy & image acquisition

Dendritic spines of hippocampal neurons were imaged on a LSM710 confocal microscope (Carl Zeiss, Germany) using a Plan-Apochromat 63x/1.40 objective with a zoom factor of two, and a DPSS 561 nm laser line for mCherry excitation.

The acquisition was made on ACSF solution (127 mM $CaCl_2$, 2.5 mM KCL, 25 mM $NaHCO_3$, 1.25 mM NaH_2PO_4, 25 mM Glucose, 300-320 mOsm) supplemented with 4 mM $CaCl_2$, 4 mM $MgCl_2$ and 1 µM of TTX added before imaging. Per condition, it was acquired 1-3 neurons, 3 apical and 3 basal dendrites per neuron in each independent experiment and no distinction was made between secondary and tertiary dendrites. Prior to acquisition, neurons were confirmed to be transfected with both GFP (which means that the neurons were transfected with sh6 or sh4 plasmid construct) and mCherry, as shown in Fig. 12.

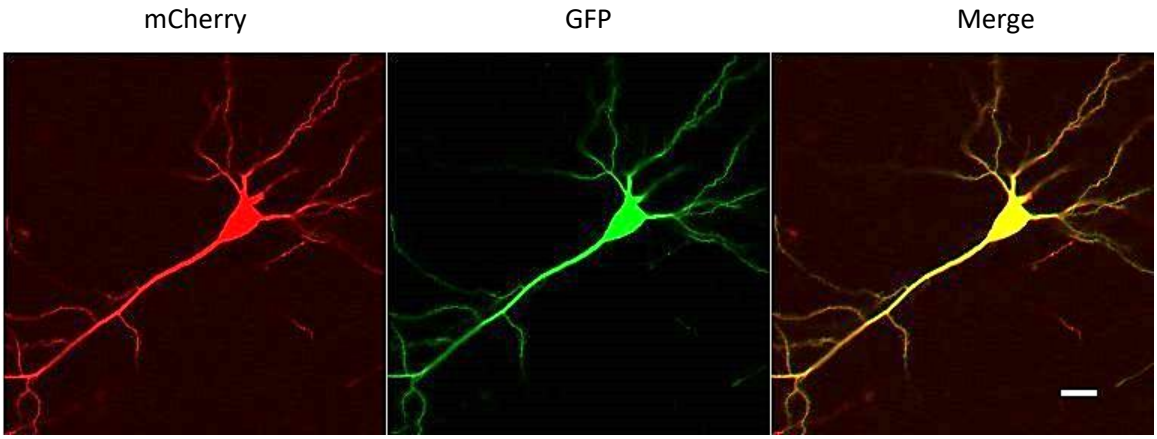

Fig. 12 - Confocal image of a hippocampal neuron double transfected with mCherry (red) and sh6/GFP (green), in a proportion of 1:1, Scale bar: 20 µm.

2.1.2. Image deconvolution

Before quantification of spine morphology, all images were deconvolved using Huygens Essential software. The deconvolution process takes into consideration parameters of the microscope and the immersion media used in order to find and remove noise due to out-of-focus light, using for that end a mathematical algorithm. Each section is then deblur due to this mathematical algorithm that considers the image as result from the sum between out of focus and in focus signal from near sections (Swedlow, 2013). The settings used for deconvolution were: number of interactions, signal to noise ratio, quality threshold and an optimized interaction mode.

2.1.3. Semi-automatic quantification of spine morphology using NeuronStudio software

NeuronStudio is program that besides reconstructing neuronal structures also allows manual and automatic spine detection and classification (Shi et al., 2014; Wearne et al., 2005). This software can be acquired for free online (http://research.mssm.edu/cnic/tools-ns.html).

To quantify spine morphology in the different conditions, we decided to train the program according to our criteria, in order to recognize different type of spines, namely:

thin, filopodia, stubby and mushroom. This training was made using different images for different conditions (sh6 and sh4) in order to give the program the characteristics of different spine morphologies to facilitate automatic spine type detection. For this, firstly dendrites were recognized automatically followed by automatic spine detection and spine building. After the spine recognition, several examples of spines were added to each category, as shown in Fig. 13, according to the following criteria (Vanderklish and Edelman, 2002):

1. Thin: elongated spine necks with small heads;
2. Filopodia: long filamentous protrusions that lacked a discernible spine head;
3. Stubby: lacked a large spine head, and did not appear to have a neck;
4. Mushroom: short neck and large spine head.

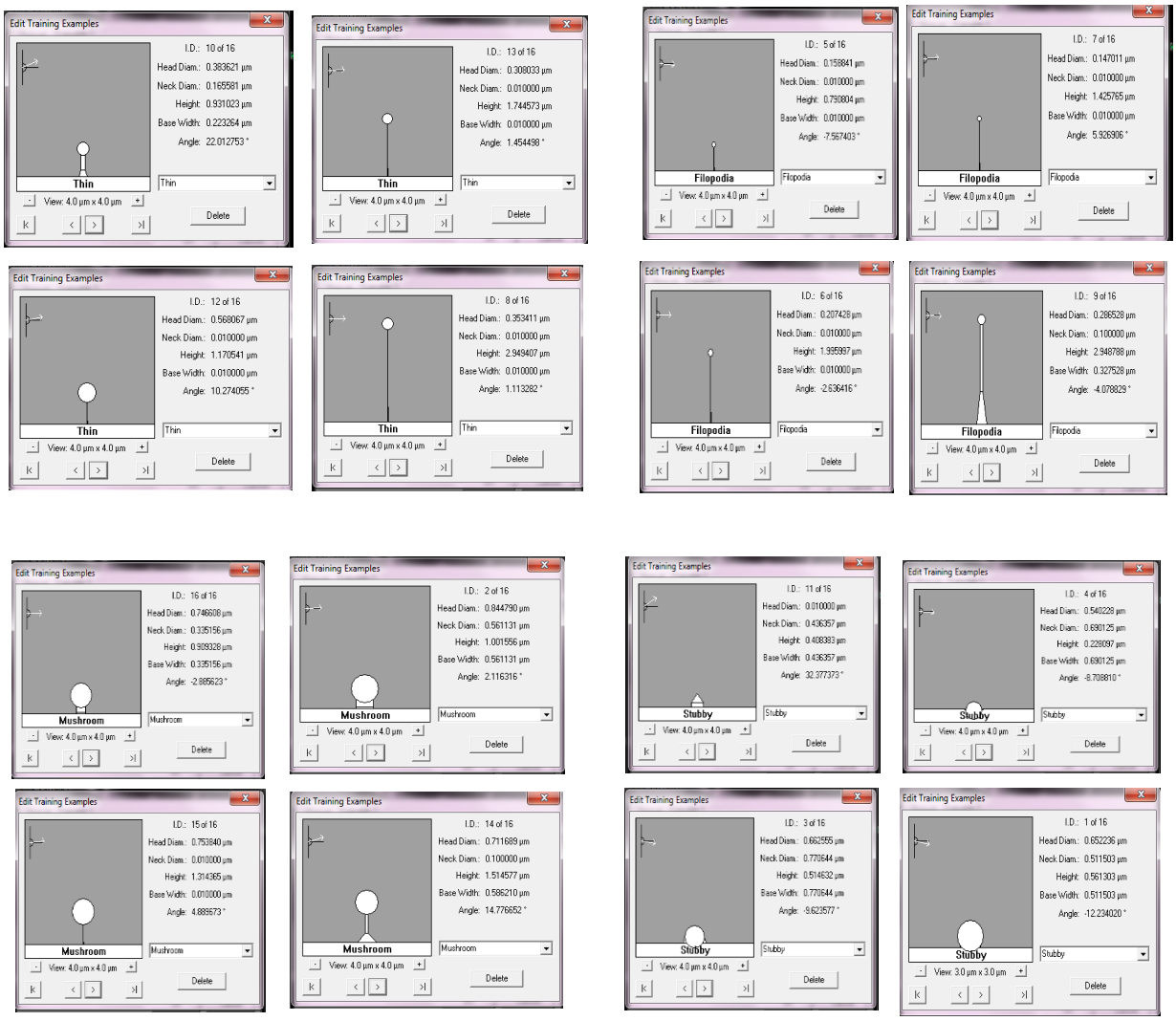

Fig. 13 – Representative training examples and their representative numerical parameters used by NeuronStudio software during classification for the several types of dendritic spines: thin, filopodia, mushroom and stubby.

After this, the best four examples of each spine type were selected and maintained for semi-automatic spine classification with a total of 16 spine examples, according to the parameters of spine head diameter and spine length shown in table 3.

Table 3 - Representative measurements of spine head diameter and spine length for different types of spines used for classification on NeuronStudio.

Type of spine	Spine head diameter	Spine Length
Thin	0.3-0.56 µm	0.9-3 µm
Filopodia	≤ 0.3 µm	0.79-3 µm
Stubby	0.01-0.66 µm	0.22-0.56 µm
Mushroom	≥ 0.7 µm	0.9-1.5 µm

3. Task two: Generation and characterization of a lentiviral vector expressing mCherry and wild-type and disease-associated variants of stargazin

3.1. Cloning

In order to perform the amplification of the desired sequence, the T2A segment which is a self-cleaving peptide that causes the ribosome to skip the formation of a peptide bound during protein translation producing two independent proteins, was amplified. The lyophilized forward and reverse primers used (table 4, Integrated DNA technologies) were rehydrated to a final concentration of 10 pmol/µl.

Table 4 - Primer sequences used.

Type of primer	Amplification target	Primer sequence
Forward sequence	T2A	5'- GCTGTACAAGTTAATTAAAGGTAGTGGAGAGGGCAGAGG-3'
Reverse sequence	T2A	5'-GCGGCGCGCCTGGGCCAGGATTCTCCTCGACG-3'
Forward sequence	Stargazin	5'-GCGGCGCGCCGATGGGGCTGTTTGATCGAGGTG-3'
Reverse sequence	Stargazin	5'-GCGGATCCTTATACGGGGGTGGTCCGGC-3'

The PCR amplification reaction contained 0,2 mM dNTPs (deoxynucleotides), 0,4 mM of 1X PrimeSTAR Buffer, 10 pmol of forward and 10 pmol of reverse primers, 100 ng of T2A DNA template, 1,25 Units/µl of Taq-polymerase enzyme (Takara) and miliQ H_2O to a final volume of 50 µl. The PCR cycle involved a first step at 98°C for 30 s, 98°C for 10 s to break the hydrogen bounds between dsDNA producing single strand bands followed by

62°C for 10 s, to allow base pairing between the referred primers and their complementary sequences on the template strands, and finally 72°C for 1 min, to replicate the single stranded DNA segments of interest. This cycle was repeated for 29 times followed by 5min at 72°C. The samples were frozen at -20°C until electrophoretic analysis.

After the PCR, 5 µl of the sample were loaded with 1x DNA loading buffer in a 3% agarose gel (NZYTech), with ethidium bromide in a TAE 1x bath at 100 Volts.

For the stargazin PCR, the solution mix was prepared with 0,2 mM dNTPs (deoxynucleotides), 0,4 mM of 1X PrimeSTAR Buffer, 10 pmol of forward and 10 pmol of reverse primers, and 100 ng of one of following DNA templates: WT stargazin or Intellectual disability mutant stargazin (ID), Schizophrenia mutant stargazin (SCZ), 1,25 Units/ µl of Takara and miliQ H_2O to adjust to 50 µl of solution. The PCR cycle involved a first step at 98°C for 30 s, 98°C for 10 s, 62°C for 0.5 s and finally 72°C for 2 min. This cycle was repeated for 29 times followed by 5 min at 72°C. The samples were frozen at -20°C until electrophoretic analyses.

After the PCR, 5 µl of the sample were loaded with 1x DNA loading buffer in a 1% agarose gel, with ethidium bromide in a TAE 1x bath at 100 Volts.

T2A and stargazin PCR products were purified using the Machery-Nagel NucleoSpin Gel and PCR clean-up kit. The total volume of PCR samples was loaded in the appropriate agarose gel (T2A in the 3% gel agarose and stargazin in the 1% gel agarose). Samples with the appropriate size were removed from the gel, and purified separately. After purification, the samples were placed separately (5 µl of the sample jointly with 2 µl of the buffer), in the appropriate agarose gel in order to verify if the purification was successful.

Purified DNA fragments were digested with restriction enzymes in order to produce cohesive extremities, which was vital for the following ligation step and to produce the final vector. Stargazin was digested with BamHI and AscI whereas T2A digestion was performed with AscI and BsrGI. The mCherry vector or the welcoming vector that is going to receive the T2A and stargazin DNA template, was also digested in

order to insert both of the referred sequences in its structure. The vector was digested with BamHI and BsrGI.

3.2. Bacterial transformation and Plasmid DNA purification (mini and maxipreps)

The ligation products were transformed into DH5α *E.coli* strain. To this end, the DNA was incubated with the bacteria for 30 min on ice, and in order to induce the heat shock, the mix was incubated at 42°C for 45s. The bacteria were allowed to recover for 1 hr in 900 µl of LB at 37°C. Afterwards, the bacteria were centrifuged at 3000 rpm during 1 min. After centrifugation, the supernatant is discarded and the cells are ressuspended in the remaining liquid. The bacteria were then plated in LB agar plates with the respective antibiotic (carbenicillin, with a final concentration of 100 µg/ml) and grown overnight (12-16 hrs) at 37°C. Plasmid DNA purification was performed accordingly to the manufacture instructions (Miniprep kit, NZYtech).

The following transformations were done in stable3 *E. coli* strain and it was used a short transformation protocol. For the short transformations protocol, the DNA was added to the cells followed by incubation on ice for a period of 30 min. After this, the bacteria were incubated at 42°C for 45 seconds, followed by a recovery period on ice during 2 min. Finally, the cells were plated in LB agar plates with the respective antibiotic (100 µg/ml) and grown overnight (12-16 hrs) at 37°C. The DNA was purified usingPureLink HiPure Plasmid Filter Maxiprep Kit, according to the manufacture indications (Invitrogen™-Life Technologies).

LB agar plates (powder, NZYtech) were produced according to the manufacture indications.

3.3. Cell cultures

Primary cultures of rat cortical neurons were prepared from dissected cortices of E18 Wistar rat embryos, after treatment with 0.06% trypsin for 15 min at 37 °C (GIBCO Invitrogen), in Ca^{2+} and Mg^{2+}-free Hank's balanced salt solution (HBSS: 5.36 mM KCl, 0.44 mM KH_2PO_4, 137 mM NaCl, 4.16 mM $NaHCO_3$, 0.34 mM $Na_2HPO_4.2H_2O$, 5 mM glucose, 1 mM sodium pyruvate, 10 mM HEPES and 0.001% phenol red). Low density cortical cells were plated in 60 mm culture dishes in neuronal plating medium at a final density of 3 x 10^5 cells/dish on poly-D-lysine-coated coverslips. After 2 to 3 h, the coverslips were flipped over an astroglial feeder layer. These neurons grew face down over the feeder layer but were kept separate from the glia by wax dots on the neuronal side of the coverslips. To prevent the overgrowth of the glial cells, neuron cultures were treated with 5 µM cytosine arabinoside after 2 days *in vitro* (DIV). Cultures were fed twice a week and maintained in Neurobasal medium supplemented with SM1, in a humidified incubator with 5% CO_2/95% air, at 37°C.

3.4. Transfection of primary neuronal culture by calcium phosphate co-precipitation

Vector expressing mCherry and wild-type or disease-associated variants of stargazin were expressed in primary neuronal cortex cultures at 10 DIV or 12 DIV using a calcium phosphate transfection protocol (adapted from Jiang et al., 2004). The plasmid, 3 µg per coverslip, was diluted in Tris-EDTA transfection buffer (10 mM Tris-HCl and 2.5 mM EDTA, pH 7.3). A $CaCl_2$ solution (2.5 M in 10 mM HEPES) was then added (12.5 µl) dropwise. The DNA/TE/$CaCl_2$ solution was gently mixed by up and down with the pipette. This DNA/TE/ $CaCl_2$ solution was added to an equivalent volume (125 µl) of 2xHEPES-buffered transfection solution (274 mM NaCl, 10 mM KCl, 1.4 mM Na_2HPO_4, 11 mM dextrose, and 42 mM HEPES, pH 7.2). This solution was gently mixed up and down with the pipette. The precipitated DNA (100 µl per coverslip) was added dropwise to the coverslips, which were in 200 µl of conditioned medium (for each coverslip) from the original culture dish and 50 µl of 10 mM Kynurenic acid (Sigma-Aldrich), dissolved in suitable un-supplemented culture medium (Neurobasal culture medium without glutamate). The cultures were incubated with the

precipitate solution for 1-2 hrs. Following this incubation step, the solution was removed and replaced by 500 µl of Neurobasal Medium without glutamate plus Kynurenic acid and slightly acidified with 5M HCL to stop transfection. Cells were incubated for 15-20 minutes in 5% CO_2/95% air at 37°C. Coverslips were then transferred to the original dish containing the conditioned medium into 37°C, 5% CO_2/95% air incubator to allow expression of the transfected construct. Cells were allowed to express the plasmid for 4 or 2 days, according to the experiment.

3.5. Immunocytochemistry

In order to perform this protocol, we have made a live ICC since our objective was to mark superficial stargazin. Coverslips of Stg^{WT}, Stg^{ID}, Stg^{SCZ} conditions were incubated with anti-HA antibody diluted in culture medium for 10 minutes at room temperature and then quickly washed in phosphate buffered saline (PBS 1x: 137 mM NaCl, 2.7 mM KCl, 1.8 mM KH_2PO_4 and 10 mM $Na_2HPO_4 \cdot 2H_2O$, pH 7.4). After this, the neurons were fixed for 15 min in 4% paraformaldehyde (PFA - Sigma-Aldrich), and 4% sucrose at room temperature. The coverslips were incubated with Alexa Fluor 488 secondary antibody diluted in 3% BSA overnight at 4°C. Following this step, cells were permeabilized with PBST (PBS + 0.25% (v/v) Triton X-100) for 5 min, at 4°C. Afterwards, the neurons were incubated in 10% (w/v) BSA (Merck), in PBS, for 30 min at 37°C, to block nonspecific staining, and incubated in anti-PSD-95 and anti-MAP2 primary antibodies diluted in 3% (w/v) BSA, in PBS, for 2 hours at 37°C or overnight, at 4°C. After washing 6 times in PBS, cells were incubated with the secondary antibodies diluted in 3% (w/v) BSA in PBS, 1 hour at 37°C. Primary and secondary antibodies used are shown in table 5 and 6, respectively. After this step the cells were further washed 6 times in PBS, after which the coverslips were mounted using fluorescent mounting medium from DAKO (Palex).

Table 5 - Primary antibodies and respective dilutions used for ICC

Primary antibodies	Application and dilution	Source
Rat anti-HA	ICC (1:200)	Roche
Rabbit anti-PSD 95	ICC (1:200)	Thermo Fisher
Chicken anti-MAP2	ICC (1:5000)	Abcam

Table 6 - Secondary antibodies and respective dilutions used for ICC.

Secondary antibodies	Application and dilution	Source
Anti-rat Alexa Fluor 488	ICC (1:500)	Jackson ImmunoResearch Laboratories, Inc.
Anti-rabbit Alexa Fluor 647	ICC (1:500)	Invitrogen
Anti-chicken AMCA	ICC (1:200)	Jackson ImmunoResearch Laboratories, Inc.

3.6. Quantification and statistical analysis

Before statistical analysis, it was determined the presence of significant outliers in our data. To this end, it was used the online calculator from GraphPad Prism 5 (http://graphpad.com/quickcalcs/Grubbs1.cfm), to perform the Grubbs' test with a significance level of Alpha = 0.05. The statistical analysis such as D'Agostino & Pearson omnibus normality test, Mann Whitney test and two tailed Unpaired t test were performed using GraphPad Prism 5 software (Graphpad software).

4. Optimization and implementation of clearing protocols: Sca*l*eA2 and Sca*l*eS

In order to apply Sca*l*eA2 protocol, Sca*l*eA2 solution was prepared with the following composition: 4 M urea crystals, 0.2% (w/v) Triton X-100 solution and 10% (w/v) of glycerol (Hama et al., 2011). The solution was mixed by stirring until every component was completely dissolved and stored at room temperature. Brain samples were incubated in Sca*l*eA2 solution at room temperature for 3 or 20 days in case of 500 µm and 1 mm brain hemispheres slices, respectively, in a 24 MW plate with constant shaking or in a see-through vial, at 4°C, for a whole hemisphere.

Sca*l*eS protocol is composed by the sequential application of several solutions: S0, S1, S2, deSca*l*ing and S4. This protocol was applied firstly to 1 mm brain hemisphere slices in order to optimize the protocol and since the incubation period for a whole hemisphere was described to be 12 hrs, we decided to shorten the protocol to 6 hours. Brain slices were incubated in a volume of 30 mg/mL in each Sca*l*eS solution and placed in an orbital shaker at 37°C with 70 rpm or at 4°C with constant rotation for the deSca*l*ing solution. All the hemispheres used in this work were a kind gift from Dr. Jorge Valero. The solutions used for this protocol are presented in table 7 (Hama et al., 2015):

Table 7 - Reagents used in Sca*l*eS protocol. Adapted from (Hama et al., 2015).

Reagent	**Sca*l*eS protocol**						
	S0	S1	S2	S3	DeSca*l*ing	S4	Source
D-(–)-sorbitol % (w/v)	20	20	27	36.4	–	40	Sigma-Aldrich
Glycerol % (w/v)	5	10	–	–	–	10	Sigma-Aldrich
Urea (M)	–	4	2.7	2.7	–	4	VWR
Triton X-100 % (w/v)	–	0.2	0.1	–	–	0.2	Acros Organics
Methyl-ß-cyclodextrin (mM)	1	–	–	–	–	–	Sigma-Aldrich
α-Cyclodextrin (mM)	1	–	–	–	–	–	Sigma-Aldrich
N-acetyl-L-hydroxyproline % (w/v)	1	–	–	–	–	–	Sigma-Aldrich
Dimethylsulfoxide % (v/v)	3	–	8.3	9.1	–	20	Sigma-Aldrich
PBS (–)	1x	–	–	–	1x	–	-
pH	7.2	8.3	8.3	7.9	7.4	7.9	-
Incubation period (hrs)	6	6	6	6	6	6	-
Incubation temperature (°C)	37	37	37	37	4	37	-

4.1. Immunohistochemistry for Sca*l*eA2

Since the 500 µm hemispheres brain slices had no endogenous fluorescent labelling we decided to apply immunohistochemistry protocol on Sca*l*eA2 processed slices and on non-processed slices (control). In order to do so, we firstly placed the slices for 12 h in blocking solution at room temperature (RT). For the Sca*l*eA2 processed slices blocking was performed with Sca*l*eA2 solution with 0.1% Triton X-100 and 3% BSA. Control slices were blocked with PBS with 0.2% Triton X-100 and 3% BSA. The following step involved an

incubation period of 24 h in primary antibody anti-GFAP in blocking solution after which we applied 3 washes, each lasting 1hr, with Sca*l*eA2 or PBS+0.1 % Triton X-100, in case of the control. The next step involved an overnight incubation with secondary antibody diluted in blocking solution at RT with constant shaking. Primary and secondary antibodies used are shown in table 8. The last step involved two washes, each lasting 1hr, with Sca*l*eA2 or PBS+0.1% Triton X-100. The samples were then imaged using the confocal microscope and stored in Sca*l*eA2 or PBS at 4ºC.

Table 8 – Primary and secondary antibodies used in IHC

Antibodies	Category	Application and dilution	Source
Mouse anti-GFAP	Primary antibody	immunohistochemistry (1:10000)	Millipore
Anti-mouse Alexa Fluor 488	Secondary antibody	immunohistochemistry (1:10000)	Thermo Fisher Scientific

4.2. Image acquisition

In order to quantify the area of the brain slices images of the entire slices were obtained using an Axio Observer.Z1 equipped with a Plan-Apochromat 20x/0.8 objective or a Axio Imager.Z2 with a EC Plan-NeoFluar 5x/0.16 using the tile module of the Zen 2 software.

In addition, in order to visualize the depth of fluorescence detection on brain slices both confocal as multiphoton microscopes were used. Confocal Z-stack images were acquired on a LSM710 confocal microscope (Carl Zeiss, Germany) equipped with a Plan-Apochromat 20x/0.8 objective and using the Argon/2 laser (488 nm) for GFP excitation. Multiphoton Z-stacks images were acquired on a LSM710 NLO multiphoton microscope (Carl Zeiss) equipped with a Plan-Apochromat 20x/1.0 objective and using a Mai-Tai DeepSee IR laser (Spectra-Physics) at 900 nm, for GFP excitation.

All the images acquisitions were made on the proper solution: PBS, Sca*l*eA2 or S4 solution for control slices, slices used in Sca*l*eA2 protocol or Sca*l*eS protocol, respectively.

Chapter III

Results

1. Influence of stargazin on dendritic spine morphology in hippocampal neurons

1.1. Selecting for a quantitative method to evaluate spine morphology: NeuronStudio semi-automatic spine classification vs. Manual classification using ImageJ

We have started this project by evaluating different methodologies for spine analysis. Organotypic hippocampal slices were transfected with a plasmid expressing a control shRNA (sh6) and co-expressing GFP, to identify transfected neurons and analyze neuronal morphology. We have imaged dendrites in transfected neurons, and manually classified dendritic spines using ImageJ. This quantification relied on manually counting of each visible spine in 3 dendrites per neuron in every layer of the z-stack. Since this counting did not require any automatic spine detection all types of spines such as branched and cup-shaped were included in the analysis (Fig. 14). The number of spines of each type was normalized to the total number of spines for each analyzed dendrite. We also analyzed the same set of images using a semi-automatic process taking advantage of the NeuronStudio software (Fig. 14). The comparison between the analysis made with the two methods did not reveal major differences, apart from the addition of cup-shaped and branched spines in the manual count that NeuronStudio does not allow. We decided to use NeuronStudio for further analysis for several reasons: 1) the criteria set in the beginning do not change over time and are always the same, reducing possible errors introduced by the observer in different days of the quantification; 2) more automatic process and less time consuming; 3) possibility of visualizing spines in 3D in case of uncertainty during correction of spine classification.

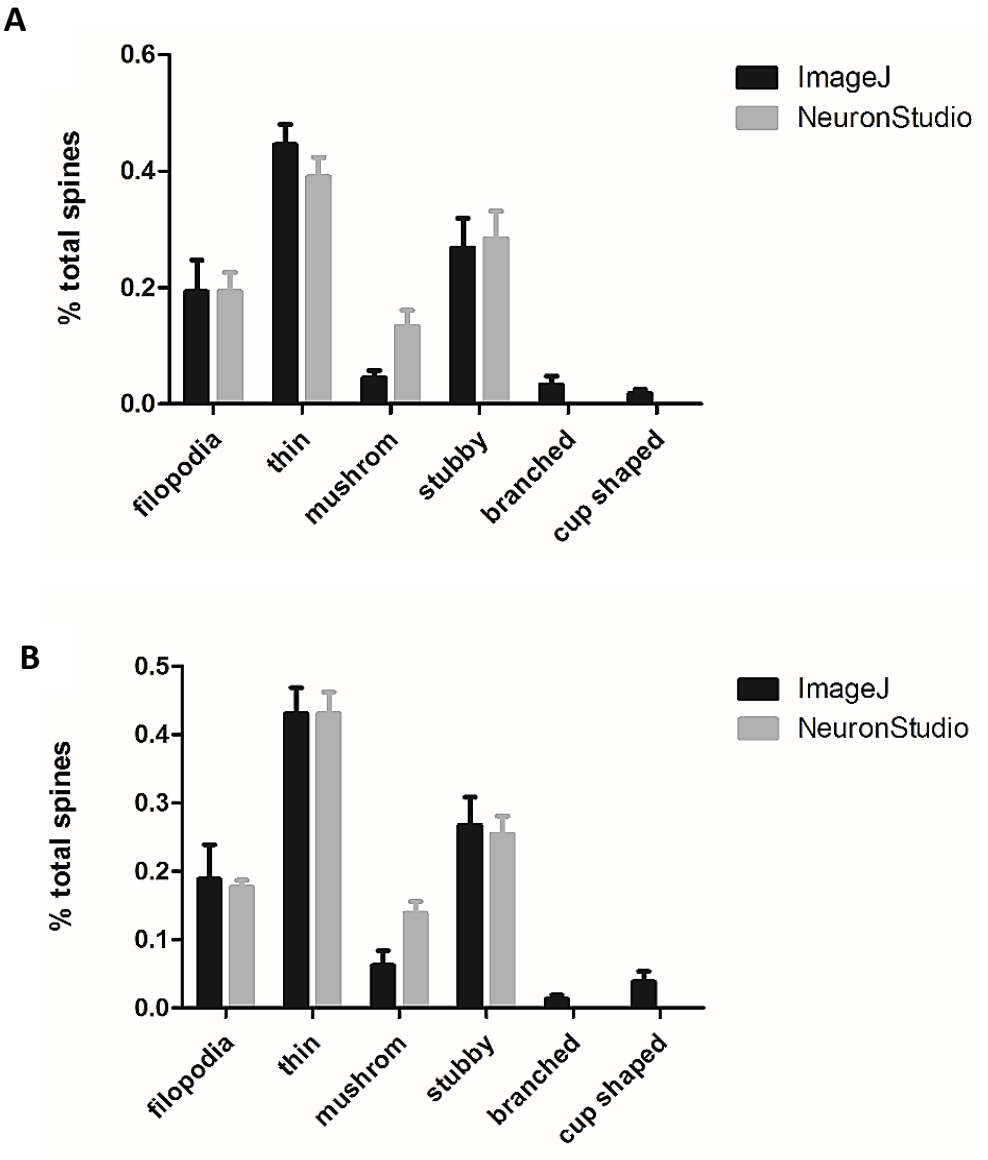

Fig. 14 - Selection of a quantitative method to evaluate spine morphology: NeuronStudio semi-automatic spine classification vs. manual classification using ImageJ. Classification of dendritic spines according to their morphology in basal **(A)** and apical **(B)** dendrites of sh6 transfected hippocampal neurons. 3 dendrites per neuron were analyzed, in 2 neurons per experiment, in 5 independent preparations. Data are presented as mean ±SEM.

1.2. Dendritic spines in apical and basal dendrites

After establishing which methodology to be used for spine analysis, we firstly characterized the distribution of each spine class in two different classes of dendrites: apical and basal. As shown in Fig. 15, there is a different distribution of spines according to the dendrite category. In particular, in apical dendrites the immature spines (filopodia and thin) are more abundant, whereas in basal dendrites mature spines are more abundant. This difference is not related to differences in spine density, since there are no significant differences in spine density between apical and basal dendrites (Fig. 15). Even though we could only find statistical significant differences in thin spines between apical and basal dendrites, probably due to the low number of dendrites analyzed, we have still decided to analyze separately basal and apical dendrites for the following experiments, since this initial experiment points to differences in the prevalence of mature and immature spines in apical and basal dendrites.

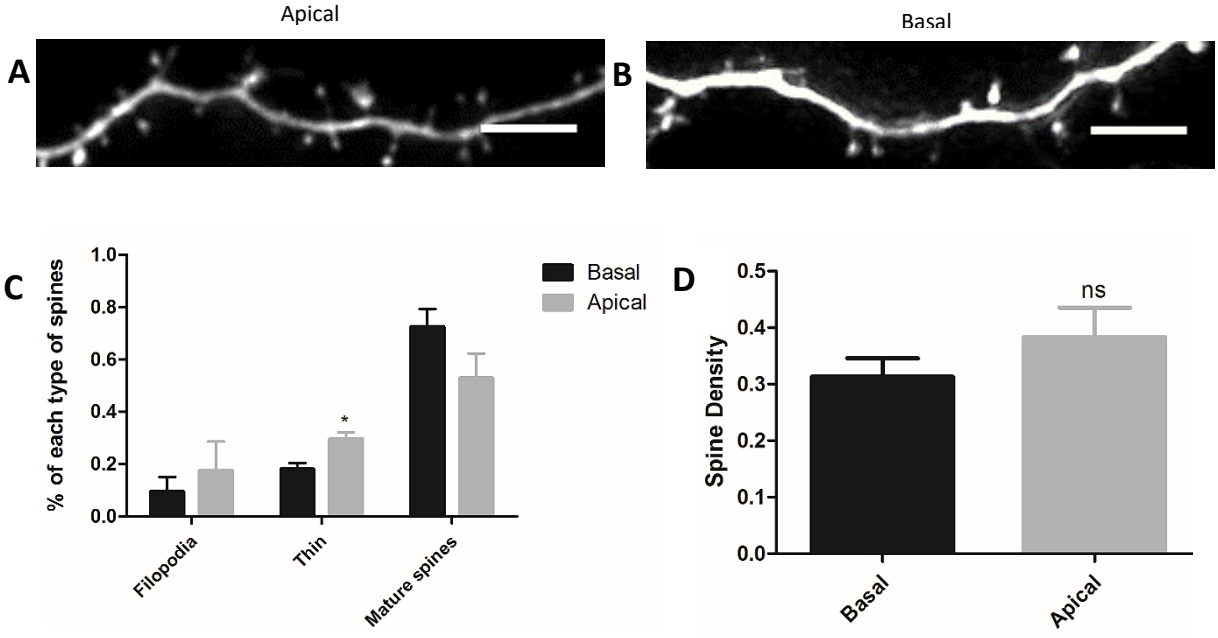

Fig. 15 - Characterization of the distribution of each spine class in apical and basal dendrites. Representative image of apical **(A)** and basal **(B)** dendrites in neurons expressing mCherry. Scale bar: 5 µm. **(C)** Spine morphology in apical and basal dendrites. The graph represents the % of each spine type in apical and basal dendrites. **(D)** Spine density in apical and basal dendrites in hippocampal neurons. 3 dendrites per neuron were analyzed with a total of 4 neurons, in 3 independent preparations. Non-parametric t-test (Mann Whitney), for the comparisons between basal and apical dendrites spine density and filopodia apical-basal, thin apical-basal, mature spines apical-basal. n.s (non-significant) $p>0.05$; *$p<0,05$, significantly different. Data are presented as mean ±SEM.

1.3. Role of stargazin in modulating spine morphology

Before trying to understand the role of stargazin within our system, through the use of an shRNA to knockdown the expression of the protein, we tested whether expression of an shRNA, and therefore activation of the siRNA processing machinery, affects spine morphology. In order to so, we compared spine morphology in neurons transfected with the plasmid encoding mCherry alone with that of neurons co-transfected with the mCherry plasmid and a plasmid to express a control shRNA (targeting luciferase) – sh6. As it is possible to observe in Fig. 16 there are no significant differences in spine morphology between both conditions for either apical or basal dendrites Taking these results in to consideration, it is possible to state that sh6 does not affect spine morphology, reason why it was possible to study stargazin function through the use of a shRNA plasmid to knockdown the protein, in this system.

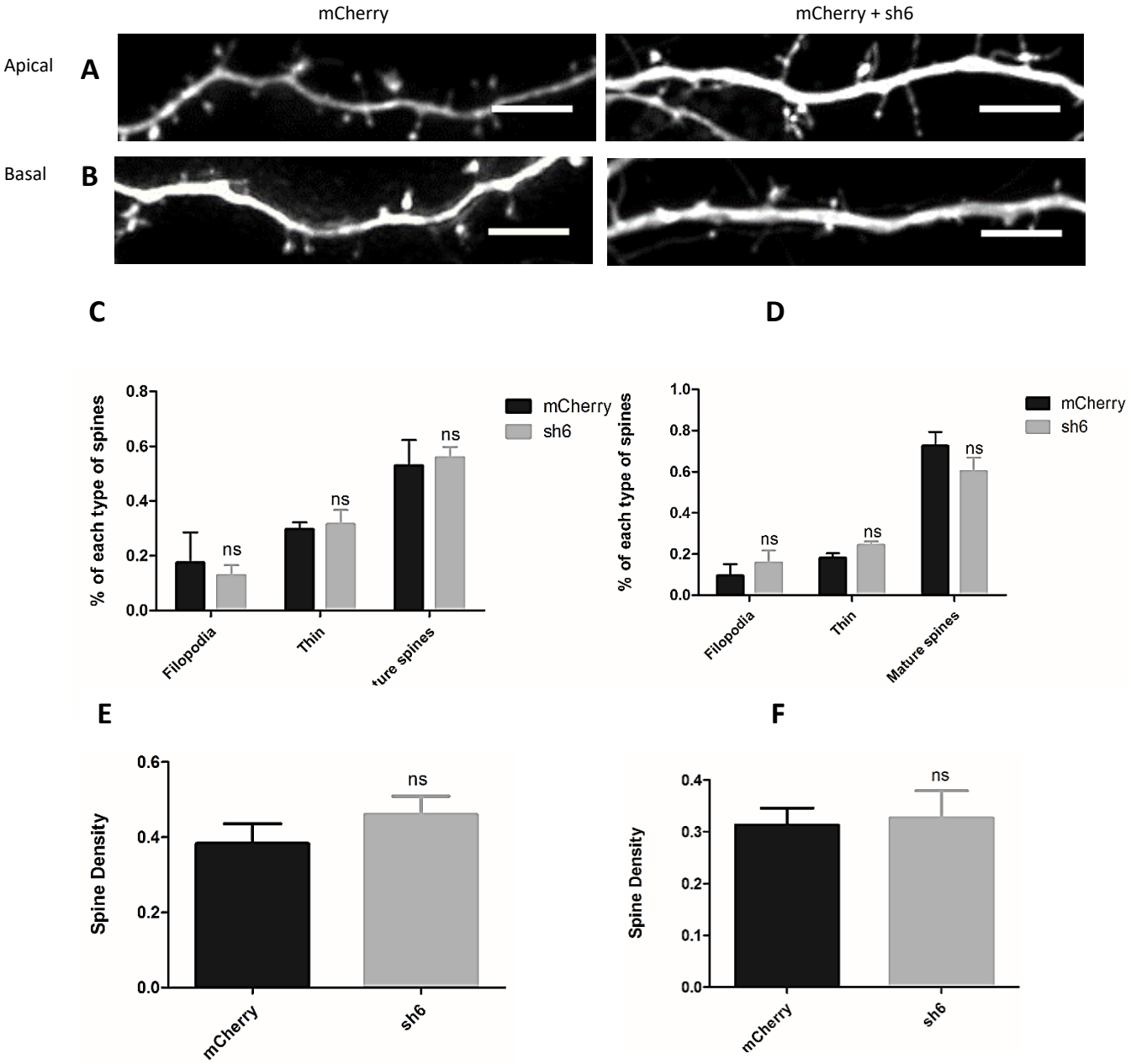

Fig. 16 - Expression of a control shRNA does not affect spine morphology in hippocampal neurons. Representative image of apical **(A)** and basal **(B)** dendrites in neurons expressing mCherry alone (left) or expressing mCherry and control shRNA (right). Scale bar: 5 µm. Spine morphology **(C)** and spine density **(E)** in apical dendrites in the mCherry and sh6 conditions. Spine morphology **(D)** and spine density **(F)** in basal dendrites; 3 dendrites per neuron were analyzed, in a total of 4 neurons in mCherry condition and 5 neurons in sh6 condition in 3 independent preparations. Mann Whitney test used to evaluate the differences between spine density and mCherry-sh6 filopodia, mCherry-sh6 thin, mCherry-sh6 mature spines. n.s (non-significant) $p>0.05$. Data are presented as mean ± SEM.

To determine whether stargazin affects spine density and morphology, we transfected organotypic hippocampal slices with the plasmid encoding mCherry together with the plasmid expressing an interference RNA for stargazin previously validated in our laboratory (sh4, Louros et al., 2014). We compared spine density and morphology in these neurons with those in neurons transfected with mCherry and the control sh6 (Fig. 17).

Even though significant statistical alterations were only found between sh6 and sh4 filopodia in basal dendrites (Fig. 17, D), comparing both conditions it is possible to see differences between sh6 and sh4 in particular in immature spines such as filopodia (as it is possible to observe in Fig. 17) in apical dendrites, with an increase of about 65% of filopodia in the conditions where the stargazin was knocked down. The increase in filopodia in the sh4 condition occurs at the expenses of both thin and mature spines, which decrease in both apical and basal dendrites in the neurons where stargazin was silenced (sh4; Fig. 17). These alterations in the sh4 condition do not appear to be related with modifications in terms of spine density, since there are no significant differences between both sh6 and sh4 conditions ($p= 0,7655$ for the basal dendrites and $p= 0,3015$ for apical dendrites, using an Unpaired t test).

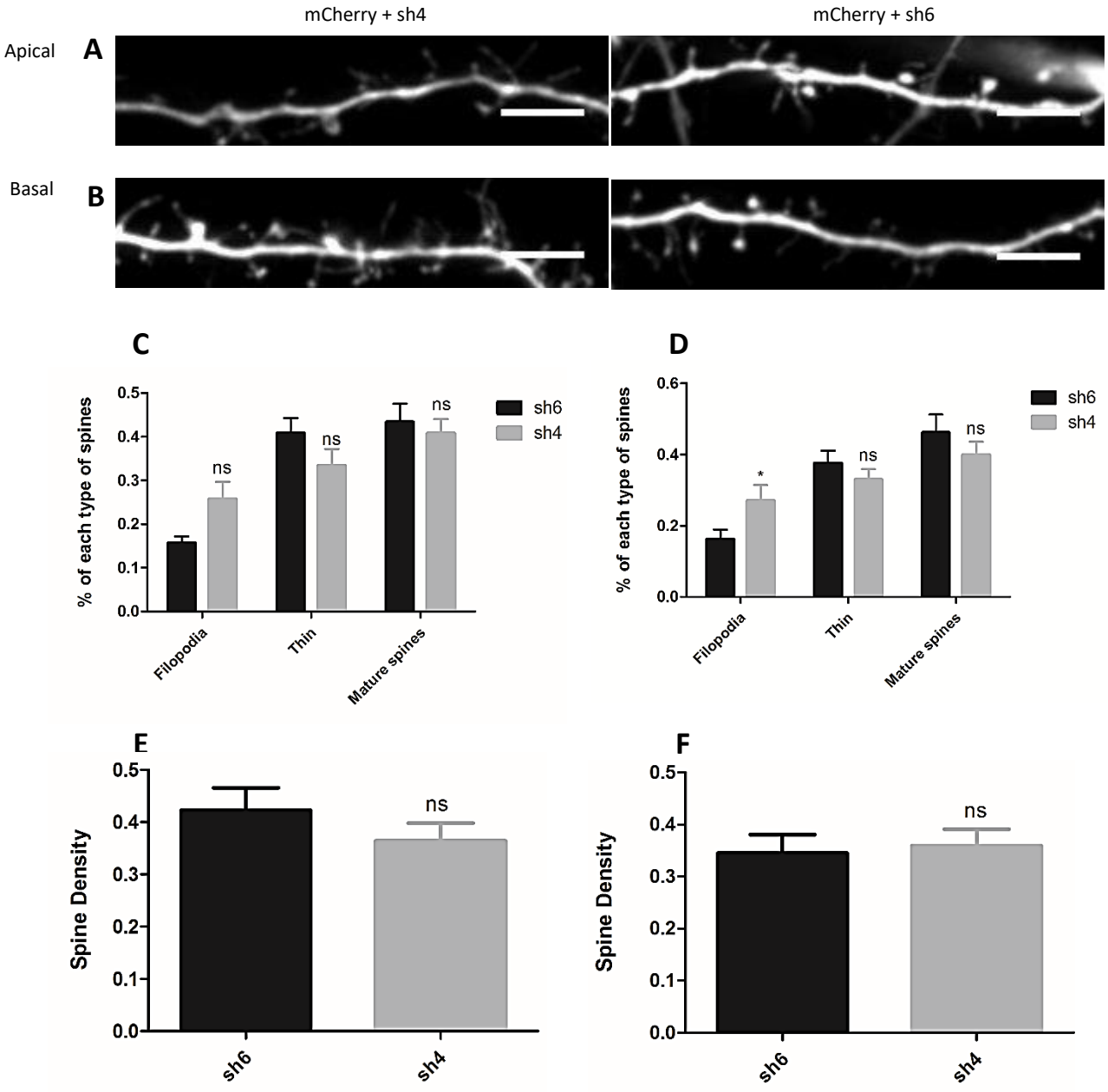

Fig. 17 - The expression of a shRNA specific for stargazin leads to an increase of 65% of the filapodia spines in hippocampal neurons in comparison to the control shRNA, sh6. Representative confocal images of **(A)** apical dendrites transfected with sh4 (left) and sh6 (right), **(B)** basal dendrites transfected with sh4 (left) and sh6 (right). Scale bar: 5 µm. Spine morphology **(C)** and spine density **(E)** in apical dendrites in the sh6 and sh4 conditions. Spine morphology **(D)** and spine density **(F)** in basal dendrites; 3 dendrites per neuron, in a total of 11 neurons per condition, in 6 independent preparations; Parametric t-test (Unpaired t test), for the comparisons between: spine density, sh6 and sh4 conditions for filopodia, thin and mature spines in basal dendrites and mature spines in apical dendrites. Non-parametric test (Mann Whitney test) for sh6-sh4 conditions in apical dendrites for thin and filopodia. n.s (non-significant) $p>0.05$; *$p<0,05$, significantly different. Data are presented as mean ±SEM.

2. Producing viral vectors to express stargazin and its disease-related mutants

Given the promising data suggesting that stargazin silencing promotes an increase on the formation of filopodia and a decrease on more mature forms of spines (Fig 17), we would like to test whether disease-related mutant forms of stargazin can perform stargazin's role in modulating spine morphology. Therefore, we produced lentiviral vectors to express HA-tagged wild-type stargazin or two mutant forms, one associated to ID (Stg^{ID}), the other associated to schizophrenia (Stg^{SCZ}). Stargazin forms were cloned in the pLL 3.7 pLentilox plasmid expressing mCherry under the control of the synapsin promoter. The self-cleaving T2A sequence was introduced between mCherry and stargazin.

PCR products were purified from the agarose gel, and the purification of the PCR products was confirmed in an agarose gel (Fig. 18, A), before proceeding for further steps in the cloning process. In the case of purified stargazin it was possible to observe a very thick band that corresponds to the stargazin sample (Stg^{WT}, Stg^{ID} or Stg^{SCZ}) and another very tenuous band (Fig. 18, panel A). In spite of the presence of this band, we continued the process and used these samples to further continue the process.

Digestion of the pLentilox vector was confirmed in an agarose gel (Fig. 18, panel B). Whereas the undigested band produces 2 bands in the gel, which correspond to the coiled and non-coiled forms of the vector, a single band for the digested vector was obtained, confirming that the digestion was successful. After ligation and bacteria transformation, several positive clones were identified by restriction analysis (Fig. 18 panel C). If the ligation step was successful, the enzymes cut in two different sites corresponding to the flanking sequences of the inserted fragment, producing two segments with different sizes, meaning that the colonies were positive. As it is possible to observe in this Fig.18, we obtained several positive clones for Stg^{WT}, Stg^{ID} and Stg^{SCZ}. These clones were confirmed by DNA sequencing (Fig. 18, D).

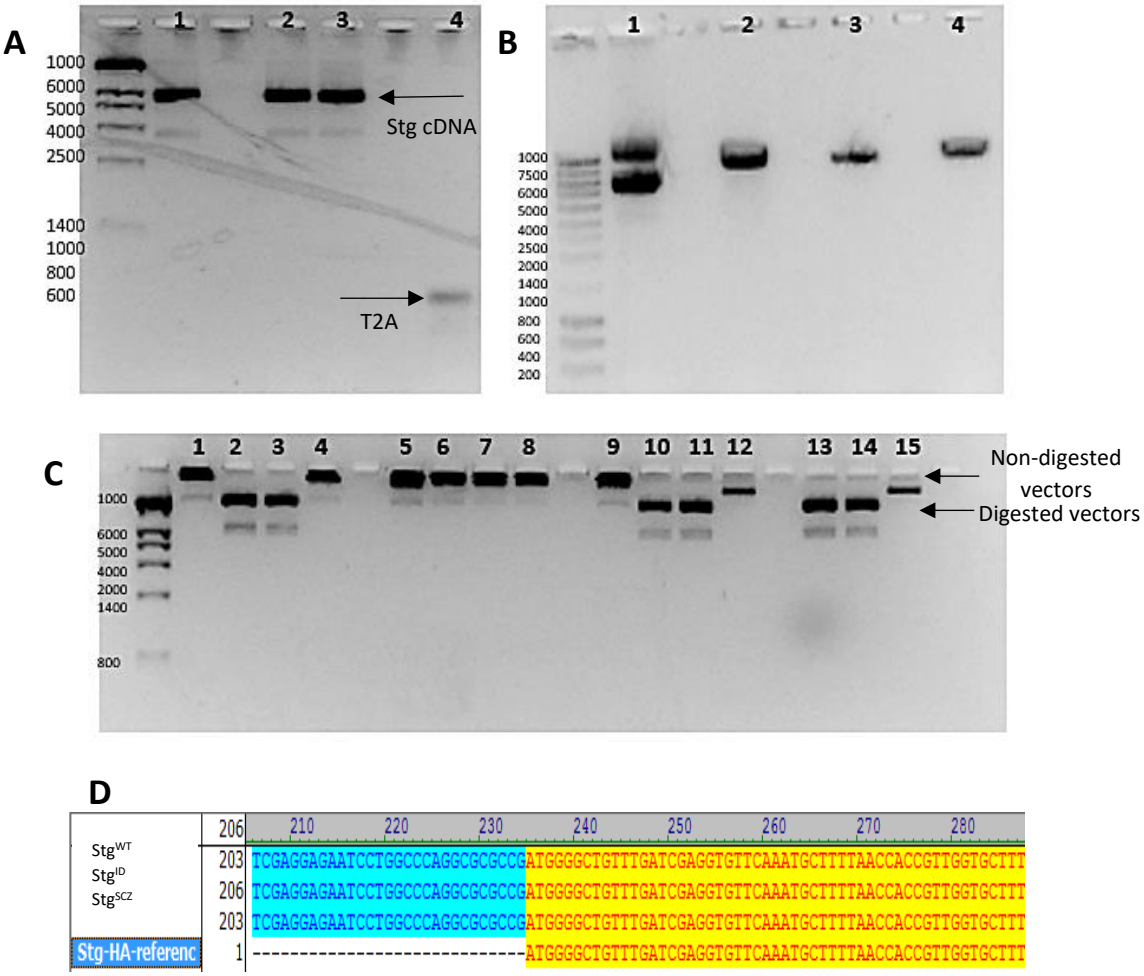

Fig. 18 - Generation of vectors that express stargazin and its disease-associated variants. **(A)** PCR results after purification directly from agarose gel. **1)** Stg^{WT}; **2)** Stg^{ID}; **3)** Stg^{SCZ} **4)** T2A. **(B)** pLentilox vector after digestion with BamHI and BsrGI restriction enzymes in a 1% agarose gel. **1)** Non-digested vector; **2)** Vector digested with both enzymes. **3)** Vector digested with BamHI; **4)** Vector digested with BsrGI**. (C)** Digestion of the final vector pLL 3.7 with BamHI and AscI restriction enzymes. **1)** Stg^{WT} non-digested control; **2-4)** Digestion of three Stg^{WT} different clones; **5)** Stg^{ID} non-digested control; **6-8)** Digestion of three Stg^{ID} different clones; **9)** Stg^{SCZ} non-digested control; **10-12)** Digestion of three Stg^{SCZ} different clones; **13-15)** Digestion of three Stg^{ID} different clones. **(D)** Homology analysis of different colonies sequence.

Even though the sequencing analysis shows that the vectors were well constructed, we tested whether the encoded proteins were expressed from these constructs, and that the T2A sequence was efficient in leading to the production of two separate proteins. Taking this into account, we transfected cortical neurons in culture with these vectors, and stained cell surface stargazin expressed from the vector by incubating live cells with the anti-HA antibody (since stargazin expressed from the vectors

was HA-tagged). As shown in Fig. 19, stargazin was expressed at the surface of neurons, whereas mCherry was expressed as a diffusible protein filling neurons; it is therefore possible to conclude that the T2A sequence is in fact leading to the production of two independent proteins– HA-stargazin and mCherry – which are appropriately trafficked in neurons.

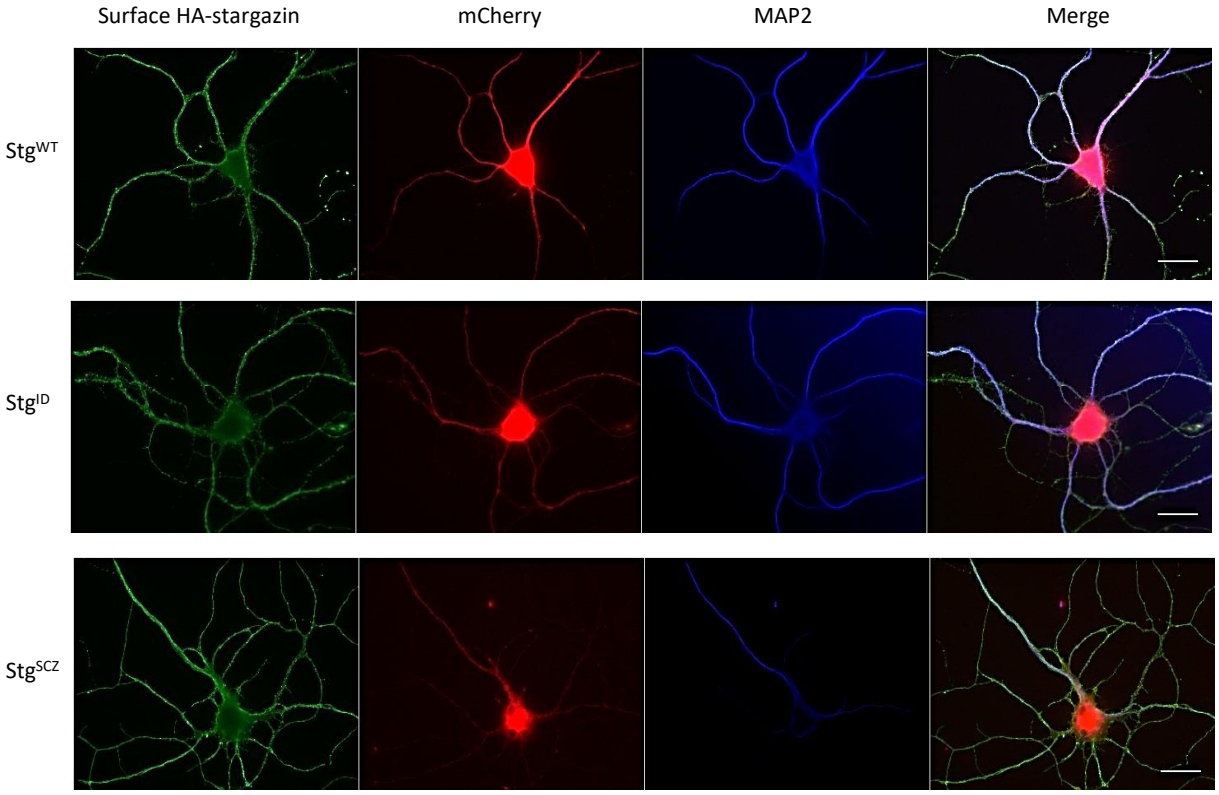

Fig. 19 - Immunocytochemistry analysis of HA-stargazin (WT form and disease associated mutants – Stg^{ID} and Stg^{SCZ}) in transfected cortical neurons. Neurons were transfected with pLL 3.7 mcherry-T2A-stargazin at DIV 10 and ICC was performed at DIV 14. Superficial HA-stargazin was live stained with anti-HA primary antibody and Alexa 488 secondary antibody. Neurons were then fixed and dendrites were labeled using an anti-MAP2 primary antibody and AMCA for secondary antibody. Scale bar: 20 µm.

We quantitatively analyzed the levels of HA-stargazin expression at the cell surface, with the objective of testing whether the disease-associated mutations in stargazin affect its traffic to the surface of neurons. For this purpose, and to attain physiological levels of expression of the protein, we transfected neurons at DIV 12, 48 h before fixing the cells and performed immunocytochemistry (as opposed to the

4 days of expression used for the experiments in Fig. 19). As shown in Fig. 20, B, the schizophrenia-associated mutant of stargazin (Stg^{SCZ}) presents lower levels of the protein at the cell surface, compared to Stg^{WT}, whereas the ID-associated variant (Stg^{ID}) is expressed at the neuronal surface with similar levels as the wild-type protein. This set of results show that the newly generated constructs effectively lead to the production of mCherry and stargazin.

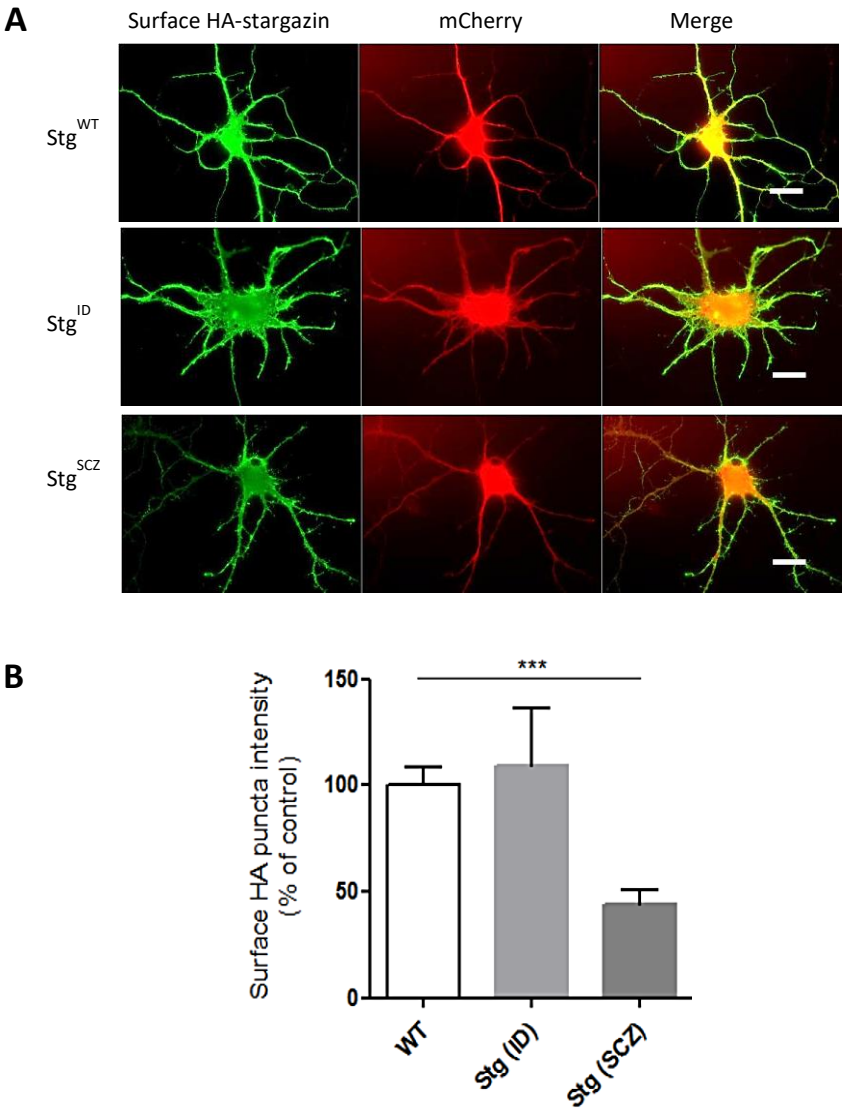

Fig. 20 Immunocytochemistry of HA-stargazin (WT form and disease associated mutants – Stg^{ID} and Stg^{SCZ}) in transfected cortical neurons and its correspondent surface HA puncta intensity analysis. **(A)** Superficial stargazin was labeled with anti-HA primary antibody and Alexa 488 secondary antibody Scale bar: 20µm. **(B)** Quantification of surface HA puncta intensity in cortical neurons transfected with Stg^{WT}, Stg^{ID}, or Stg^{SCZ} conditions. A total of 24 cells per condition were analyzed in 4 independent experiments. Non parametric test (Mann Whitney test), ***p>0,001. Data are presented as mean ± SEM.

3. New methods for imaging the brain: ScaleA2 and ScaleS

Analysis of neuronal and spine morphology benefits from newly developed methods that allow deeper brain imaging. Given our interest in investigating the role of stargazin in regulating spine morphology, we have optimized the use of these methods in our laboratory.

We started by applying Sca*l*eA2 to 500 µm brain slices as an initial step to then apply this protocol to thicker samples, such as 1 mm brain slices and whole brain hemispheres. As shown in Fig. 21 (panel A), this protocol was quite successful in terms of making the samples more transparent only by using a 3 days' incubation period.

After optimizing the incubation period to the 500 µm brain slices we set out to a more qualitative approach. Since it has been described that this procedure leads to slice expansion (Hama et al., 2011), we aimed to understand if such phenomenon also occurred in our samples by measuring the area of treated slices (Fig. 21, panel B and C). Slice areas were measured and we found that in fact the Sca*l*eA2 protocol leads to an expansion of the treated slice, Fig.21 C.

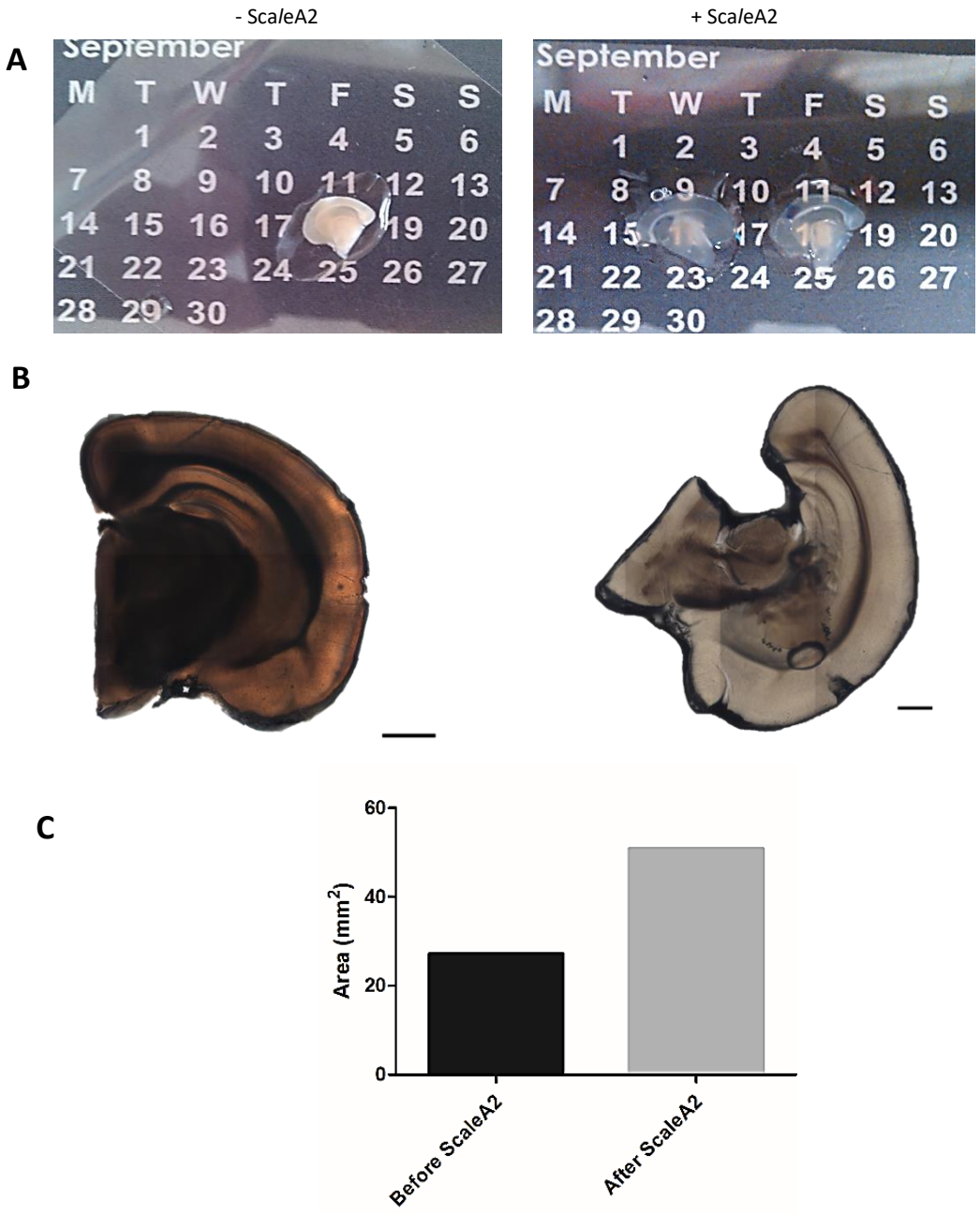

Fig. 21 - Sca*l*eA2 applied to 500 µm brain slices. **(A)** Photographs from 500 µm brain slices taken in a dark surface before clearing (left) and after clearing with the Sca*l*eA2 protocol (right). **(B)** Image of 500 µm brain slice before clearing (left) and after clearing with the Sca*leA2* protocol (right). **(C)** Area of slice before and after Sca*leA2* protocol. Scale bar:1 mm.

Afterwards, we decided to apply immunohistochemistry protocol to stain GFAP in our samples in order to understand if it was possible to image in greater depths after the application of Sca*l*eA2, since the main objective of these type of protocols is to allow higher light penetrance by reducing light scattering, allowing a greater information

gathering since there is no need for brain sectioning. As shown in Fig. 22, panel A, with standard PFA fixation protocols it is possible to acquire images up to around 60 µm in depth, whereas after the Sca*l*eA2 clearing protocol (Fig. 22, panel B) there is an increase in the depth acquisition up to 90 µm in the confocal microscope and to around 200 µm in the case of multiphoton microscopy imaging (Fig. 22, panel C).

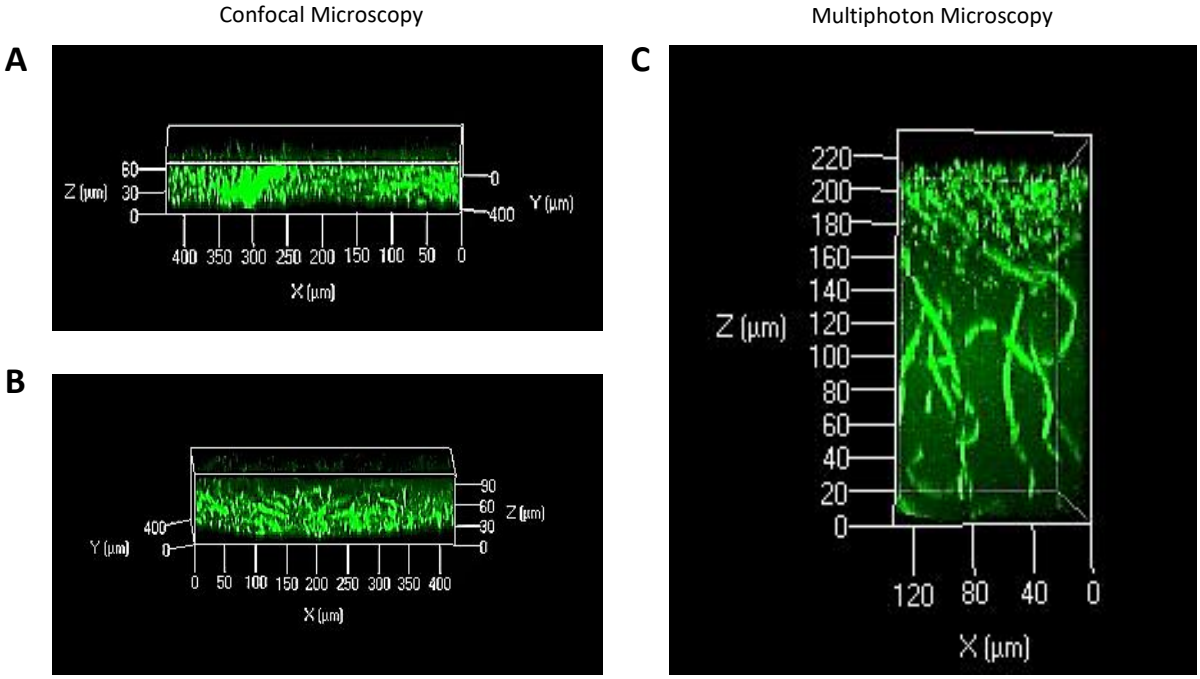

Fig. 22. Imaging of GFAP-labeled 500 µm brain slices. Confocal image of 500 µm brain slice without clearing, imaged in PBS, 2% Triton X-100 solution **(A)** or after clearing in Sca*l*eA2 solution **(B)**. Brain slice was labelled with anti-GFAP antibody (Alexa 488). **(C)** Multiphoton image of 500 µm brain slice after clearing in Sca*l*eA2 solution.

The next step involved qualitative analysis of 1 mm brain slices after an incubation period of 15 days in Sca*l*eA2. In this case we used transgenic mice expressing GFP under the control of the Nestin promoter (mice brains kindly provided by Dr. Jorge Valero, Achucarro Basque Center for Neuroscience). Once again, brain slice increased its area after the Sca*l*eA2 protocol (Fig. 23).

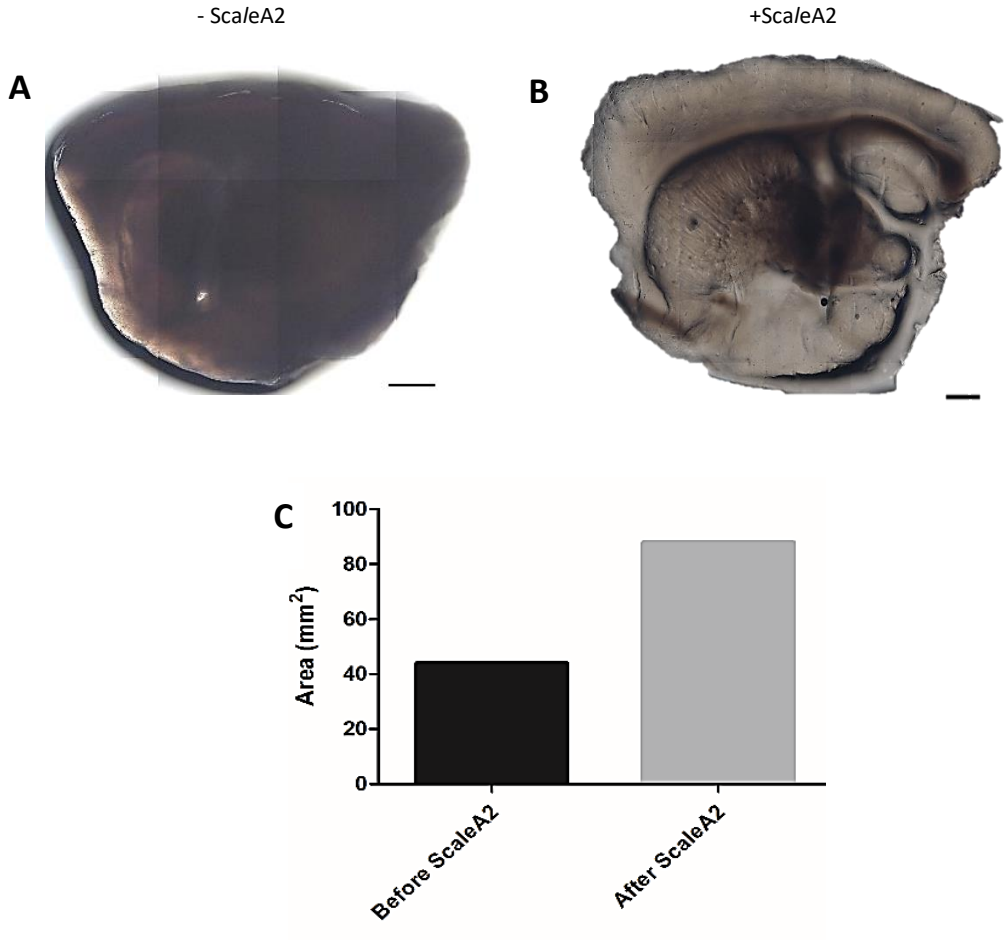

Fig. 23 - Imaging of transgenic mice expressing GFP under the control of the nestin promoter. **(A)** Image of 1 mm brain slice before clearing with Sca*l*eA2 and after an incubation period of 15 days with Sca*l*eA2 **(B)**. **(C)** Area of the slice before and after clearing in Sca*l*eA2 solution. Scale bar: 1 mm.

As it happened in the previous case, use of the Sca*l*eA2 clearing protocol increased the depth of image acquisition under the confocal microscope from 200 µm up to 500 µm (Fig. 24, panels A and C). When the untreated slices were imaged using multiphoton microscopy (Fig. 24, panel B), the range of depth acquisition even before Sca*l*eA2 application is by far bigger than the depth acquisition on the confocal mode at the same microscope (Fig. 24, panel A), highlighting the benefits of multiphoton microscopy.

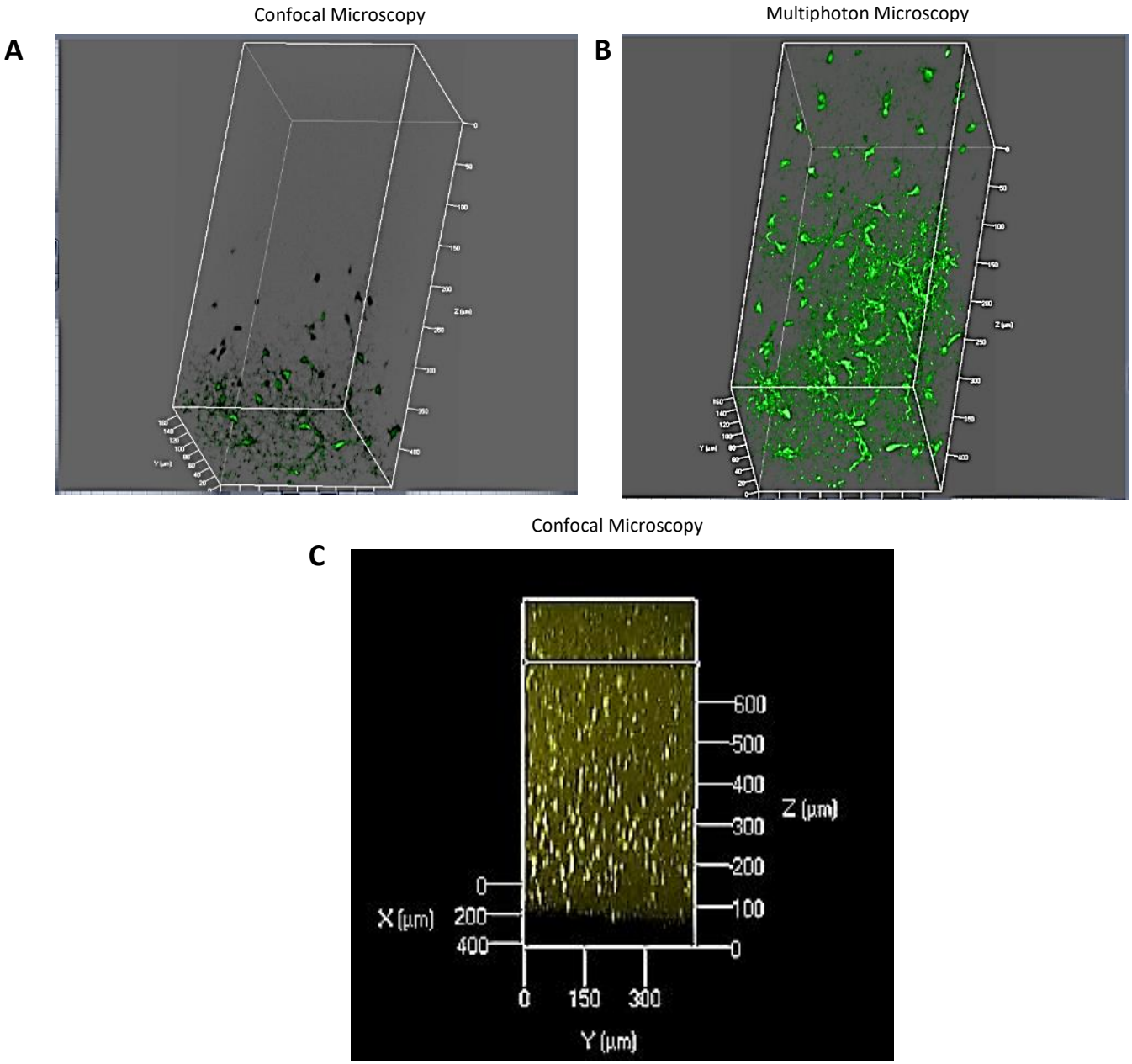

Fig. 24 - Imaging of GFP expressing cells in 1 mm brain slices from mice expressing GFP under the control of the nestin promoter. **(A)** Confocal image of 1 mm brain slice before clearing, imaged in PBS solution and multiphoton image of 1 mm brain slice before clearing, in PBS solution **(B).** Confocal image of 1 mm brain slice after Sca*l*eA2 protocol **(C).**

We then proceeded to improve the Sca*l*eA2 method for 1 mm brain slices, this time by increasing the incubation period from 15 to 20 days, as shown in Fig. 25 A and Fig. 26 A, since, after 15 days, slices still revealed some opacity in some regions, as it is possible to observe by Fig. 26, A.

Once more, the slices that were analyzed presented an increase of area of 1.45 times (Fig. 27). This protocol leads once more to an increase in depth of acquisition from 45 to 200 µm (slice 1, Fig. 25, panel C) by confocal microscopy.

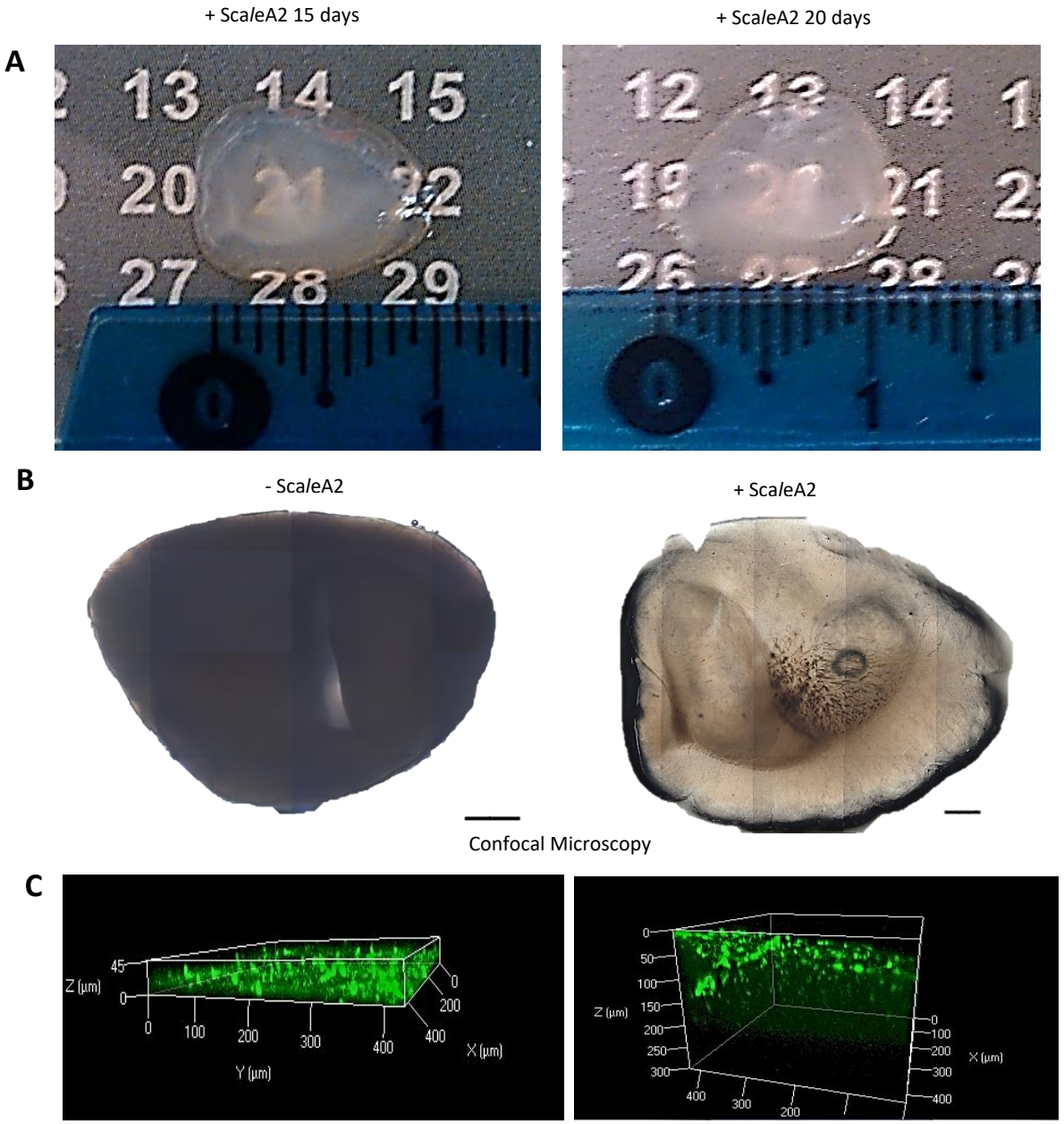

Fig. 25 - Imaging of GFP expressing cells in 1 mm brain slices from mice expressing GFP under the control of the the Nestin promoter. **(A)** Images from 1 mm brain slice after Sca*l*eA2 at incubation day 15 (left) and 20 (right) **(B)** Image of 1 mm brain slice before clearing (left) and after clearing with Sca*l*eA2 for 20 days (right). **(C)** Confocal image of 1 mm brain slice before (left) and after (right) clearing in Sca*l*eA2 solution. Scale bar: 1 mm.

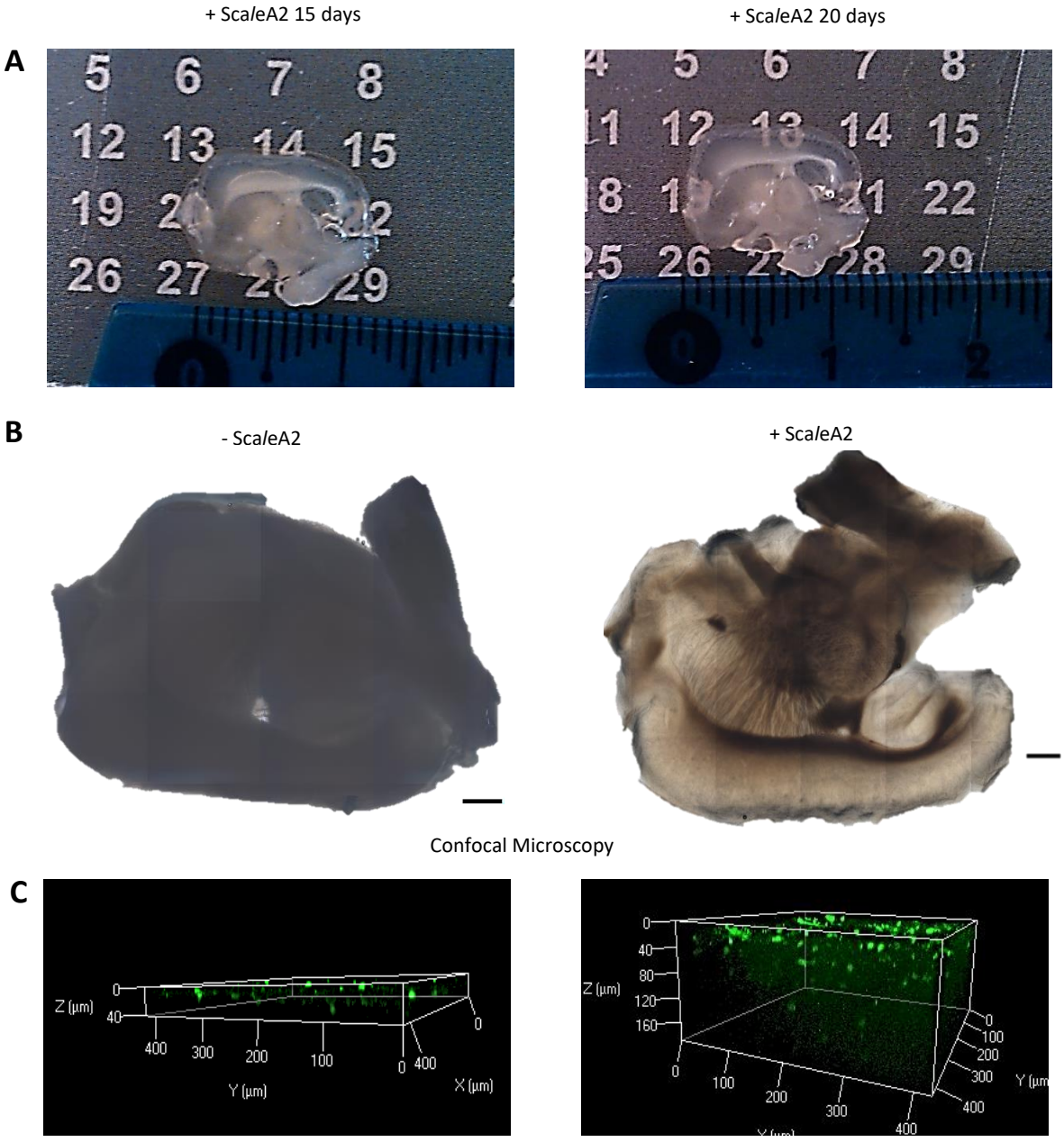

Fig. 26 - Imaging of GFP expressing cells in 1 mm brain slices from mice expressing GFP under the control of the nestin promoter. **(A)** Images from 1 mm brain after clearing at incubation day 15 (left) and 20 right on Sca*/e*A2. **(B)** Image of 1 mm brain slice before (left) and after clearing with Sca*/e*A2 for 20 days (right). **(C)** Confocal image of 1 mm brain before (left) and after (right) clearing in Sca*/e*A2 solution. Scale bar: 1 mm.

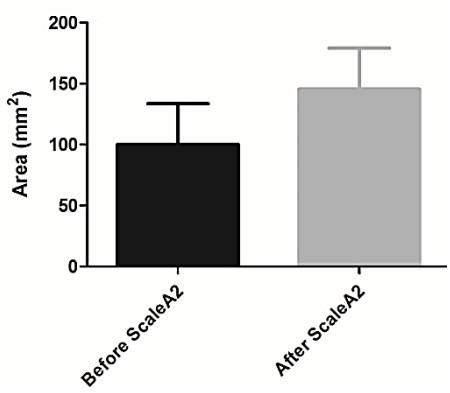

Fig. 27 - Normalized area of 1 mm brain slices before and after application of Sca*l*eA2 protocol N=3. Data are presented as mean ± SEM.

We then tried to clear a whole brain hemisphere using Sca*l*eA2 method following the protocol of Hama and co-workers. However, our results were not the same as reported. As it had been done in this work, we also placed the brain hemisphere in a 20 mL of solution per g of tissue, at 4°C with constant rotation. However, after two weeks we only obtained hemispheres with a lighter color in comparison to the original. These samples after two weeks revealed no transparency (Fig. 28, B) contrary to what was shown in their work (Fig. 29). The same samples continued to reveal no transparency after two months, as shown in Fig. 28 C.

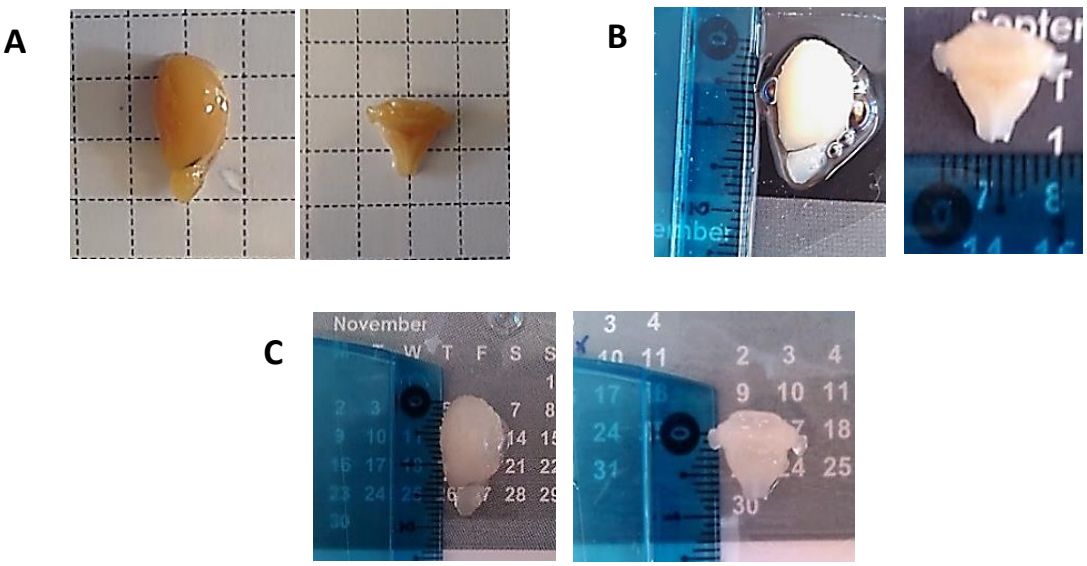

Fig. 28 - Whole brain hemisphere before Sca*l*eA2 **(A)**, after two weeks' incubation period on Sca*l*eA2 **(B**), and after 2 months in Sca*l*eA2 **(C).**

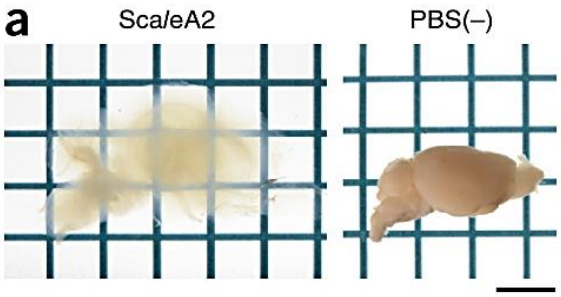

Fig. 29 - Mouse (10 weeks old) hemispheres after treatment with Sca*l*eA2 and PBS after two weeks. Adapted from Hama et al., 2015.

The next protocol we decided to apply was the Sca*l*eS protocol, using 1 mm brain slices from transgenic mice expressing GFP under the control of the LPAR promoter. This protocol relies on the application of 5 sequential solutions during 6 h each. During this process, we followed each slice in terms of transparency by placing the samples in a dark surface with a number in order to understand in which phases the samples started to become more transparent and when they suffered expansion or retraction, since it was one of the modifications reported during the procedure (Hama et al., 2015).

As shown in Fig. 30, slices started to become more transparent from the S1 stage, a phenomenon that is followed by an increase in size as it is possible to observe by the figures in the millimetric paper. This increase in transparency and size is however reverted after the descaling protocol (Fig. 30-6), when the slice becomes quite opaque and smaller. As described by Hama and co-workers, our samples also suffered from an expansion phase (Fig. 30-3-5) followed by a retraction phase (Fig. 30-6). Nevertheless, the samples did not return to their original size, not even approximately 100% of that of the original after transient shrinkage and expansion, as stated in the same work (Fig. 31).

-Sca/eS

1

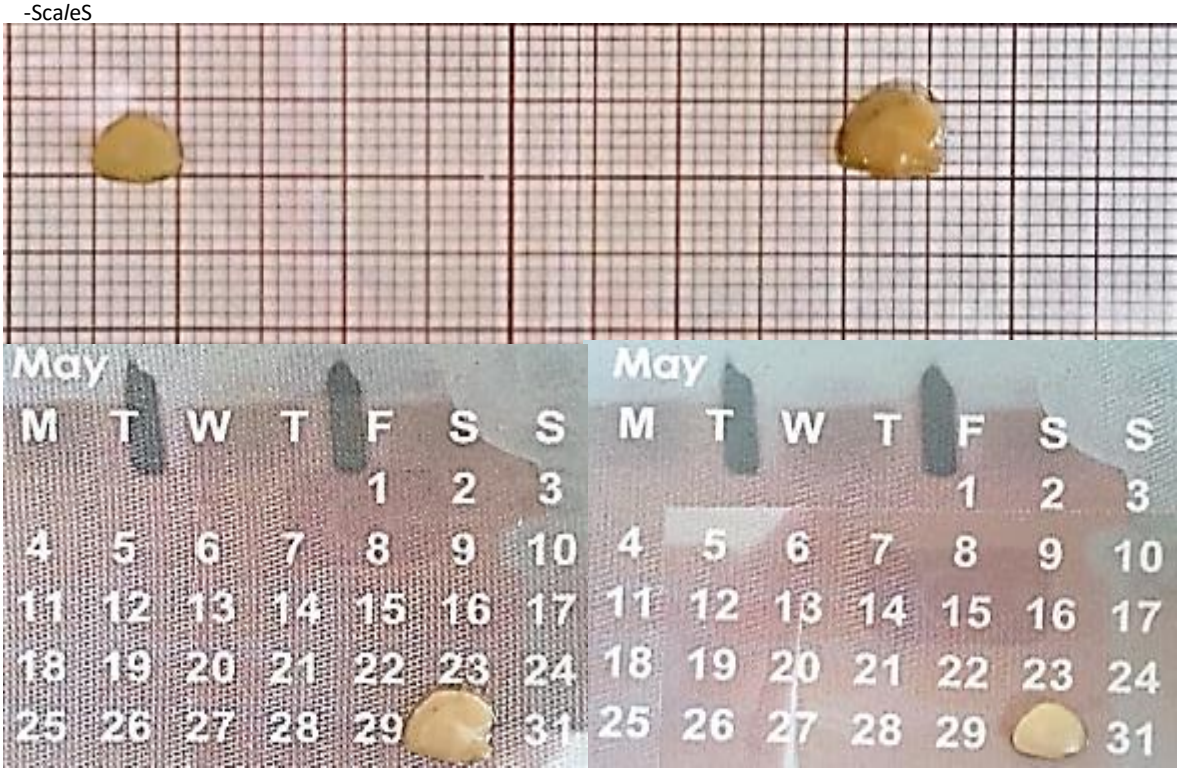

Sca/eS0

2

Sca/eS1

3

4 Sca*l*eS2

5 Sca*l*eS3

6 Desca*l*ing

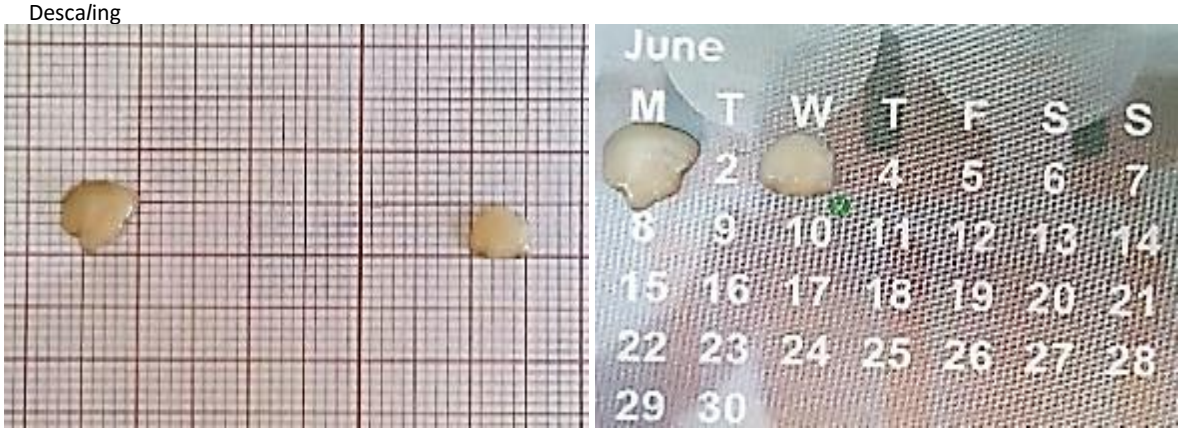

7 Sca*l*eS4

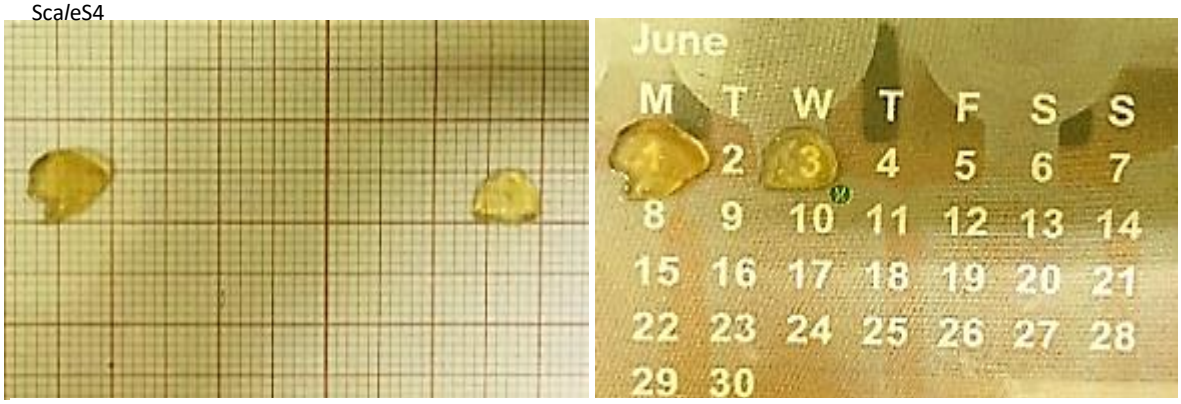

Fig. 30 - Images concerning different stages of the Sca*l*eS protocol applied to a 1 mm brain slice **1)** Slices before Sca*l*eS; **2)** Slices after S0; **3**) Slices after S1; **4)** Slices after S2; **5)** Slices after S3; **6)** Slices after deSca*l*ing; **7)** Slices after S4.

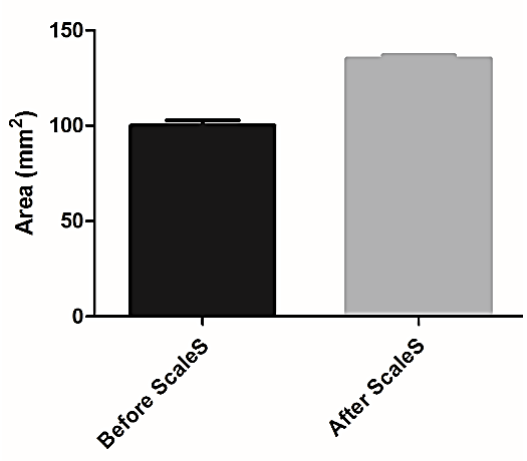

Fig. 31 - Normalized area of 3 slices before and after application of the Sca*l*eS protocol to 1 mm brain slices. Data are presented as mean ± SEM.

Once again we could still see an increase the depth of image acquisition with the application of Sca*l*eS (from approximately 60 µm up to 250 µm in confocal microscopy – Fig. 32, C). In the multiphoton microscope we were able to increase the depth acquisition to about 1 mm, approximately the slice size.

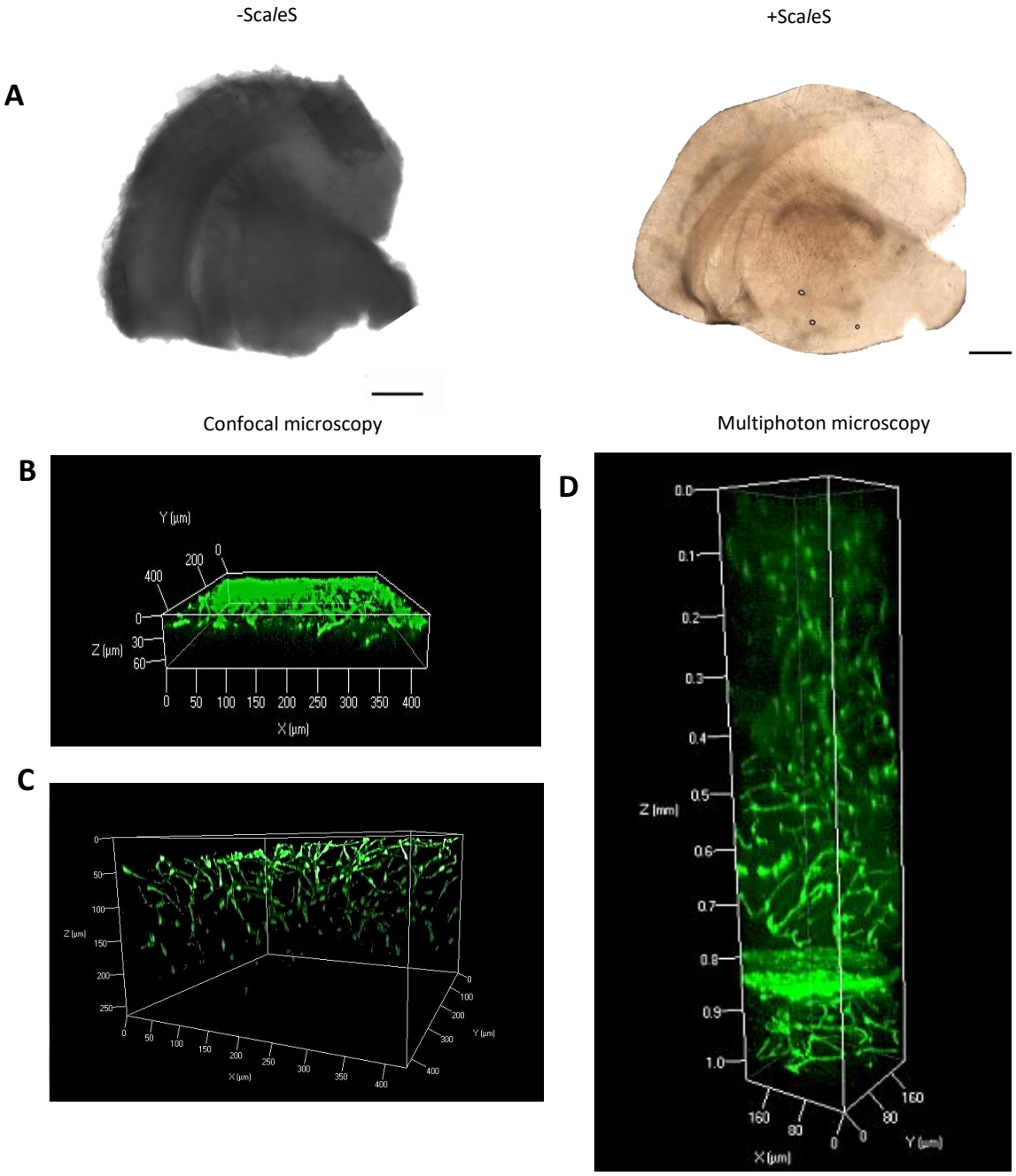

Fig. 32 - Imaging of GFP expressing cells in 1 mm brain slices from mice expressing GFP under the control of the LPAR promoter. **(A)** Image of 1 mm brain slice before clearing with Sca*l*eS (left) and after clearing with Sca*l*eS (right). Confocal image of 1 mm brain slice before clearing, imaged in PBS solution **(B)** and after Sca*l*eS protocol clearing in S4 solution **(C)**. Multiphoton images of 1 mm brain slice after Sca*l*eS protocol, in S4 solution **(D).** Scale bar: 1 mm.

Chapter IV

Discussion

1. Discussion

This work has focused on the study of the influence of stargazin on determining spine morphology in hippocampal neurons. To this end, we have used organotypic hippocampal neurons transfected with control shRNA, sh6, or shRNA specific for stargazin, sh4.

Dendritic spines are highly dynamic specialized structures whose form varies across development (Zuo et al., 2005) and can be classified as thin, stubby and mushroom (Harris et al., 1992; Hering and Sheng, 2001; Peters and Kaiserman-Abramof, 1970). These structures offer a specialized microenvironment able to receive inputs. These inputs are received due to the presence of several receptors in the membrane such as AMPAR and NMDAR, which activate several downstream pathways, leading to morphological and dendritic density modifications (as reviewed in Hering & Sheng 2001). Besides spines, it is also possible to find protrusions called filopodia. Filopodia have been referred as precursors of dendritic spines and, in comparison to spines, have a smaller AMPAR content (Matsuzaki et al., 2001; Zuo et al., 2005). Moreover, filopodia are pointed out as environmental detectors, detecting environment changes which might lead to cell migration, cell contacts, signal transmission and cell dynamics, all activities highly dependent on actin cytoskeleton (Blanchoin et al., 2014).

Besides this, we have also optimized and implemented new clearing methods which, in the future, will allow the study of this protein in a more complex *in vivo* system. These clearing methodologies were Sca*l*eA2 and Sca*l*eS.

1.1. Is stargazin relevant for spine morphology in hippocampal neurons?

Stargazin has been associated in the past few years with AMPAR traffic and gating, Hebbian and homeostatic plasticity (Louros et al., 2014; Tomita et al., 2005a). In this work, using hippocampal organotypic slices, we have analyzed if stargazin has indeed a role in the definition of spine morphology. Through the use of a shRNA to knockdown stargazin in our system, we have shown an increase of about 65% in the density of filopodia in dendrites of neurons lacking stargazin, compared to neurons transfected with the control shRNA sh6, meaning that when stargazin is absent the spines become more

immature. One possible and most obvious explanation for this might be related with some previous experiments conducted by our Lab, regarding AMPAR trafficking to the synapse. Stargazin in these experiments has been shown to be indispensable for GluA1 trafficking to the synapse since upon stargazin silencing, the GluA1 levels are significantly reduced. So, the absence of stargazin will lead to a decreased trafficking of GluA1 to the synapse, a smaller content in GluA1-containing AMPARs, which could be related to the maintenance of the synapse in a constant immature state. On the other hand, stargazin has been associated with several cytoskeleton-associated proteins: microtubule-associated protein 1 light chain 2, forming a complex with GluA2 AMPAR, Arc protein which is important for GluA1 downregulation during homeostatic plasticity, and MAGI-2. So, if stargazin is in lower amounts in the knockdown condition, the interaction between stargazin and cytoskeleton components in this case might be compromised, leading to morphological modifications. However, the exact cause of this morphological change is not yet known.

One of the questions that arises from this study, in face of these results, is the following: do synapses take longer to develop when the protein is in lower concentrations or do they remain immature over longer periods of time?

In this work we have focused in the physiological modifications of dendritic spines when stargazin is absent. However, after these results, several are the questions that start to emerge. Such questions are related with structural modifications over time in the presence of diverse stimuli since the spines are highly dynamic structures: 1) Are spines in neurons lacking stargazin as plastic as in control neurons? 2) How do neurons lacking stargazin behave in terms of spine structure in the presence of different plasticity stimuli? 3) Can we visualize any structural (such as, volume spine modifications) alterations in neurons lacking stargazin in comparison to control neurons?

Taking this study regarding the influence of stargazin in hippocampal neurons, into consideration, it is of most pivotal importance the study of the role of this protein, in a disease context.

1.2. Role of stargazin in disease

In the future, one of our goals is to understand the impact of stargazin disease-associated mutants (for ID and schizophrenia) on the function of stargazin. In order to do so, we aim to transfect organotypic hippocampal neurons with sh4 and perform rescue of stargazin levels with pLentilox mCherry-T2A-stargazinHA vector also produced in this work, in task 2.

Even though we have no indications so far of how spine morphology will be in the presence of disease related mutants, we also expect some degree of alteration. Alterations are expected in particular in the Stg^{SCZ} condition, since surface levels of this variant are reduced in comparison to the WT form.

Furthermore, in previous experiments, the surface and synaptic GluA1 levels were significantly reduced when disease-related variants were expressed, suggesting that these mutations impact stargazin function.

1.3. Sca*l*eA2 and Sca*l*eS

A second objective of this thesis was to implement and optimize Sca*l*eA2 and Sca*l*eS protocols. These set of methodologies will be, in a near future, a really important since they will allow scientists to acquire much more informative and naturalistic images.

Even though Sca*l*eS is an evolution of Sca*l*eA2, these protocols have several differences between them. One of such differences are the reagents used: Sca*l*eA2 uses one single solution composed by urea, triton X-100, glycerol and water, whereas Sca*l*eS protocol uses 6 solutions each with 8-9 reagents such as D-(–)-sorbitol, Glycerol, Urea, Triton X-100, Methyl-ß-cyclodextrin, α-Cyclodextrin, N-acetyl-L-hydroxyproline, Dimethylsulfoxide, PBS and water. Another very important difference is the incubation periods and the temperature at which these incubations occurs. Sca*l*eA2 in this work needs 20 days of incubation at RT, for 1 mm slice, whereas Sca*l*eS protocol only takes 36 h for 1 mm slice, each solution requiring an incubation period of 6 hrs at 37°C or 4°C.

In terms of transparency, it seems that slices in the Sca*l*eS protocol become uniformly transparent, which does not happen in Sca*l*eA2. We have also tried to apply Sca*l*eA2 protocol to whole-brain hemispheres. However, this protocol did not work, since

the hemispheres remained opaque and did not become transparent, even after two months after applying the solution. To these larger samples, Hama and colleagues (Hama et al., 2011) only used an incubation period of 15 days and as seen in Fig. 29. and their sample become much more transparent than ours. One reason that might help to explain this discrepancy is the age of brains, since we used older samples. One of the possible alterations to be made in the future might be an incubation period at higher temperatures such as stated by Hama and coworkers (2015), in comparison to what the authors have firstly stated (Hama et al., 2011). In the future, we also aim to apply Sca*l*eS to whole hemispheres.

In terms of the depth of image acquisition attained with the different protocols, it seems to be quite similar between Sca*l*eA2 and Sca*l*eS by confocal or multiphoton microscopy. Comparing confocal and multiphoton microscopy we could see some significant increase in terms of depth acquisition in both types of slices (Sca*l*eA2 and Sca*l*eS) when comparing image taken before and after the protocol. This increase of depth of image acquisition is obviously related with the fundamentals of each type of microscopy, making the multiphoton microscopy a better choice for imaging thicker samples.

In Sca*l*eA2, we report here an increase in slice area of 1.45, which was also reported by Hama and coworkers (2011), in all types of slices after the protocol. However, the authors have also reported that even though they could see an increase of sample volume, the proportions of the regions still remain the same. An increase in the area was also observed in Sca*l*eS.

Rethinking both techniques, we can point out as positive aspects of Sca*l*eS (regarding Sca*l*eA2) that it is not as time consuming as Sca*l*eA2, it is more effective in terms of transparency and the fact that this protocol allows sample contraction to its original size, due to the presence of sorbitol, a hydrophilic sugar alcohol that causes dehydration. However, Sca*l*eS is more labor consuming and more expensive than Sca*l*eA2. Weighting the pros and cons of both techniques, it seems more feasible to use Sca*l*eS for the future investigations.

Chapter V

References

Abidi, F.E., Holinski-Feder, E., Rittinger, O., Kooy, F., Lubs, H. a, Stevenson, R.E., and Schwartz, C.E. (2002). A novel 2 bp deletion in the TM4SF2 gene is associated with MRX58. J. Med. Genet. *39*, 430–433.

Ackermann, M., and Matus, A. (2003). Activity-induced targeting of profilin and stabilization of dendritic spine morphology. Nat. Neurosci. *6*, 1194–1200.

Alonso, M., Medina, J.H., and Pozzo-miller, L. (2004). ERK1 / 2 Activation Is Necessary for BDNF to Increase Dendritic Spine Density in Hippocampal CA1 Pyramidal Neurons. Cold Spring Harb. Lab. Press, *11,* 172–178.

Amtul, Z., and Atta-ur-Rahman (2015). Neural plasticity and memory: molecular mechanism. Rev. Neurosci. *26*, 253–268.

Bassani, S., Cingolani, L. a., Valnegri, P., Folci, A., Zapata, J., Gianfelice, A., Sala, C., Goda, Y., and Passafaro, M. (2012). The X-Linked Intellectual Disability Protein TSPAN7 Regulates Excitatory Synapse Development and AMPAR Trafficking. Neuron *73*, 1143–1158.

Bats, C., Groc, L., and Choquet, D. (2007). The Interaction between Stargazin and PSD-95 Regulates AMPA Receptor Surface Trafficking. Neuron *53*, 719–734.

Bats, C., Soto, D., Studniarczyk, D., Farrant, M., and Cull-Candy, S.G. (2012). Channel properties reveal differential expression of TARPed and TARPless AMPARs in stargazer neurons. Nat. Neurosci. *15*, 853–861.

Beards, S., Gayer-Anderson, C., Borges, S., Dewey, M.E., Fisher, H.L., and Morgan, C. (2013). Life events and psychosis: A review and meta-analysis. Schizophr. Bull. *39*, 740–747.

Blanchoin, L., Boujemaa-Paterski, R., Sykes, C., and Plastino, J. (2014). Actin dynamics, architecture, and mechanics in cell motility. Physiol. Rev. *94*, 235–263.

Borgdorff, A.J., and Choquet, D. (2002). Regulation of AMPA receptor lateral movements. Nature *417*, 649–653.

Chater, T.E., and Goda, Y. (2014). The role of AMPA receptors in postsynaptic mechanisms of synaptic plasticity. Front. Cell. Neurosci. *8*, 1–14.

Chazeau, a., Mehidi, a., Nair, D., Gautier, J.J., Leduc, C., Chamma, I., Kage, F., Kechkar, a., Thoumine, O., Rottner, K., et al. (2014). Nanoscale segregation of actin nucleation and elongation factors determines dendritic spine protrusion. EMBO J. *33*, 2745–2764.

Chazeau, a., Garcia, M., Czondor, K., Perrais, D., Tessier, B., Giannone, G., and Thoumine, O. (2015). Mechanical coupling between transsynaptic N-cadherin adhesions and actin flow stabilizes dendritic spines. Mol. Biol. Cell *26*, 859–873.

Chen, L., Chetkovich, D.M., Petralia, R.S., Sweeney, N.T., Kawasaki, Y., Wenthold, R.J., Bredt, D.S., and Nicoll, R. a (2000). Stargazin regulates synaptic targeting of AMPA receptors by two distinct mechanisms. Nature *408*, 936–943.

Chen, Y., Liang, Z., Fei, E., Chen, Y., Zhou, X., Fang, W., Fu, W.-Y., Fu, A.K.Y., and Ip, N.Y. (2015). Axin Regulates Dendritic Spine Morphogenesis through Cdc42-Dependent Signaling. PLoS One *10*, e0133115.

Chetkovich, D.M., Chen, L., Stocker, T.J., Nicoll, R. a, and Bredt, D.S. (2002). Phosphorylation of the postsynaptic density-95 (PSD-95)/discs large/zona occludens-1 binding site of stargazin regulates binding to PSD-95 and synaptic targeting of AMPA receptors. J. Neurosci. *22*, 5791–5796.

Choi, J., Ko, J., Park, E., Lee, J.R., Yoon, J., Lim, S., and Kim, E. (2002). Phosphorylation of stargazin by protein kinase A regulates its interaction with PSD-95. J. Biol. Chem. *277*, 12359–12363.

Chung, K., and Deisseroth, K. (2013). CLARITY for mapping the nervous system. Nat. Methods *10*, 508–513.

Chung, K., Wallace, J., Kim, S.-Y., Kalyanasundaram, S., Andalman, A.S., Davidson, T.J., Mirzabekov, J.J., Zalocusky, K. a, Mattis, J., Denisin, A.K., et al. (2013). Structural and molecular interrogation of intact biological systems. Nature *497*, 332–337.

Corcoran, C., Mujica-Parodi, L., Yale, S., Leitman, D., and Malaspina, D. (2002). Could stress cause psychosis in individuals vulnerable to schizophrenia? CNS Spectr. *7*, 33–38, 41–42.

Corcoran, C., Walker, E., Huot, R., Mittal, V., Tessner, K., Kestler, L., and Malaspina, D. (2003). The Stress Cascade and Schizophrenia: Etiology and Onset. Schizophr. Bull. *29*, 671–692.

Cuadra, A.E., Kuo, S.-H., Kawasaki, Y., Bredt, D.S., and Chetkovich, D.M. (2004). AMPA receptor synaptic targeting regulated by stargazin interactions with the Golgi-resident PDZ protein nPIST. J. Neurosci. *24*, 7491–7502.

Datta, D., Arion, D., Corradi, J.P., and Lewis, D. a. (2015). Altered Expression of CDC42 Signaling Pathway Components in Cortical Layer 3 Pyramidal Cells in Schizophrenia. Biol. Psychiatry *68*, 1–11.

Day, R., Nielsen, J. a., Korten, a., Ernberg, G., Dube, K.C., Gebhart, J., Jablensky, a., Leon, C., Marsella, a., Olatawura, M., et al. (1987). Stressful life events preceding the acute onset of schizophrenia: A cross-national study from the World Health Organization. Cult. Med. Psychiatry *11*, 123–205.

Deng, F., Price, M.G., Davis, C.F., Mori, M., and Burgess, D.L. (2006). Stargazin and other transmembrane AMPA receptor regulating proteins interact with synaptic scaffolding protein MAGI-2 in brain. J. Neurosci. *26*, 7875–7884.

Durand, C.M., Perroy, J., Loll, F., Perrais, D., Fagni, L., Bourgeron, T., Montcouquiol, M., and Sans, N. (2012). SHANK3 mutations identified in autism lead to modification of dendritic spine morphology via an actin-dependent mechanism. Mol. Psychiatry *17*, 71–84.

Elias, G.M., Funke, L., Stein, V., Grant, S.G., Bredt, D.S., and Nicoll, R. a. (2006). Synapse-Specific and Developmentally Regulated Targeting of AMPA Receptors by a Family of MAGUK Scaffolding Proteins. Neuron *52*, 307–320.

Ertürk, A., Becker, K., Jährling, N., Mauch, C.P., Hojer, C.D., Egen, J.G., Hellal, F., Bradke, F., Sheng, M., and Dodt, H.-U. (2012). Three-dimensional imaging of solvent-cleared organs using 3DISCO. Nat. Protoc. *7*, 1983–1995.

Faludi, G., and Mirnics, K. (2011). Synaptic changes in the brain of subjects with

schizophrenia. Int. J. Dev. Neurosci. *29*, 305–309.

Fink, C.C., Bayer, K.U., Myers, J.W., Ferrell, J.E., Schulman, H., and Meyer, T. (2003). Selective regulation of neurite extension and synapse formation by the β but not the α isoform of CaMKII. Neuron *39*, 283–297.

Guzowski, J.F., Lyford, G.L., Stevenson, G.D., Houston, F.P., McGaugh, J.L., Worley, P.F., and Barnes, C. a (2000). Inhibition of activity-dependent arc protein expression in the rat hippocampus impairs the maintenance of long-term potentiation and the consolidation of long-term memory. J. Neurosci. *20*, 3993–4001.

Hafner, A.-S., Penn, A.C., Grillo-Bosch, D., Retailleau, N., Poujol, C., Philippat, A., Coussen, F., Sainlos, M., Opazo, P., and Choquet, D. (2015). Lengthening of the Stargazin Cytoplasmic Tail Increases Synaptic Transmission by Promoting Interaction to Deeper Domains of PSD-95. Neuron *86,* 1–15.

Hama, H., Kurokawa, H., Kawano, H., Ando, R., Shimogori, T., Noda, H., Fukami, K., Sakaue-Sawano, A., and Miyawaki, A. (2011). Scale: a chemical approach for fluorescence imaging and reconstruction of transparent mouse brain. Nat. Neurosci. *14*, 1481–1488.

Hama, H., Hioki, H., Namiki, K., Hoshida, T., Kurokawa, H., Ishidate, F., Kaneko, T., Akagi, T., Saito, T., Saido, T., et al. (2015). ScaleS: an optical clearing palette for biological imaging. Nat. Neurosci., *18*, 1518-1529.

Hamdan, F.F., Gauthier, J., Araki, Y., Lin, D.T., Yoshizawa, Y., Higashi, K., Park, a. R., Spiegelman, D., Dobrzeniecka, S., Piton, A., et al. (2011). Excess of de novo deleterious mutations in genes associated with glutamatergic systems in nonsyndromic intellectual disability. Am. J. Hum. Genet. *88*, 306–316.

Han, K., Holder, J.L., Schaaf, C.P., Lu, H., Chen, H., Kang, H., Tang, J., Wu, Z., Hao, S., Cheung, S.W., et al. (2013). SHANK3 overexpression causes manic-like behaviour with unique pharmacogenetic properties. Nature *503*, 72–77.

Harris, K.M., Jensen, F.E., and Tsao, B. (1992). Three-dimensional structure of dendritic spines and synapses in rat hippocampus (CA1) at postnatal day 15 and adult ages:

implications for the maturation of synaptic physiology and long-term potentiation. J. Neurosci. *12*, 2685–2705.

Hering, H., and Sheng, M. (2001). Dendritic spines: structure, dynamics and regulation. Nat. Rev. Neurosci. *2*, 880–888.

Hirabayashi, S., Nishimura, W., Iida, J., Kansaku, A., Kishida, S., Kikuchi, A., Tanaka, N., and Hata, Y. (2004). Synaptic scaffolding molecule interacts with Axin. J. Neurochem. *90*, 332–339.

Holtmaat, A.J.G.D., Trachtenberg, J.T., Wilbrecht, L., Shepherd, G.M., Zhang, X., Knott, G.W., and Svoboda, K. (2005). Transient and persistent dendritic spines in the neocortex in vivo. Neuron *45*, 279–291.

Howard, R., Rabins, P. V., Seeman, M. V., and Jeste, D. V. (2000). Late-onset schizophrenia and very-late-onset schizophrenia-like psychosis: An international consensus. Am. J. Psychiatry *157*, 172–178.

Inamura, M., Itakura, M., Okamoto, H., Hoka, S., Mizoguchi, A., Fukazawa, Y., Shigemoto, R., Yamamori, S., and Takahashi, M. (2006). Differential localization and regulation of stargazin-like protein, γ-8 and stargazin in the plasma membrane of hippocampal and cortical neurons. Neurosci. Res. *55*, 45–53.

Ives, J.H., Fung, S., Tiwari, P., Payne, H.L., and Thompson, C.L. (2004). Microtubule-associated protein light chain 2 is a stargazin-AMPA receptor complex-interacting protein in vivo. J. Biol. Chem. *279*, 31002–31009.

Jégou, A., Carlier, M.-F., and Romet-Lemonne, G. (2013). Formin mDia1 senses and generates mechanical forces on actin filaments. Nat. Commun. *4*, 1883.

Ke, M.-T., Fujimoto, S., and Imai, T. (2013). SeeDB: a simple and morphology-preserving optical clearing agent for neuronal circuit reconstruction. Nat. Neurosci. *16*, 1154–1161.

Kim, K.S., Yan, D., and Tomita, S. (2010). Assembly and stoichiometry of the AMPA receptor and transmembrane AMPA receptor regulatory protein complex. J. Neurosci. *30*, 1064–1072.

Kim, S.Y., Chung, K., and Deisseroth, K. (2013). Light microscopy mapping of connections in the intact brain. Trends Cogn. Sci. *17*, 596–599.

Knott, G.W., Holtmaat, A., Wilbrecht, L., Welker, E., and Svoboda, K. (2006). Spine growth precedes synapse formation in the adult neocortex in vivo. Nat. Neurosci. *9*, 1117–1124.

Kourosh Arami, M., and Jameie, B. (2015). Synaptic Neuronal Plasticity. Thrita *4*, 1–4.

Kovar, D.R., Harris, E.S., Mahaffy, R., Higgs, H.N., and Pollard, T.D. (2006). Control of the assembly of ATP- and ADP-actin by formins and profilin. Cell *124*, 423–435.

Kuwajima, T., Sitko, A. a, Bhansali, P., Jurgens, C., Guido, W., and Mason, C. (2013). ClearT: a detergent- and solvent-free clearing method for neuronal and non-neuronal tissue. Development *140*, 1364–1368.

Lee, S.H., Liu, L., Wang, Y.T., and Sheng, M. (2002). Clathrin Adaptor AP2 and NSF Interact with Overlapping Sites of GluR2 and Play Distinct Roles in AMPA Receptor Trafficking and Hippocampal LTD. Neuron *36*, 661–674.

Letts, V. a, Felix, R., Biddlecome, G.H., Arikkath, J., Mahaffey, C.L., Valenzuela, a, Bartlett, F.S., Mori, Y., Campbell, K.P., and Frankel, W.N. (1998). The mouse stargazer gene encodes a neuronal Ca2+-channel gamma subunit. Nat. Genet. *19*, 340–347.

Lin, Y.-C., and Redmond, L. (2008). CaMKIIbeta binding to stable F-actin in vivo regulates F-actin filament stability. Proc. Natl. Acad. Sci. U. S. A. *105*, 15791–15796.

Louros, S.R., Hooks, B.M., Litvina, L., Carvalho, A., and Chen, C. (2014). A role for stargazin in experience-dependent plasticity. Cell Rep. *7*, 1614–1625.

Ma, T.M., Paul, B.D., Fu, C., Hu, S., Zhu, H., Blackshaw, S., Wolosker, H., and Snyder, S.H. (2014). Serine Racemase Regulated by Binding to Stargazin and PSD-95. J. Biol. Chem. *289*, 29631–29641.

Martens, M.B., Celikel, T., and Tiesinga, P.H.E. (2015). A Developmental Switch for Hebbian Plasticity. PLOS Comput. Biol. *11*, e1004386.

Marx, V. (2016). Optimizing probes to image cleared tissue. Nat. Methods *13*, 205–209.

Matsuda, S., Kakegawa, W., Budisantoso, T., Nomura, T., Kohda, K., and Yuzaki, M. (2013). Stargazin regulates AMPA receptor trafficking through adaptor protein complexes during long-term depression. Nat. Commun. *4*, 2759.

Matsuzaki, M., Ellis-Davies, G.C., Nemoto, T., Miyashita, Y., Iino, M., and Kasai, H. (2001). Dendritic spine geometry is critical for AMPA receptor expression in hippocampal CA1 pyramidal neurons. Nat. Neurosci. *4*, 1086–1092.

Murakoshi, H., and Yasuda, R. (2012). Postsynaptic signaling during plasticity of dendritic spines. Trends Neurosci. *35*, 135–143.

Nägerl, U.V., Eberhorn, N., Cambridge, S.B., and Bonhoeffer, T. (2004). Bidirectional activity-dependent morphological plasticity in hippocampal neurons. Neuron *44*, 759–767.

Nägerl, U.V., Köstinger, G., Anderson, J.C., Martin, K. a C., and Bonhoeffer, T. (2007). Protracted synaptogenesis after activity-dependent spinogenesis in hippocampal neurons. J. Neurosci. *27*, 8149–8156.

Nissen, S., Liang, S., Shehktman, T., Kelsoe, J.R., Greenwood, T. a, Nievergelt, C.M., McKinney, R., Shilling, P.D., Smith, E.N., Schork, N.J., et al. (2012). Evidence for association of bipolar disorder to haplotypes in the 22q12.3 region near the genes stargazin, IFT27 and parvalbumin. Am. J. Med. Genet. B. Neuropsychiatr. Genet. *159B*, 941–950.

Nomura, T., Kakegawa, W., Matsuda, S., Kohda, K., Nishiyama, J., Takahashi, T., and Yuzaki, M. (2012). Cerebellar long-term depression requires dephosphorylation of TARP in Purkinje cells. Eur. J. Neurosci. *35*, 402–410.

Okamoto, K., Bosch, M., and Hayashi, Y. (2009). The roles of CaMKII and F-actin in the structural plasticity of dendritic spines: a potential molecular identity of a synaptic tag? Physiology (Bethesda). *24*, 357–366.

Okamoto, K.-I., Narayanan, R., Lee, S.H., Murata, K., and Hayashi, Y. (2007). The role of CaMKII as an F-actin-bundling protein crucial for maintenance of dendritic spine structure. Proc. Natl. Acad. Sci. U. S. A. *104*, 6418–6423.

Opazo, P., Labrecque, S., Tigaret, C.M., Frouin, A., Wiseman, P.W., De Koninck, P., and Choquet, D. (2010). CaMKII triggers the diffusional trapping of surface AMPARs through phosphorylation of stargazin. Neuron *67*, 239–252.

Palmer, C.L., Cotton, L., and Henley, J.M. (2005). The Molecular Pharmacology and Cell Biology of Acid Receptors. Pharmacol. Rev. *57*, 253–277.

Park, E., Chi, S., and Park, D. (2012). Activity-Dependent Modulation of the Interaction between CaMKII and Abi1 and Its Involvement in Spine Maturation. J. Neurosci. *32*, 13177–13188.

Peebles, C.L., Yoo, J., Thwin, M.T., Palop, J.J., Noebels, J.L., and Finkbeiner, S. (2010). Arc regulates spine morphology and maintains network stability in vivo. Proc. Natl. Acad. Sci. U. S. A. *107*, 18173–18178.

Peters, a, and Kaiserman-Abramof, I.R. (1970). The small pyramidal neuron of the rat cerebral cortex. The perikaryon, dendrites and spines. Am. J. Anat. *127*, 321–355.

Pozo, K., and Goda, Y. (2010). Unraveling mechanisms of homeostatic synaptic plasticity. Neuron *66*, 337–351.

Ramiro-Cortés, Y., and Israely, I. (2013). Long Lasting Protein Synthesis- and Activity-Dependent Spine Shrinkage and Elimination after Synaptic Depression. PLoS One *8*, 1–10.

Renier, N., Wu, Z., Simon, D.J., Yang, J., Ariel, P., and Tessier-lavigne, M. (2014). Resource iDISCO : A Simple , Rapid Method to Immunolabel Large Tissue Samples for Volume Imaging. Cell *Im*, 1–15.

Richardson, D.S., and Lichtman, J.W. (2015). Clarifying Tissue Clearing. Cell *162*, 246–257.

Roberts, M.F., Taylor, D.W., and Unger, V.M. (2011). Two modes of interaction between the membrane-embedded TARP stargazin's C-terminal domain and the bilayer visualized by electron crystallography. J. Struct. Biol. *174*, 542–551.

Rosch, J.H., and Bonhoeffer, T. (2003). Analysis of activity-dependent morphological plasticity of dendritic spines on hippocampal neurons.

Saarikangas, J., Zhao, H., and Lappalainen, P. (2010). Regulation of the actin cytoskeleton-plasma membrane interplay by phosphoinositides. Physiol. Rev. *90*, 259–289.

Sala, C., and Segal, M. (2014). Dendritic spines: the locus of structural and functional plasticity. Physiol. Rev. *94*, 141–188.

Schnell, E., Sizemore, M., Karimzadegan, S., Chen, L., Bredt, D.S., and Nicoll, R. a (2002). Direct interactions between PSD-95 and stargazin control synaptic AMPA receptor number. Proc. Natl. Acad. Sci. U. S. A. *99*, 13902–13907.

Schubert, V., Da Silva, J.S., and Dotti, C.G. (2006). Localized recruitment and activation of RhoA underlies dendritic spine morphology in a glutamate receptor-dependent manner. J. Cell Biol. *172*, 453–467.

Shanks, N.F., Maruo, T., Farina, A.N., Ellisman, M.H., and Nakagawa, T. (2010). Contribution of the global subunit structure and stargazin on the maturation of AMPA receptors. J. Neurosci. *30*, 2728–2740.

Shelton, M. a., Newman, J.T., Gu, H., Sampson, A.R., Fish, K.N., MacDonald, M.L., Moyer, C.E., DiBitetto, J. V, Dorph-Petersen, K.-A., Penzes, P., et al. (2015). Loss of Microtubule Associated Protein 2 Immunoreactivity Linked to Dendritic Spine Loss in Schizophrenia. Biol. Psychiatry 1–12.

Shen, K., and Meyer, T. (1999). Dynamic control of CaMKII translocation and localization in hippocampal neurons by NMDA receptor stimulation. Science *284*, 162–166.

Shen, K., Teruel, M.N., Subramanian, K., and Meyer, T. (1998). CaMKIIβfunctions as an F-actin targeting module that localizes CaMKIIα/β heterooligomers to dendritic spines. Neuron *21*, 593–606.

Shi, P., Huang, Y., and Hong, J. (2014). Automated three-dimensional reconstruction and morphological analysis of dendritic spines based on semi-supervised learning. Biomed. Opt. Express *5*, 1541–1553.

Shi, Y., Lu, W., Milstein, A.D., and Nicoll, R. a (2009). The stoichiometry of AMPA receptors and TARPs varies by neuronal cell type. Neuron *62*, 633–640.

Siddoway, B., Hou, H., and Xia, H. (2011). Glutamatergic Synapses: Molecular Organisation. eLS.

Soto, D., Coombs, I.D., Kelly, L., Farrant, M., and Cull-candy, S.G. (2008). Europe PMC Funders Group Stargazin attenuates intracellular polyamine block of calcium- permeable AMPARs. *10*, 1260–1267.

Stoppini, L., Buchs, P.A., and Muller, D. (1991). A simple method for organotypic cultures of nervous tissue. J. Neurosci. Methods *37*, 173–182.

Sumioka, A., Yan, D., and Tomita, S. (2010). TARP Phosphorylation Regulates Synaptic AMPA Receptors through Lipid Bilayers. Neuron *66*, 755–767.

Susaki, E. a., Tainaka, K., Perrin, D., Kishino, F., Tawara, T., Watanabe, T.M., Yokoyama, C., Onoe, H., Eguchi, M., Yamaguchi, S., et al. (2014). Whole-brain imaging with single-cell resolution using chemical cocktails and computational analysis. Cell *157*, 726–739.

Swedlow, J.R. (2013). Quantitative fluorescence microscopy and image deconvolution Methods in Cell Biology *114,* 407-426.

Tardin, C., Cognet, L., Bats, C., Lounis, B., and Choquet, D. (2003). Direct imaging of lateral movements of AMPA receptors inside synapses. EMBO J. *22*, 4656–4665.

Tomer, R., Ye, L., Hsueh, B., and Deisseroth, K. (2014). Advanced CLARITY for rapid and high-resolution imaging of intact tissues. Nat. Protoc. *9*, 1682–1697.

Tomita, S. (2010). Regulation of ionotropic glutamate receptors by their auxiliary subunits. Physiology (Bethesda). *25*, 41–49.

Tomita, S., Nicoll, R. a., and Bredt, D.S. (2001). PDZ protein interactions regulating glutamate receptor function and plasticity. J. Cell Biol. *153*, 19–23.

Tomita, S., Fukata, M., Nicoll, R. a, and Bredt, D.S. (2004). Dynamic interaction of stargazin-like TARPs with cycling AMPA receptors at synapses. Science *303*, 1508–1511.

Tomita, S., Adesnik, H., Sekiguchi, M., Zhang, W., Wada, K., Howe, J.R., Nicoll, R. a, and Bredt, D.S. (2005a). Stargazin modulates AMPA receptor gating and trafficking by distinct

domains. Nature *435*, 1052–1058.

Tomita, S., Stein, V., Stocker, T.J., Nicoll, R. a., and Bredt, D.S. (2005b). Bidirectional synaptic plasticity regulated by phosphorylation of stargazin-like TARPs. Neuron *45*, 269–277.

Tomita, S., Sekiguchi, M., Wada, K., Nicoll, R. a, and Bredt, D.S. (2006). Stargazin controls the pharmacology of AMPA receptor potentiators. Proc. Natl. Acad. Sci. U. S. A. *103*, 10064–10067.

Topper, S., Ober, C., and Das, S. (2011). Exome sequencing and the genetics of intellectual disability. Clin. Genet. *80*, 117–126.

Toyoizumi, T., Kaneko, M., Stryker, M.P., and Miller, K.D. (2014). Modeling the dynamical interaction of Hebbian and homeostatic plasticity. Neuron *84*, 1–40.

Turrigiano, G. (2007). Homeostatic signaling: the positive side of negative feedback. Curr. Opin. Neurobiol. *17*, 318–324.

Turrigiano, G. (2012). Homeostatic synaptic plasticity: Local and global mechanisms for stabilizing neuronal function. Cold Spring Harb. Perspect. Biol. *4*, 1–17.

Vandenberghe, W., Nicoll, R. a, and Bredt, D.S. (2005). Interaction with the unfolded protein response reveals a role for stargazin in biosynthetic AMPA receptor transport. J. Neurosci. *25*, 1095–1102.

Vanderklish, P.W., and Edelman, G.M. (2002). Dendritic spines elongate after stimulation of group 1 metabotropic glutamate receptors in cultured hippocampal neurons. Proc. Natl. Acad. Sci. U. S. A. *99*, 1639–1644.

Vitureira, N., Letellier, M., and Goda, Y. (2012). Homeostatic synaptic plasticity: From single synapses to neural circuits. Curr. Opin. Neurobiol. *22*, 516–521.

Volk, L., Chiu, S.-L., Sharma, K., and Huganir, R.L. (2015). Glutamate Synapses in Human Cognitive Disorders. Annu. Rev. Neurosci. *38*, 127–149.

Wearne, S.L., Rodriguez, A., Ehlenberger, D.B., Rocher, A.B., Henderson, S.C., and Hof, P.R.

(2005). New techniques for imaging, digitization and analysis of three-dimensional neural morphology on multiple scales. Neuroscience *136*, 661–680.

Woods, G., and Zito, K. (2008). Preparation of gene gun bullets and biolistic transfection of neurons in slice culture. J. Vis. Exp. *e675*, 3–6.

Yang, B., Treweek, J.B., Kulkarni, R.P., Deverman, B.E., Chen, C.K., Lubeck, E., Shah, S., Cai, L., and Gradinaru, V. (2014). Single-Cell Phenotyping within Transparent Intact Tissue through Whole-Body Clearing. Cell *158*, 945–958.

Yang, Y., Wang, X., Frerking, M., and Zhou, Q. (2008). Spine expansion and stabilization associated with long-term potentiation. J. Neurosci. *28*, 5740–5751.

Yu, L., Rostamiani, K., Hsu, Y.T., Wang, Y., Bi, X., and Baudry, M. (2011). Calpain-mediated regulation of stargazin in adult rat brain. Neuroscience *178*, 13–20.

Zhang, W., Wu, J., Ward, M.D., Yang, S., Chuang, Y.-A., Xiao, M., Li, R., Leahy, D.J., and Worley, P.F. (2015). Structural Basis of Arc Binding to Synaptic Proteins: Implications for Cognitive Disease. Neuron *86,* 1–11.

Ziff, E.B. (2007). TARPs and the AMPA Receptor Trafficking Paradox. Neuron *53*, 627–633.

Zito, K., and Scheuss, V. (2009). NMDA Receptor Function and Physiological Modulation. In: Encyclopedia of Neuroscience. Elsevier 276–283.

Zuo, Y., Lin, A., Chang, P., and Gan, W.B. (2005). Development of long-term dendritic spine stability in diverse regions of cerebral cortex. Neuron *46*, 181–189.